ACIBADEM MEHMET ALI AYDINLAR UNIVERSITY
INSTITUTE OF HEALTH SCIENCES

PROTEIN PROFILING OF HUMAN GASTRIC ORGANOID MODEL INFECTED WITH OUTER MEMBRANE INFLAMMATORY PROTEIN A (OIPA) ON AND ΔOIPA *H. PYLORI* STRAINS

SÜMEYYE AKÇELİK DEVECİ

PH.D. THESIS

DEPARTMENT OF MEDICAL BIOTECHNOLOGY

SUPERVISOR
Assist. Prof. Sinem Öktem Okullu

ISTANBUL-2023

ACIBADEM MEHMET ALI AYDINLAR UNIVERSITY
INSTITUTE OF HEALTH SCIENCES

PROTEIN PROFILING OF HUMAN GASTRIC ORGANOID MODEL INFECTED WITH OUTER MEMBRANE INFLAMMATORY PROTEIN A (OIPA) ON AND ΔOIPA *H. PYLORI* STRAINS

SÜMEYYE AKÇELİK DEVECİ

PH.D. THESIS

DEPARTMENT OF MEDICAL BIOTECHNOLOGY

SUPERVISOR
Assist. Prof. Sinem Öktem Okullu

ISTANBUL-2023

DECLARATION

I declare that this thesis work is my own work, I had no unethical behavior at any stage from the planning to the writing of the thesis, I obtained all the information in this thesis in accordance with academic and ethical rules, I cited all the information and comments that were not obtained with this thesis work, and I provided resources in the list of references. I also declare that there was no violation of any patents and copyrights during the study and writing of this thesis.

06/06/2023
Sümeyye AKÇELİK DEVECİ

PREFACE AND ACKNOWLEDGEMENT

I would like to express my sincere gratitude to my thesis advisor, Assist. Prof. Sinem ÖKTEM OKULLU, for her unwavering support and guidance throughout my doctoral journey. Her trust in me and my research, even in times of uncertainty, has been invaluable. Additionally, her willingness to stand by my side, offering encouragement and constructive feedback, has helped me grow both personally and professionally. I could not have completed this work without her mentorship and expertise, and for that, I am truly grateful.

I also want to express my sincere thanks to the esteemed professors of my Ph.D. thesis review committee, Prof. Dr. Tanıl KOCAGÖZ, and Assoc. Prof. Dr. Ayça Sayı Yazgan, for their valuable time, for sharing their precious opinions with me, and for their support throughout the study. I also want to thank to Orhan ÖZCAN for his suggestions on whole omics data analysis.

I would like to express my heartfelt gratitude to my dear friend, colleague, and Ph.D. partner, Ph.D. Nesteren Mansur Özen, for her kind friendship and invaluable contributions to my life since the day we first met. Throughout the doctoral period, our coffee breaks and brainstorming sessions have been a source of inspiration and motivation for me. I am deeply grateful for the wonderful memories we have shared and for her endless support and encouragement throughout our journey together.

I owe an appreciation to our research group member and colleague, Yaren BÜYÜKÇOLAK for her great support and kind friendship. It was a great joy doing PCR with her during the days and nights. I would also thank to Tuana AYDINLAR for her friendship and help.

I would like to thank Selma ÇAT for patiently helping and answering every question under any circumstances. I am grateful to meet Ayşegül EKMEKÇİ and Başak KAVAKLIOĞLU, who always help me with their smiling faces during long cell culture experiments, and Gökçen ÖZGÜN, who help me with histological

experiments, for their kindness. I would also like to thank Simge ŞENAY, Esma AYBAKAN, Tayyip KARAMAN, Elif SEVER, Hale MUŞLU, and other graduate researchers from the fifth floor of ACU for always being kind and gentle. Spending seven years with these lovely people has been so precious.

I would like to express my heartfelt thanks to Zeliha Nur MUTLU, Huriye YILDIRIM, and Gülnaz TÜRKCAN, who have been my greatest luck in life. They have always supported and understood me throughout my doctoral study, even when I couldn't be there for them on special occasions. I would like to express my deepest gratitude to Ahmet Çevik for his encouragement and belief in me. Also, would like to thank all my friends for their support.

I gratefully thank my mother, Emine AKÇELİK, father, Recep AKÇELİK, and my sister, Şeyma ŞAHİN who makes me who I am and accepts me for who I am, for their support, encouragement, and endless love not only during this study but also throughout my life.

I express my deepest and sincerest gratitude from the bottom of my heart to my dearest husband, Cihad DEVECİ, who completed this study with me, worked with me during long nights, and shared life with me. It brings me great joy to have you by my side, and I thank you with all my love.

I would like to thank my professors who contributed to my doctoral education and TÜBİTAK for supporting me within the scope of the BİDEB 2211-A National PhD Scholarship Program.

This research was completed within the scope of the project numbered 119S127 and titled "Protein profile identification of stomach organoid model infected with outer membrane inflammatory protein A (OipA) on or off *H. pylori* strain and comparison with the protein profile obtained by MALDI imaging method in OipA on and off strain infected patient stomach tissues" supported by TUBITAK (1001 - The Scientific and Technological Research Projects Funding Program).

TABLE OF CONTENTS

LIST OF ABBREVIATIONS AND SYMBOLS

AGS	Human gastric adenocarcinoma
ALI	Air-liquid interface
AlpA / AlpB	Adherence associated proteins A/B
Ambic	Ammoniumbicarbonate
ASCs	Adult stem cells
BabA	Blood-antigen binding protein A
BACs	Bacterial artificial chromosomes
BB	Brucella Broth
BCA	Bicinchoninic acid
Bcl-2	B-cell lymphoma 2
cagA	Cytotoxin-associated gene A
cagPAI	Cag pathogenicity island
CBA	Colombia Blood agar
CD40	Cluster of differentiation 40
CLO	Campylobacter-Like Organism
DMEM	Dulbecco's Modified Eagle Medium
DMSO	Dimethyl sulfoxide
DNA	Deoxyribonucleic acid
DTT	Dithiothreitol
EGF	Epidermal Growth Factor
ESCs	Embryonic stem cells
ECM	Extracellular matrix
FBS	Fetal bovine serum
FC	Fold changes
FDR	False Discovery Rate
FGF	Fibroblast growth factors
GO	Gene ontology
H. pylori	*Helicobacter pylori*
HC	Hierarchical Clustering
HEK-293T	Human embryonic kidney 293

hGOs	Human gastric organoids
IARC	International Agency for Research on Cancer
IL-8	Interleukin-8
iPSCs	Induced pluripotent stem cells
KanR	Kanamysin resistant
Le^b	Lewis b
LFQ	Label-free quantification
LGR-5	Leucine-rich-repeat-containing G-protein-coupled receptor 5
LPS	Lipopolysaccharide
MALT	Mucosal lymphoid tissue
MHC-II	Major histocompatibility complex-2
µg	Microgram
µm	Micrometer
mL	Milliliter
MMP-1	Matrix metalloproteinase 1
NCBI	National Center for Biotechnology Information
NFκB	Nuclear Factor kappa B
ng	Nanogram
NGS	Next generation sequencing
NOG	Noggin
OipA	Outer inflammatory protein A
OMPs	Outer membrane proteins
PCA	Principal Component Analysis
PCR	Polymerase chain reaction
PDOs	Patient-derived organoids
PEI	Polyethylenimine
PFA	Paraformaldehyde
PPIs	Proton- pump inhibitors
PSCs	Pluripotent stem cells
RHOKi	Rho-associated coiled coil forming protein serine/ threonine kinase inhibitor
RL	Renilla luciferase

RNA	Ribonucleic Acid
RUT	Rapid urease test
SabA	Sialic acid-binding adhesin
SAT	Stool antigen test
SOE PCR	Splicing by overlap extension PCR
SPE	Solid-phase extraction
SPEM	Spasmolytic polypeptide-expressing metaplasia
SRY	Sex-determining region Y
T4SS	Type IV secretion system
TFF1	Trefoil factor 1
TGF-β	Transforming growth factor beta
TNF-α	Tumor necrosis factor-alpha
UBT	Urea breath test
UreA	Urease A
vacA	Vacuolating cytotoxin A
WGS	Whole genome dequencing
WHO	World Health Organization
xCT	Cystine–glutamate transporter

LIST OF FIGURES

LIST OF TABLES

ÖZET

Dış Zar Inflamatuar Protein A (oipA) ON ve ΔoipA *Helicobacter pylori* Suşları ile Enfekte Olmuş İnsan Mide Organoid Modelinin Protein Profillerinin Belirlenmesi

Helicobacter pylori dünya nüfusunun yaklaşık yarısını enfekte ederek midede inflamasyonun oluşmasına yol açan bir patojendir. Bakterinin sebep olduğu enfeksiyonda en önemli adımlarından biri mide epitel hücrelere tutunmasıdır. Tutunmada, yüzey proteinleri ile etkileşime girebilen ve enfeksiyon seyrine etki edebilen virülans faktörlerinden dış zar proteinleri görev alır. Dış zar proteinlerinden, Outer inflamatory protein A (OipA) tutunmada rol alarak mide epitel hücrelerinde pro-enflamatuar sinyallerin oluşmasını ve IL-8 salgılanmasını indükler. Bu çalışmada enfeksiyon seyrine etkilerinin tam olarak bilinmediği OipA proteininin gastrik hücreler üzerindeki etkisi, hücrelerin enfeksiyon sonrasındaki protein profilleri ile araştırılmıştır. Enfeksiyon için *H. pylori* G27 suşu kullanılarak *oipA* geni silinmiş, bakteriden bakteriye fark edebilecek diğer virülans faktörlerin, virülans gen profiline bilinen etkisi ortadan kaldırılmıştır. Doğal dokunun taklit edildiği gastrik organoid modeli kullanılarak fizyolojik olarak daha güvenilir bir enfeksiyon modeli oluşturulması amaçlanmıştır. İnsan korpus dokusundaki yetişkin kök hücreler kullanılarak oluşturulan model karakterize edilmiş, gastrik dokuya ait dört ana hücre kökeninin ifade edildiği gözlemlenmiştir. Elde edilen proteomik veri analiz edilmiş, 1922 adet protein tanımlanmıştır. Yapılan kantifikasyon çalışmaları ile 97 adet proteinin miktarlarının, enfeksiyonda OipA'nın varlığında ve yokluğunda istatistiksel olarak anlamlı bir şekilde değiştiği tespit edilmiştir. Biyoinformatik analizlerle proteinlerin hücre içerisindeki görevleri ve dahil oldukları yolaklar araştırılmıştır. Sonuç olarak OipA proteininin varlığı *H. pylori* enfeksiyonunda hangi protein ve yolakları etkiliyor analiz edilmiş, enfeksiyon seyrinin anlaşılmasında kullanılabilecek biyobelirteç, tedavi ve aşı çalışmalarına hedef protein adayları belirlenmiştir.

Anahtar Sözcükler: *Helicobacter pylori*, Virulans faktörleri, OipA, Gastrik organoid kültürü, Proteomiks

ABSTRACT

Protein Profiling of Human Gastric Organoid Model Infected with Outer Membrane Inflammatory Protein A (oipA) ON and ΔoipA *Helicobacter pylori* Strains

Helicobacter pylori, a pathogenic bacterium, infects about half of the world's population and causes inflammation in the stomach. A crucial step in its infection is its attachment to the stomach epithelial cells, which is facilitated by outer membrane proteins. Among these proteins, outer inflammatory protein A (OipA) induces pro-inflammatory signals and IL-8 secretion, playing a significant role in bacterial attachment. The present study focuses on the effects of the OipA protein on gastric cells during infection using protein profiling. To eliminate the effects of other virulence factors, the *oipA* gene was deleted using the *H. pylori* reference strain G27 for the infection study. Moreover, to create a more physiologically reliable infection model that mimics natural tissue without using animal models or cancer cell lines, a gastric organoid model was developed by using adult stem cells from human corpus tissue. The model exhibited four lineages of stomach cells and used as an infection model in this study. As a result of LC-MS/MS data analysis, out of the 1922 proteins identified through quantification studies, 97 proteins were identified that were statistically significantly different in their quantities in the presence and absence of OipA during infection. The intracellular functions and pathways of these proteins were investigated using bioinformatic analysis. This study examined the impact of the OipA protein on gastric cells during *H. pylori* infection and identified promising protein candidates that could serve as targets for biomarker, treatment, and vaccine development studies to improve the prognosis of *H. pylori*-associated diseases.

Keywords: Helicobacter pylori, Virulence Factors, OipA, Gastric organoid culture, Proteomics

1 INTRODUCTION AND AIM

Helicobacter pylori (*H. pylori*) is a Gram-negative, spiral-shaped, and microaerophilic pathogen that infects more than half of the world's population at some point in their lives. *H. pylori* is defined by the World Health Organization (WHO) as a first-class carcinogen that colonizes the mucous layer of the gastric epithelium of infected organisms, leading to chronic gastric infections such as chronic gastritis, peptic ulcer, and mucosa-associated lymphoid tissue lymphoma (MALT).

The prevalence of *H. pylori* infection varies based on several factors, such as age, ethnicity, gender, geography, and socioeconomic status, with a higher incidence reported in developing countries compared to developed ones. In our country, the prevalence of the bacterium is approximately 70–80% in adults and 40% in children. While the majority of individuals infected with *H. pylori* remain asymptomatic, around 20% experience symptoms, which may be influenced by the host immune response, environmental factors, and bacterial virulence factors. Understanding the virulence factors of *H. pylori* and their impact on the host can provide crucial insights into the prognosis of the disease. Thus, it is essential to investigate the interplay between bacterial and host factors to develop effective strategies for the prevention and management of *H. pylori*-associated diseases.

The pathogenesis of the bacterium begins with its entry into the stomach tissue and continues with adherence and proliferation on the gastric mucosal surface. The first step of successful colonization is the attachment of bacteria to the gastric mucosal surface, where the bacterium's outer membrane proteins play a critical role. These proteins help the bacteria attach to the stomach surface and protect against the cleaning mechanisms in the stomach, such as fluid flow, peristaltic movements, and spillage of the mucosal surface. Outer inflammatory protein A (OipA) is one of the outer membrane proteins of *H. pylori*.

The *H. pylori* OipA protein is involved in the colonization of bacteria, the secretion of interleukin-8 (IL-8) from gastric epithelial cells, inducing apoptosis, and altering the cytoskeleton of host gastric epithelial cells, which leads to severe gastroduodenal diseases. OipA is encoded by the *oipA* gene, which is regulated by a slipped-strand mispairing mechanism based on the number of CT dinucleotide repeats in the 5' region. Some studies suggest that the functional status of *oipA* varies by geographical location. Although recent studies have associated the "on" status of the *oipA* gene with an increased risk of peptic ulcers and gastric cancer, other studies have not reached a consensus on this association. Further investigation is required to fully understand the multifactorial role of OipA protein in the pathogenesis of *H. pylori* infection. Both bacterial and host factors play important roles in the development of *H. pylori*-associated diseases, and OipA is one of the key virulence factors that contribute to the pathogenicity of the bacteria. To develop effective treatment and prevention strategies, a deeper understanding of the mechanisms underlying the involvement of OipA in *H. pylori* pathogenesis is essential.

The use of cancer cell lines as infection models for *H. pylori* studies can present limitations since they are often obtained from malignant samples or immortalized through viral infection, cell fusion, or the introduction of oncogenes. Such models may not accurately represent protein profiles in infected tissue organs. Recent studies propose a potential solution to this issue by using gastric organoid models derived from healthy tissue cells in three-dimensional cell culture. Organoids exhibit long-term growth, cellular diversity, and cellular organization capabilities specific to the organ of origin. Gastric organoid models mimic the human gastric tissue, and utilizing organoid models for infection studies enables the observation of changes in healthy tissues after infection, offering new insights into the pathogenesis of *H. pylori*-associated diseases.

1.1 Aim of the Study

The interaction between *H. pylori* OipA protein and host cells, as well as the downstream signaling pathways activated by OipA during infection, are critical areas

of investigation for understanding the pathogenesis of *H. pylori* infection. In this proposed thesis study, we aim to elucidate the protein profiles expressed after infection in a three-dimensional gastric organoid model that closely mimics the physiological and cellular features of the stomach tissue. To achieve this goal, we infected the gastric organoid model with *H. pylori* wild-type G27 strain and mutant G27 strain in which the *oipA* gene was deleted. The use of a gastric organoid model, developed without animal models or cancer cell lines, allowed us to obtain more reliable and physiologically relevant proteome data.

The identified and quantified protein data were further investigated using bioinformatic analysis to determine their intracellular functions and pathways. By examining these pathways, we hope to gain insight into the specific mechanisms by which OipA interacts with host cells and causes infection. The findings from this study will contribute to a better understanding of the role of OipA in *H. pylori* infection, which could be useful in the development of new therapeutic strategies to combat this common bacterial infection.

2 BACKGROUND

2.1 *Helicobacter pylori*

Helicobacter pylori (*H. pylori*) is a Gram-negative, microaerophilic bacterium with a helical, curved shape that infects the stomach and causes inflammation leading to a range of gastroduodenal diseases. *H. pylori* has two to six flagella which provide motility and allow rapid movement in the mucous layer on the gastric epithelial cells (1).

This bacterium, in which more than half of the world's population is infected, has been discovered in human samples from various gastric diseases, including gastric ulcers and cancer under a microscope by W. Jaworski, a professor at Cracow Medical Academy, published this information in Jaworski's Handbook of Gastric Diseases and named them “Vibrio rugula”, in 1889 (2). He was the first to purpose a possible role of this organism in the pathogenesis of gastric diseases and the idea was confirmed by Warren and Marshall independently. They cultured *H. pylori* for the first time in 1982 at the microbiology lab of the Royal Perth Hospital from a gastric biopsy of a duodenal ulcer patient. Although they originally named the bacterium Campylobacter-Like Organism (CLO) because it was thought to be a species of Campylobacter, ribonucleic acid sequencing results indicated that it could not be included in the genus Campylobacter. The organism’s name was changed to *H. pylori*, which represents a new species of *Helicobacter* (3,4).

To demonstrate the effect of *H. pylori* on gastric disease development, Marshall, who had normal gastric mucosa, drank a Petri dish of *H. pylori* culture. Eventually, he developed gastritis and histologically proven on the tenth day after the ingestion of bacteria (3).

In the continuation of their works, Warren and Marshall proved antibiotics are effective in treating gastritis. The National Institutes of Health (USA) published an opinion in 1994 indicating that *H. pylori* was the primary cause of the majority of

recurrent stomach ulcers and advising antibiotic therapy as part of the recommended course of treatment (5). For their research on *H. pylori*, Warren and Marshall received the Nobel Prize in Medicine in 2005. According to these data, *H. pylori* studies, which have continued to increase until today showed *H. pylori* colonization in the stomach can cause several gastrointestinal conditions, including chronic gastritis, duodenal or gastric ulcers, gastric mucosal lymphoid tissue (MALT) lymphoid, and gastric cancer and provided us with detailed information about the epidemiology of the bacterium, the diagnosis, treatment, and pathogenesis of the diseases it causes.

2.1.1 Epidemiology of the *H. pylori*

H. pylori is responsible for various gastrointestinal diseases. It is estimated that around 50% of the world's population is infected with *H. pylori*, making it one of the most common bacterial infections globally (6).

The prevalence of *H. pylori* infection varies depending on the region, with higher rates of infection seen in developing countries and lower rates in developed countries. Infection is more common in areas with poor sanitation and hygiene, as well as in populations with lower socioeconomic status (7). In terms of transmission, *H. pylori* is mainly spread through fecal-oral or oral-oral routes. Infection can occur through ingestion of contaminated food or water, as well as through close contact with an infected person (8).

The majority of people infected with *H. pylori* do not experience any symptoms, but in some cases, it can cause various gastrointestinal diseases, including gastritis, peptic ulcer disease, and gastric cancer which is the of the most common malignancies in the world (9). The studies showed that infection with *H. pylori* is the strongest known risk factor for gastric cancer and the International Agency for Research on Cancer (IARC), a subordinate organization of the World Health Organization (WHO), identified *H. pylori* as a "group 1 (definite carcinogen)" based on the results of epidemiologic studies (10).

2.1.2 *H. pylori* associated diseases

It is well acknowledged that *H. pylori* infection is the primary cause of the histological characteristics leading to severe gastro-duodenal diseases, such as peptic ulcer disease, gastric cancer, and gastric MALT lymphoma.

H. pylori infection usually occurs in childhood, while infectious diseases occur in adulthood. Although *H. pylori* infection typically results in chronic active gastritis, most (85%) infected individuals remain asymptomatic for their entire life (11). The gastric inflammation may develop into more serious diseases such as duodenal or gastric ulcers, gastric mucosa-associated lymphoid tissue (MALT) lymphoma, non-cardia gastric adenocarcinoma or gastric cancer. Variations in host immunity, bacterial virulence factors, and timing of infection are likely the causes of individual variances in stomach mucosal damage brought on by *H. pylori* infection (12).

There are many studies in the literature on extra-gastric diseases associated with *H. pylori* infection. These diseases include neurological, dermatological, hematological, ocular, cardiovascular, metabolic and allergies (13). Many of the evidence presented in the research results from epidemiological studies where several confounding factors have not been analyzed in depth. Therefore, it is impossible to establish a cause-effect relationship, and further investigation is needed (14).

2.1.3 Diagnosis and treatment of *H. pylori* infection

H. pylori infection can be detected by two types of diagnostic methods, invasive and non-invasive tests, which are categorized according to whether endoscopy is required or not. While invasive tests include histological evaluation, culture, polymerase chain reaction (PCR), and rapid urease test (RUT) on tissue obtained during endoscopy, urea breath test (UBT), serology, and stool antigen test (SAT) are categorized in non-invasive *H. pylori* diagnostic tests. The advancement of current diagnostic techniques enables a more precise diagnosis of *H. pylori* infection, which

enhances the management of disorders linked to *H. pylori*. The best test to use to identify *H. pylori* infection depends on several factors, including the prevalence and strains of the illness in endemic locations, accessibility, the benefits and drawbacks of each technique, and the unique clinical circumstances of each patient. Efforts to improve the diagnostic yield of *H. pylori* infection for various clinical uses, particular demographics, and genotypic characterizations may lead to more accurate and practical *H. pylori* infection diagnostic methods in the future (15).

H. pylori is a globally prevalent, high-risk pathogen. After diagnosing of the infection, while no treatment is recommended in asymptomatic patients, the classic therapy, which contains a proton pump inhibitor, clarithromycin, and amoxicillin or metronidazole, is generally the first choice for treatment of symptomatic patients (16). There are numerous methods for treating *H. pylori* infection, but no single antibiotic treatment has been found to completely remove it. Historically, the illness has been treated with a combination of different medicines, including clarithromycin, amoxicillin, metronidazole, tetracycline, fluoroquinolones, tinidazole, and others. These antibiotics are often combined antisecretory agents, bismuth salts or proton-pump inhibitors (PPIs). Different combinations of these medicines have demonstrated varying levels of efficacy in eradicating *H. pylori* infection. These therapies of *H. pylori* generally consist of two groups, which are classified as first-line therapies and second-line therapies. If the first-line therapy is unsuccessful, second-line therapy should be applied. The widespread use of standard therapies has become less effective due to the rapid emergence of antibiotic-resistant strains of *H. pylori*, along with noncompliance with treatment by patients. As a result, the effectiveness of these therapies has decreased to unacceptable levels of 80% or lower in many geographic regions (17). Due to the rapidly increasing antibiotic-resistant *H. pylori* strains, the bacteria listed in the WHO's high-priority pathogens list of bacteria for which new antibiotics are urgently needed (18).

Alternative methods of eradicating *H. pylori* have been explored. Some of these avenues are the use of novel antibiotics or traditional antibiotics used in various combinations in routine clinical practice to create innovative and more effective

treatments. Another method is the use of probiotics and antibiotics together in the treatment of infection (17). The ongoing searches for novel therapeutic approaches and the expanding knowledge of the molecular mechanisms behind *H. pylori* infection are major factors in the development of the most recent therapeutics and vaccines.

2.1.4 Bacterial mechanisms of pathogenesis

The human gastric epithelial cell inhibits the adhesion, growth, and migration of invasive pathogens. Due to the synthesis of toxic soluble components, pathogens like *H. pylori* disturb the gastrointestinal barrier. Furthermore, it binds to a variety of epithelial cell receptors and activates several host signaling pathways. *H. pylori* colonization, development of illnesses and infections rely on four main stages: adaptation to the gastric mucosa's acidic environment, movement toward and penetration of the epithelial cell barrier, attachment to particular receptors, and finally, tissue damage (11).

H. pylori pathogenesis is started by adaptation and adhesion of the bacterium to the mucosal surface of the stomach. During the first stage of the infection the bacteria produce a urease enzyme that converts urea to ammonia and bicarbonate, neutralizing the acidic environment of the stomach and allowing the bacterium to survive. Besides the urease enzyme the bacterium uses it’s polar flagella which helps bacteria to stay in the mucus layer and maintained colonization with both the ability to swim with movement (19). Once *H. pylori* colonizes the mucosal layer of the gastric epithelium, its adhesins interact with cellular receptors to prevent it from being displaced by the stomach's natural movements. *H. pylori* has many known adhesives involved in attachment such as blood-antigen binding protein A (BabA) and sialic acid-binding adhesin (SabA), adherence associated proteins (AlpA and AlpB) and outer inflammatory protein A (OipA). After adherence, the bacteria obtain nutrients and metabolic substrates, and release toxins that damage the host cells, promoting bacterial growth (20). The bacterium penetrates the epithelial layer through a process known as type IV secretion, which allows the injection of

virulence factors, like cytotoxin-associated gene A (cagA) and vacuolating cytotoxin A (vacA), into the host cell and causes changes that affect the cytoskeleton's overall organization as well as cell motility, proliferation, and apoptosis (21). *H. pylori* virulence factors play a major role in both pathogenesis of bacteria and infection causing disease development.

2.2 Virulence Factors

H. pylori is a highly virulent pathogen that has evolved multiple strategies to evade the host immune system and thrive in the harsh acidic environment of the stomach. The bacterium's virulence factors, including urease, cagA, vacA, and other outer membrane proteins, aid in its survival within the host and contribute to the pathogenesis of the disease, play a crucial role in these strategies (Figure 1) (22).

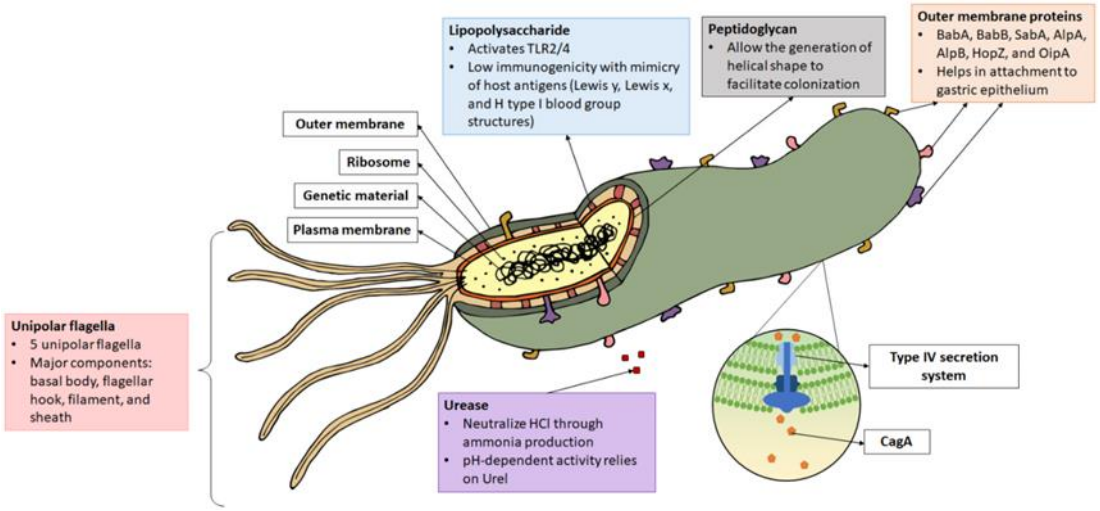

Figure 1. *Helicobacter pylori*'s structure. The virulence factors include the type IV secretion system (T4SS), flagella, urease, peptidoglycan, outer membrane proteins, and lipopolysaccharide (LPS). Figure reproduced here under the terms of the Creative Common CC BY license (22).

Urease is an essential virulence factor of *H. pylori*, which is an enzyme that converts urea to carbon dioxide and ammonia, creating a more alkaline environment favorable for bacterial survival in the stomach. The urease enzyme is present on the bacterial cell surface and secreted into the extracellular space, forming a protective layer around the bacteria. This process contributes to the bacterium's ability to adhere

to and colonize the gastric epithelium, which is the first stage of pathogenesis. Studies have shown that mutants deficient in urease activity exhibit a significant decrease in *H. pylori* colonization and pathogenicity, highlighting the importance of this virulence factor in the bacterium's survival and pathogenesis (23). According to studies, this enzyme may contribute to the development of peptic ulcers, gastric cancer, and gastric inflammation. The production of pro-inflammatory cytokines and chemokines can be stimulated by urease activity, which can then attract inflammatory cells to the stomach and cause chronic inflammation. The presence of *H. pylori* urease can also damage the stomach's epithelial cells, leading to cell death and tissue damage (24).

H. pylori involves around 1600 genes, and some virulence genes have been identified and characterized (25). One well-established *H. pylori* virulence gene is CagA, which is located in the 35-40 kb cag pathogenicity island (cagPAI) containing 27-33 genes. The cagPAI also encodes proteins that are involved in a type IV secretory system (T4SS), which is responsible for injecting the CagA protein into gastric epithelial cells (26). T4SS creates an extracellular, needle-like pilus that requires several protein-protein interactions as well as some pilus-associated components to be assembled. The pilus is activated upon contact with the host cell and *H. pylori's* adhesion, then it exports CagA through the bacterial and epithelial membranes and into the host cell cytoplasm (27). Following entry, CagA interacts with host cell molecules, causes cellular changes (28), and triggers gastric inflammation with an NFκB signal and increased IL-8 secretion (29,30). Consensus exists regarding the fact that the expression of CagA by *H. pylori* strains in vivo is associated with an amplified inflammatory response from the host, it correlates with an elevated likelihood of developing peptic ulcers or gastric cancer (25).

The other well-studied classical secreted virulence factor of *H. pylori* is the VacA. VacA is a secreted toxin that exhibits several biological activities, including the ability to induce vacuolization (31), act as an immune modulator (32,33), alter membrane permeability (34), and trigger apoptosis in host cells (35,36). The *vacA* gene is located in the plasticity region of the *H. pylori* genome, which is

characterized by genetic variability and diversity. The genetic diversity of *vacA* results in the production of different VacA isoforms, which vary in their cytotoxic activities and antigenic properties (37). Studies have shown that there is an antagonistic relationship between CagA and VacA toxins (38). It is thought that this antagonistic interaction occurs to prolong the life of the host cell (39). The more active version of VacA is frequently linked to the more active form of CagA and is thus further linked to more severe gastric disease (40).

Adhesion of *H. pylori* on the surface of gastric epithelial cells, is mediated via numerous outer membrane proteins (OMPs) which are virulence factors that play a pivotal role in binding to human cells.

2.1.1 Outer membrane proteins (OMPs)

The outer membrane proteins of *H. pylori* play a crucial role in the pathogenesis of the bacterium by mediating the interaction between the bacterium and the host cells. OMPs are a diverse group (Figure 2) (41), consisting of Hop, Hor, Hof, Hom, iron-related outer membrane proteins, and efflux pump-associated outer membrane proteins that are involved in various functions; colonization and persistence by preventing the bacteria from being eliminated from the stomach (19), evasion from the human immune system (42), and efficient delivery of toxins into the gastric cell, such as the CagA oncoprotein. *H. pylori* expresses a wide range of OMPs, including BabA, SabA, and OipA.

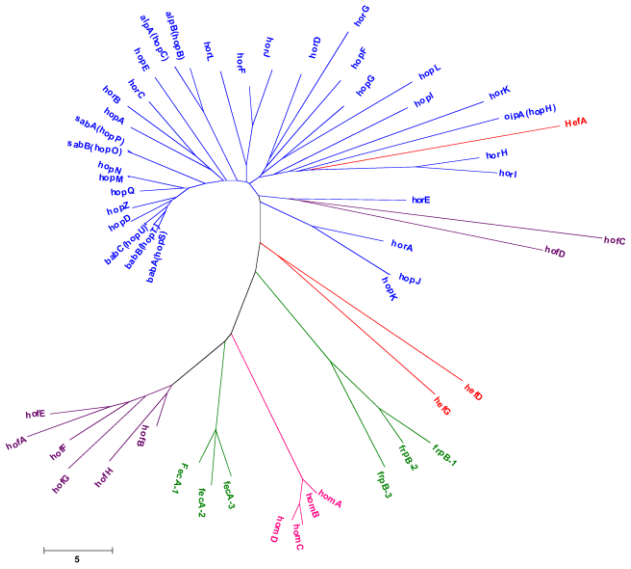

Figure 2. Phylogenetic analysis of the OMPs identified in *H. pylori* (41). Figure reproduced here under the terms of the Creative Common CC BY license.

Blood group antigen-binding adhesin (BabA) is a well-identified *H. pylori* adhesin protein that binds to certain blood group antigens, specifically the H-type 1 antigen and the ABO/Lewis b (Le^b) antigens found in the gastric epithelium. Through this binding, BabA facilitates the activity of the type IV secretion system TSS4, leading to the release of excessive amounts of pro-inflammatory factors and potentially promoting the development of cancer in the stomach (43,44). Besides the severity of gastrointestinal diseases, the expression of BabA also correlates with higher mucosal inflammation. BabA facilitates *H. pylori* adhesion to the spasmolytic polypeptide-expressing metaplasia (SPEM) glands by working with sialic acid-binding adhesion (SabA), producing metaplastic changes that aid at the beginning of carcinogenesis (45).

Sialic acid-binding adhesin is another adhesin belonging to the OMP family that facilitates *H. pylori* adherence to gastric epithelial cells via binding to the Le^x antigen. There is a correlation between SabA expression and the degree of bacterial colonization. SabA expression is linked to the advancement of gastric illnesses, excessive neutrophil infiltration, and gastric atrophy during infection (46,47). Studies have shown that one of the factors that cause an iron shortage in *H. pylori*-infected patients is the increased expression of the *sabA* gene (48).

In literature, it has been suggested that the outer membrane proteins BabA, SabA, and OipA, may aid in improving the accuracy of *H. pylori* diagnosis. As a result, they may have potential as diagnostic biomarkers for both active *H. pylori* infection and *H. pylori*-induced gastric cancer (49).

2.1.2 Outer inflammatory protein A (OipA)

Outer inflammatory protein A (OipA) is a 34-kDa adhesin protein that is a member of the Hop protein family, also known as HopH. The protein is encoded by an inflammation-related gene (HP0638/*hopH*) located approximately 100 kb from cag PAI on the *H. pylori* chromosome. The encoded gene of the OipA protein is present in all *H. pylori* strains but can be either functional or non-functional due to variations in the promoter region of the gene. The functional status of *oipA* is regulated by slipped-strand mispairing based on the number of CT dinucleotide repeats in the 5′ region of the genes that can be either switched 'on' (functional) or switched 'off' (nonfunctional) (50). While functional OipA is associated with enhanced adhesion to gastric epithelial cells, increased colonization and production of pro-inflammatory cytokines, neutrophil infiltration, activation of focal adhesion kinase, and re-organization of cytoskeleton (51–53), non-functional OipA is associated with a reduced ability to adhere to host cells and decreased virulence (54,55).

Epidemiological studies have indicated that the existence of OipA is linked to both duodenal ulcers and gastric cancer (50). When scientists studied host-bacteria interaction, the results have shown that the OipA protein modulates host immune responses. It can induce the production of pro-inflammatory cytokines, such as interleukin-8 (IL-8), IL-1, IL-6, IL-11 IL-17, matrix metalloproteinase 1 (MMP-1), tumor necrosis factor-alpha (TNF-α), and interleukin-1 beta (IL-1β), by gastric epithelial cells and immune cells. These cytokines promote inflammation and tissue damage, contributing to the development of gastric diseases (56–58). Considering the connection between OipA and the host immune system, one study focused on the interaction between dendritic cells and the OipA protein. Dendritic cells are the most

powerful antigen-presenting cells, with a potent capacity to stimulate naive T cells, and the result of this study shows the OipA suppresses the maturation of the dendritic cells by downregulating CD40, CD86, and MHC-II expression on the cell surface, as well as the release of IL-10 (59).

The *oipA* "on" gene correlated strongly with other virulence factors such as cytotoxin-associated gene (*cagA*) and toxigenic vacuolating cytotoxin (*vacA*). Studies have shown that *H. pylori* has an effect on mitochondria, and it has also been studied that CagA and VacA virulence factors affect mitochondria through different mechanisms (60–62). Because of the high correlation between these virulence factors the effect of OipA on mitochondria and cellular apoptosis is also investigated. There is a study resulted as, the attachment of OipA to the gastric epithelial cells also triggers a process of apoptosis in the host cells. This is mainly achieved through the Bcl-2 family pathway and higher levels of Bax and cleaved-caspase 3 within the cells (63).

The studies show that *H. pylori*-induced gastric diseases are significantly reduced by a glutamate supplement and an oral glutamate precursor (64,65). Since OipA promotes inflammatory cytokines secretion and heightens gastric inflammation, the effect of oipA on the miRNA/glutamate pathway in *H. pylori*-induced mucosal injury was investigated (66). The recombinant OipA protein increased miR-30b levels, accompanied by a reduction in cystine–glutamate transporter (xCT) activity which regulates extracellular levels of glutamate (67). In conclusion, decreasing glutamate levels brought on by a decrease in xCT activity have a significant impact on the damage that *H. pylori* causes to the stomach mucosa. Additionally, by controlling miRNA-30b, OipA decreased the protective effects of the xCT/glutamate pathway on the stomach mucosa (66).

Although numerous investigations have been conducted to explore the impact of the OipA protein on the pathogenesis of *H. pylori* and the mechanism of infection-related diseases, the association of OipA with host proteins and protein pathways necessitates further investigation. Studies on *H. pylori* infection have been performed

in cell cultures and animal models. Various animal species are used in research related to infections, including mice, gerbils, pigs, cats, and dogs; however, they have limitations due to genetic variances. Both primer and secondary cell cultures are used in *H. pylori* research. Commonly used secondary human cancer lines AGS and KATO lines carry oncogenic mutations that limit their ability to accurately represent healthy cells in research analyses. Although the gastric primary cell lines are purer than the secondary lines, they cannot be grown and maintained in culture for an extended period since they are unable to regenerate. To address this issue, recent advances in three-dimensional organoid models have emerged as a promising solution. Organoids are constructed from healthy tissue-derived cells, and they have the ability to mimic disease-causing cellular expressions more accurately in humans due to their long-term growth, cellular diversity, and organ-specific cellular organization (68). Consequently, organoids provide a better model to investigate the complex interplay between *H. pylori*, host proteins, and protein pathways.

2.3 Organoids

The human body contains stem cells, which are unspecialized, possess the capacity for self-renewal, and have the ability to develop into any type of organismal cell. Through cellular renewal, migration, differentiation, and apoptosis, stem cells are essential for preserving organ size, shape, and function (69). The fate of stem cells is regulated by their unique surroundings, which is commonly known as the stem cell niche (70). After the discovery of the Matrigel which is a basement membrane extracellular matrix (ECM) containing a unique mixture of ECM components and growth factors, was extracted from mouse sarcoma tumor (71), and used to mimic the stem cell niche in vitro studies (72). Sato et al. achieved a significant milestone in 2009 by creating a three-dimensional culture technique that allowed the growth of mouse intestinal epithelial organoids from a single Lgr5+ crypt base columnar stem cell, which maintained lineage development and self-renewal with rapid cycling (73,74). Further research results show organoids can be grown and specialized in a laboratory environment, closely resembling the structure and function of actual tissue (75,76).

Organoids provide simplified and replicable models that simulate the intricate dynamics of human tissue development, homeostasis, and disease. These models can be utilized by multiple laboratories and are straightforward to manipulate, image, and analyze biochemically, without the complexities associated with in vivo studies. If developed from human cells, organoids enable the transition from animal models to human biology with acceptable ethical considerations. The organoid models have been developed for a wide range of tissues, including intestine (73), stomach (77), liver (78), brain (79), kidney (80), and pancreas (81).

Organoid models have several advantages over traditional in vitro and in vivo models. They are more physiologically relevant than 2D cell culture systems, as they allow cells to interact with each other and the ECM in a 3D environment. They are also more accessible and less expensive than animal models, and they can be easily manipulated and analyzed using a variety of techniques, including microscopy, gene expression analysis, and drug screening.

Organoid models are a powerful tool for studying human tissue development, function, and disease. They offer a more physiologically relevant and accessible alternative to traditional in vitro and in vivo models, and they have the potential to accelerate the development of new therapies and personalized medicine.

2.3.1 Construction of the organoid models

The basic principle behind the construction of organoid models is to recreate the in vivo environment by providing the stem cells with the necessary signals and cues that enable them to self-organize and differentiate into specialized cell types, forming a functional organ-like structure.

Organoid culture assembly is starting with the isolation of stem cells from the target tissue. Stem cells can be obtained from fetal tissue, adult tissue, or induced pluripotent stem cells (iPSCs) derived from reprogrammed somatic cells. The starting cell source is highly important for obtaining the structure and function of the

target model and affects the variability and heterogeneity of the model (82). Organoids can develop from either early multicellular structures like intestinal crypts (83,84), cell aggregates (85), micropatterned cells (86), or from spherical colonies produced by single cells (73,78). Using multicellular structure seeks to create a cellular niche from the start that includes other cells of the same or different type.

After the stem cell isolation, cells are cultured in a specialized 3D matrix that provides the necessary signals and cues for their self-organization and differentiation. Extracellular matrix (ECM) mainly provides structural support to cells in vivo. Different types of ECM can be used, depending on the target tissue. One of widely used matrix is Matrigel which is mainly composed of laminin, collagen IV, entactin, perlecan and growth factors, and is similar in composition to the basement membrane (87).

In addition to ECM, other components of the culture medium, such as growth factors, cytokines, and small molecules, are added to promote stem cell survival, self-renewal, and differentiation. Although many small-molecule drugs can affect several pathways, leading to poor repeatability (88), and growth factors may be expensive and unstable, some organoid regimens have merged the use of both biologics and small-molecule drugs (89). It is possible to substitute frequently used growth factors, such as WNT3A ligands (90), with conditioned media produced by engineered cell lines that produce biologically active growth factors, such as L-Wnt-3A. Similar batch-to-batch fluctuation affects these conditioned media, and rigorous studies are needed to ensure repeatability (91). Since in vivo soluble markers are often coordinated in time and location to cells via the ECM or neighboring cells, it is important to consider how and when they are added to organoid cultures.

The growth processes of organoids involve aggregation, proliferation, migration, and differentiation of the initial cells. To assess the success of organoid formation, it is essential to evaluate the presence of desired cell types and the degree to which the organoids replicate the functions of corresponding tissues in vivo (92). The formation of the desired organoid pattern is evaluated using both gene expression

verification and whole-genome transcriptome analyses (78,93). Various techniques can be performed to characterize the organoid models, including real-time polymerase chain reaction for gene expression analysis, western blot analysis for protein profiling and signaling pathway analysis, antibodies for staining specific cell markers, and immunofluorescence techniques for imaging (94). These methods are crucial for assessing the quality of organoids and evaluating their potential use in various applications, including drug screening and disease modeling. Given optimal conditions, it is possible to sustain organoids in culture for extended periods, lasting several months. This provides a valuable opportunity to conduct long-term investigations into tissue development, function, and disease (82).

2.3.2 Applications of organoid technology

2.3.2.1 Therapeutics and drug development

There are numerous 2D cell lines that have multiple culture-induced mutations or contamination from other cell lines, which limits their usefulness as precise models for disease modeling or drug screening applications (95,96). The use of patient-derived organoids, which are more stable and physiologically relevant, has increased interest in developing high-throughput screening methods for early drug discovery programs and toxicity screens (97,98). In a recent study, within a week of surgery, personalized medication sensitivity profiles were obtained by screening 240 tyrosine kinase inhibitors on organoids generated from individuals with ovarian or peritoneal tumors. The study also included sporadic ovarian cancer, for which no established line therapy was available (99). Tumor organoids can be used for screening to identify successful treatments from candidates with similar structural properties (100), and to look into the synergistic effects of several medications for combination therapy (101). To verify the tumor-specific efficacy of the tested drugs, non-tumor cells from nearby normal tissue in biopsy samples or surgically removed samples can be used to create healthy organoids as control (102). Libraries of immune cells that have been modified to express chimeric antigen receptors against various neo-antigens can be used to screen organoids (103). In tumor organoid

models that contain immune cells, checkpoint inhibitors, and other immuno-oncology medications can also be tested (104). The viability, size, and form of organoid cultures are frequently intrinsically diverse, which makes it difficult to analyze the toxicity and effectiveness of medications. To get over this restriction, live imaging techniques that enable an in-the-moment analysis of the organoid response and thorough characterization of the heterogeneity within the culture would be developed.

2.3.2.2 Regenerative medicine

Organoids have shown great potential for use in regenerative medicine, including tissue engineering and cell transplantation. Organ function was restored after the successful transplantation of organoids from mouse intestines (105), livers (102),(106),(107), and pancreas (108,109) into mice. Studies have shown, the transplantation of pancreatic islets that were grown in an artificial extracellular matrix (ECM) proved to be effective in reversing hyperglycemia and restoring insulin production in mouse models of diabetes induced by either streptozocin or autoimmune factors (110). Apart from organoids created from mice, liver organoids that were derived from EpCAM+ ductal cells taken from human liver samples have been successfully transplanted into immunodeficient mice with induced acute liver damage (111). Despite the fact that there is still a significant amount of work required before organoids can be effectively utilized in regenerative medicine, progress has been made in developing protocols that can generate normal tissue organoids, implementing good manufacturing practices to ensure high levels of reproducibility, as well as establishing the grafting and functional capacities of organoids (112). To generate xenografts with high engraftment rates, intact organoids (113,114) or individual cells obtained after digestion (115,116) are frequently used. Patient-derived organoids have also proven to be useful in generating xenografts, confirming their tumorigenic capacity, and reproducing the histology of parental tumors. In a study examining colorectal cancer, benign tumor organoids exhibited little to no engraftment in mice, while colorectal cancer organoids derived from metastases were more invasive than those obtained from

primary tumors (113). Glioblastoma multiforme cells were cultivated as either tumor spheres or organoids, and the morphology of these xenografts was compared. It was found that while the cells from tumor spheres showed a solid growth pattern, the cells from organoids were more diffusive, similar to the originating tumor (116).

2.3.2.3 Precision medicine applications

Precision medicine is a medical strategy that considers individual differences in genetics, environmental factors, and lifestyle to personalize healthcare decisions and treatments for each patient. The goal of this approach is to achieve improved health outcomes by enabling more precise diagnoses and more effective treatments for patients (117). One of the technologies developed to achieve this goal is patient-derived organoids (PDOs), which are models of organs that are generated using tissue from individual patients. These models accurately mimic various aspects of the patient's physiology and disease characteristics, such as genetic traits and responsiveness to drugs. Thus, PDO platforms offer an unprecedented opportunity for enhancing preclinical drug discovery, validating clinical trials, and ultimately, improving patient care (118). In a study, as a treatment for a patient with recurrent triple-negative breast cancer, eribulin was used in organoids made from patient-derived xenografts. The patient showed a 3.5-fold increase in progression-free survival time on the eribulin regimen compared to the previous treatment received, highlighting the potential of organoids in clinical care. These findings imply that functional drug testing using PDOs is practical and that it can provide useful information in real time for clinical care (119).

The use of PDOs in cancer research has resulted in the creation of extensive biobanks containing breast (120), pancreas (121), brain (122), gastric (123), liver (124), and some other cancer types. These biorepositories preserve the histopathological and genetic features of the original tissue and can be cultivated for research purposes, rendering them valuable tools for investigating the effectiveness of treatments across various cancer subtypes and patient populations (118).

2.3.2.4 Diseases modelling

Organoids have shown to be quite useful for modeling and researching both common and unusual diseases originating from several different organs (82). An example of this is the genetic disorder Cystic Fibrosis, for which organoids of various organs such as the colon (117), liver and bile ducts (125), rectum (126), respiratory system (127), and small intestine (128) have been developed using adult stem cells from either mouse models or patients. These models have a variety of uses, from examining the biology of the disease to simulating patients' drug responses (126). Another one is liver organoids which were created to represent liver disorders like primary sclerosing cholangitis, α1-antitrypsin deficiency, and Alagille syndrome (129,130).

Over the years, many types of organoids have been constructed as models of many diseases; some of them are microcephaly, Alzheimer's, glaucoma, hepatitis B, diabetes mellitus, congenital and early-onset hearing loss, systemic sclerosis, Barth syndrome, influenza, coronavirus, and some host-pathogen interaction models like gastric organoids for *H. pylori* infection (131).

2.3.2.5 Host-pathogen interaction studies

The use of organoid models in research on the interactions between hosts and pathogens is becoming more prevalent. Organoids generated from various tissues and organs, such as the gut (132), liver (133), lung (134), oral mucosa (135), and stomach (136), have been co-cultured with pathogens like bacteria, viruses, and parasites (137). Gastric organoids are commonly used to study the interaction between the gastric epithelium and *H. pylori* bacteria. This approach enables the investigation of the natural host-pathogen interaction occurring at the apical side of the stomach epithelium.

2.3.3 Gastric organoids as an infection model

The stomach is a crucial organ for both storing and digesting food with enzymes and digestive acids. The cardia, fundus, corpus (body), and antrum (pylorus) make up the four major components of the stomach. While the corpus secretes digestive enzymes and acid, the antrum releases hormones and mucus into the stomach (123). The human stomach is lined with a columnar epithelium that forms multiple regular invaginations called gastric pits. These pits lead to gastric units, which are further divided into the isthmus, neck, and base regions. The glands are the collective term used to describe the neck and base regions (138). Massive cell multiplication occurs in the isthmus, from which the cells go either toward the pit or the gland. Pit cells have a limited lifespan of about 3 days and have thick apical mucus (139). Cells migrating to the bottom of the gland differentiate into chief cells, which can live up to six months, or mucus neck cells, which secrete pepsinogen (140). The parietal cells are secreting acids, migrates bidirectionally and presents in all parts of the gastric glands more found in neck region (141). Enteroendocrine cells are rarely found in the gastric epithelium, where they scatter around gastric glands and release regulating hormones such as serotonin, somatostatin, ghrelin, and gastrin (138).

The epithelium of the stomach undergoes constant renewal, with certain parts turning over every three days. It has a remarkable regenerative capacity fueled by stem cells, which were believed to be present within the tissue itself (137). Early studies have identified undifferentiated cells in the isthmus region of the gastric glands (142). Advances in genetic lineage tracing which provides information about the number of progeny of the founder cell, their location, and their differentiation status, have allowed scientists to map the fate of the progeny from specific cells (143). By marking cells expressing the leucine-rich-repeat-containing G-protein-coupled receptor 5 (LGR-5) gene, it was discovered that LGR-5 identifies peculiar, slender cells located between the paneth cells in the intestine and cells at the base of the gastric glands. Lineage tracing using Lgr5-Egfp-IRES-CreERT2 mice showed that Lgr5-expressing cells and their offspring can generate all cell lineages of both the intestine and the stomach. Additionally, cells expressing villin (144), sex-

determining region Y (SRY)-box 2 (145), gastrin receptor cholecystokinin B receptor (146), and transcription factor basic helix-loop-helix family member a15 (147) have stem cell capacity in the stomach.

The discovery of Lgr5+ stem cells and their niche factors provided the basis for their maintenance in organoid culture. The first successful murine intestinal Lgr5+ stem cell culture was established in 2009 by seeding single sorted cells into an extracellular matrix, followed by embedding in a medium containing the essential niche factors R-spondin1 (RSPO), EGF and noggin (NOG) to promote stem cell proliferation and expansion (73). Subsequently, a gastric organoid culture was also established using adult stem cells (ASCs) (77) and pluripotent stem cells (PSCs) such as induced PSCs (iPSCs) and embryonic stem cells (ESCs) (148). The presence of mesenchymal cells is the primary distinction between organoids produced from ASC and PSC. Both types of organoids start with a mixture of mesenchymal and epithelial cells, but subsequent splitting and re-seeding make ASC-derived organoids exclusively epithelial, allowing for the study of mesenchymal-epithelial interactions during initial observation and the long-term study of pure epithelium. Some other differences are in the maintenance and lifespan of the cultures. While ASC-derived gastric organoid cultures mature within 1-2 weeks and can expand for an unlimited time, PSC-derived organoids require differentiation from PSCs to the adult epithelium, which typically takes about 30–60 days and has a limited lifespan (138).

One of the essential features that make gastric organoids, as well as other organoids, so desirable for the laboratory, is that they are long-lived, which means they can be divided and re-seeded, frozen and thawed, and appear to have an infinite capacity for expansion. Additionally, a variety of common laboratory procedures can be used on them, including microscopy, RNA analysis, protein analysis, genetic modification using lentiviruses, bacterial artificial chromosomes (BACs), or genome editing utilizing the CRISPR/Cas9 system (149–152). Over the past ten years, scientists have used gastric organoids to better understand the biology of the stomach, identify cell plasticity, gain important knowledge about the

development and treatment of gastric cancer, and examine interactions between the gastric epithelium and pathogens like *H. pylori* (153).

Due to their resemblance to the human stomach in vivo, their simplicity of use, and their ability to be cultured for an extended period of time, human gastric organoids (hGOs) have many benefits over conventional in vivo and in vitro models (154). In the earlier studies, *H. pylori* infection was performed by microinjection into the spheroid lumen because the interior formed the luminal edge of the epithelial cells (149). However, subsequent work that used Matrigel to create the initial antral and corpus spheroids was further developed, enabling spheroids to be successfully cultivated in 2D monolayers on collagen-coated surfaces which is not required microinjection but has a limited lifespan (68). A further study detailed the use of an air-liquid interface (ALI) system to produce mucosoid cultures from antral glands. The collagen-coated trans-well technique used for this, allowed for the co-incubation of bacteria to the luminal side of the culture for infection and discovery of the soluble factors in experiment with a life of up to one month (155). This system is also suitable for experiments that contain co-culturing of *H. pylori* for several days.

Gastric organoids have provided new insights into various aspects of *H. pylori* infection that were previously difficult to investigate using other models. These include chemotaxis (156), intracellular effects of *H. pylori* virulence factors (157–159), interactions with the apical-junctional complex (160), activation of the innate immune system (161), and the initiation of inflammation by *H. pylori* (162). Moreover, the effects of *H. pylori* on gland stem cells and the induction of DNA damage have enhanced our knowledge of the mechanisms underlying cancer initiation, leading to the identification of potential targets for therapeutic intervention (163–165).

3 MATERIALS AND METHODS

3.1 Materials

3.1.1 *H. pylori* strain

Helicobacter pylori G27 strain used in the *oipA* gene deletion and infection experiments which was kindly gifted by Prof. Dr. Anne Müller, University of Zurich Institute of Molecular Cancer Research.

3.1.2 *H. pylori* culture

The agar plates used for *H. pylori* cultivation was Colombia Blood agar (OXOID) supplemented with 0,1% 1000X antibiotic cocktail which includes 5 mg/mL Trimethoprim (ChemCruz) and 8 mg/mL Amphotericin B (Bristol-Myers Squibb and 0,5% 200X antibiotic cocktail which contains 2 mg/mL Vancomycin (Koçak Pharma), 1 mg/mL Cefsulodin (Koçak Pharma) and 30,3 mg/mL Polymyxins B Sulfate (ChemCruz), 2 g/L β-cyclodextrin (SIGMA Life Science) and 5% of defibrinated horse blood. 20 μg/mL Kanamycin (GeneMark) antibody was added to plates depending on needs of experimental design.

Ingredients of *H. pylori* liquid culture were Brucella Broth (Remel) supplemented with 10% fetal bovine serum (FBS, GIBCO®), 2 mg/mL Vancomycin. 20 μg/mL Kanamycin antibody was added to plates depending on needs of experimental design.

The contents of the freezing medium of *H. pylori* G27 strain is a mixture of 50% of Brucella Broth and 50 % of Glycerol (SIGMA Life Science).

3.1.3 Cell lines

Cultrex HA-R-Spondin 1-Fc 293T cells were purchased from R&D Systems for use in condition medium production. The cells are stably transfected to express R-Spondin-1, which contains an N-terminal HA epitope tag and is fused to a C-terminal murine IgG2a Fc fragment.

L Wnt-3A, a cell line presently the best source for the production of Wnt-3A conditioned medium, was purchased from ATCC (American Type Culture Collection) for use in this study.

A human epithelial cell line, human embryonic kidney 293 (HEK-293T) cells were kindly provided by Assoc. Prof. Zeynep Tokcaer Keskin, Acibadem Mehmet Ali Aydinlar University, Istanbul, Turkey.

3.1.4 Gastric glands

Gastric glands were obtained from bariatric surgery patients who had no prior history of *H. pylori* infection and had negative *H. pylori* test results. Samples were collected from eligible patients who had given their informed consent at the Bariatric Surgery Department of Maslak Acıbadem Hospital. Tissue samples measuring approximately 3 cm^2 were taken from the corpus of the stomach and placed in a solution of Advanced DMEM/F12 (Thermo Scientific) containing 100 µg/mL of Primocin (Invivogen) antibiotic. The samples were then transported to the laboratory on ice.

The gastric glands were isolated in a chelating buffer. The chelating buffer ingredients used during gastric glands isolation are shown in Table 1.

Table 1. Chelating buffer ingredients

Chemicals	Final Concentrations	Supplier Company
Na_2HPO_4	5.6 mM	Merck
KH_2PO_4	8.0 mM	Merck
NaCl	96.2 mM	Sigma
KCl	1.6 mM	Sigma
Sucrose	43.4 mM	Sigma
D-sorbitol	54.9 mM	Sigma
DL-dithiothreitol	0.5 mM	Sigma
EDTA	10 mM	Sigma

3.1.5 Cell culture

2D cell lines were maintained in a complete Dulbecco's Modified Eagle Medium (DMEM) media and similar growth conditions. The solutions used in 2D and 3D cell cultures throughout the study are given in Table 2.

Freezing of 2D cell lines was performed with a freezing media which is a composition of 50% of growth medium, 40 % of FBS and 10% of DMSO.

Table 2. The Solution used in cell culture experiments

Chemicals/Medium	Supplier Company
Advanced DMEM/F-12	Gibco
GlutaMAX™ Supplement	Gibco
Sodium Pyruvate (100 mM)	Gibco
HEPES (1 M)	Gibco
DMEM, high glucose	Gibco
Roswell Park Memorial Institute (RPMI) Medium	Gibco
Fetal Bovine Serum (FBS)	Gibco
Penicillin/Streptomycin	Gibco
Primocin	Invivogen
Zeocin	Invivogen
Geneticin™	Thermo Scientific
Matrigel growth factor reduced, phenol red free	BD Biosciences
EGF Recombinant Mouse Protein	Thermo Scientific
FGF-Basic Recombinant Human Protein	Thermo Scientific
B-27™ Supplement	Thermo Scientific
N-Acetyl-L-cysteine	Sigma
A 83-01	Sigma
[Leu15]-Gastrin I human	Sigma
Y-27632 dihydrochloride	Sigma
Recombinant Human Noggin	Peprotech
Recovery™ Cell Culture Freezing Medium	Thermo Scientific
Trypan Blue	Sigma
DMSO (Dimethyl sulfoxide)	Sigma
Pei-max	Sigma
0.25%Trypsin-EDTA (1X)	Gibco
Dispase	StemCell Technologies

Table 2 (cont'd). The Solution used in cell culture experiments

TrypLE™ Express Enzyme	**Thermo Scientific**
collagen type 1	Corning
HumanKine® recombinant human Wnt3A protein	Proteintech

3.1.6 Primers

Primers sequences were designed by using National Center for Biotechnology Information (NCBI) primer blast for the indicated DNA sequences. Sequences of primers used in experiments and expected product lengths are given in Tables 3-5.

Table 3. Primers used in the *oipA* gene deletion of the *H. pylori* G27 strain

Primers	**Primer Sequence 5'->3'**	**Product length**
P1	CATTAAGCGGTGGTTTTGTG	172 bp
P2	TGACCAAAATCCCTTAACGTGAGCTTTTTTCATGGTT	
P3	TGCCACCTGAAATTGTAAACGTGCAAGTAACAATCTCA	325 bp
P4	AGCCAACTAAAGAGCGGTAA	
K1	CGTTTACAATTTCAGGTGGCA	990 bp
K2	TCACGTTAAGGGATTTTGGTCA	
S2/P1	CCTCTTCCGACCATCAAGCA	947 bp
S1/P4	AACAGGCCAGCCATTACGCT	899 bp
q-Kan-F	GATAATGTCGGGCAATCAGG	138 bp
q-Kan-R	CGTCAGCCAGTTTAGTCTGA	
q-UreA-F	CGTGGCAAGCATGATCCAT	77 bp
q-UreA-R	GGGTATGCACGGTTACGAGTTT	

Table 4. Primer sequences used for gene level characterization of gastric organoids

Primers	**Forward primer 5'->3'**	**Reverse primer 5'->3'**	**length**
LGR5	CCGCTTCCTGGAGGAGTTAC	GCATCCAGACGCAGGGATTG	174 bp
MUC5AC	GACACACTGGAGAACCTCCG	GGTAGTTGTAGCAGAGCCCC	187 bp
PGC	GAAGAGTTCCTCATCGGCGG	CAGTAGCCGTTGTTACTGAGG	226 bp
TFF1	GTCCCTCCAGAAGAGGAGTG	AGCCGAGCTCTGGGACTAAT	105 bp
MUC6	GTGGCTGTGGTCTACCTCTC	CCGTGATGTTGCGAGTCTTG	112 bp
SST	CACTCTCCAGCTCGGCTTTC	AGTACTTGGCCAGTTCCTGC	185 bp
EPCAM	AGCGAGTGAGAACCTACTGGA	ACGCGTTGTGATCTCCTTCTG	110 bp
MUC2	CGGACCTGTGCCCCATATTC	AGATGTTGGAGTGGATGCCG	126 bp

Table 5. Primer sequences used in infection optimization experiment

Primers	**Forward primer 5'->3'**	**Reverse primer 5'->3'**	**length**
GAPDH	CTCATGACCACAGTCCATGC	TTCAGCTCTGGGATGACCTT	155 bp
IL-8	GACATACTCCAAACCTTTCCACC	AACTTCTCCACAACCCTCTGC	162 bp

3.1.7 Commercial kits

Commercial kits used in the study are listed in Table 6.

Table 6. Commercial kits used

Kits	Supplier Company
Tissue & Cell Genomic DNA Purification Kit	GeneMark
Plasmid MiniPrep Purification Kit	GeneMark
Hot Start Master Mix (5X)	GeneMark
Quick-DNA/RNA Microprep Plus Kit	Zymo Research
Clean & Concentrator-100 Kiti	Zymo Research
ZymocleanTM Gel DNA Recovery Kit	Zymo Research
Phusion™ High-Fidelity PCR Master Mix	Thermo Scientific
Gram Staining Kit	Novolab
High-Capacity cDNA Reverse Transcription Kit	Thermo Scientific
Dual-Luciferase® Reporter Assay System	Promega
Tissue & Cell Genomic DNA Purification Kit	GeneMark
Plasmid MiniPrep Purification Kit	GeneMark
Pierce BCA Protein Assay	Thermo Scientific

3.1.8 General chemicals

General chemicals and their supplier companies were indicated in Table 7.

Table 7. General chemicals that used in the studies

Chemicals	Supplier Company
Hydrocloric Acid Fuming 37%	Merck
Sodium Hydroxide	Merck
Ethanol 100%	Merck
Methanol 100%	Merck
2-Propanol Merck	Merck
Agarose	NORGEN
50X TAE Buffer	GeneMark
Agar	Sigma
Xylene	Sigma
target retrieval solution	Dako

3.1.9 Equipments

General labware equipments, machines and their accessories are shown in Table 8 with their supplier companies.

Table 8. General equipments used in the studies

Equipments	Supplier Company
Biosafety Class II Cabinet	Thermo Scientific
Thermo Cycler, PCR	BIO-RAD, T100
NanoDrop	Thermo Scientific
LightCycler® 96	Roche
Microplate Spectrophotometer	BioTek, PowerWave XS2
Light microscope	Leica DM500
Water purification system	Merck Millipore, Milli-Q® Advantage A10
Fluorescence microscope	ZEISS, AXIO
Imaging System	BIO-RAD, ChemiDocTM MP
pH meter	Thermo Scientific, ORION STAR A211
Electrophoresis system	MS Measure Science, BIO-RAD, Mini Protean
Power supply	BIO-RAD, PowerTM Pac Basic
Microcentrifuges	Thermo Scientific, MICROCL 21R
Centrifuges	Beckman CoulterTM Allegra 64R, Thermo Scientific, SL16R
Vortex	bioSan Combi-Spin FVL-2400N
Incubator	Thermo Scientific, HERATHERM
Shaker	Witeg
Magnetic shaker with heat	Thermo Scientific, CIMAREC
Autoclave	Witeg,Nüve steamArt
Dry heat sterilizator	Nüve FN120
Pipettes	Eppendorf
Syringe Filters 0.45µm-0.22 µm	Sartorius
Water Bath	EMCO, ESM-3710
Dry Block Heating Thermostat	BIOSAN, Bio TDB-100
Microwave	SAMSUNG T.D.S
Weighing Machine	UNIBLOC, SHIMADZU UW620H
Fridges	Arctiko/ Kirsch
Confocal microscopy	Zeiss LSM 700

3.1.10 Bioinformatics tools

GraphPad Prism 6, Inkscape, Proteome Discoverer 2.5, Geneious Prime, and Cytoscape and Excel softwares were used in the thesis. Bioinformatics tools and web servers used in the identification of properties of proteins are given in Table 9.

Table 9. Bioinformatics tools and web servers used in the proteomics data analysis

Tools	
Panther	http://www.pantherdb.org
SRplot	http://www.bioinformatics.com.cn/srplot
Reactome	https://reactome.org/
KEGG	https://www.genome.jp/kegg/
String	https://string-db.org/

3.2 Methods

3.2.1 Construction of *H. pylori* ΔoipA-G27 strain

3.2.1.1 Cultivation of *H. pylori*

H. pylori was grown in Colombia Blood agar (CBA) media including 0,1% 1000X antibiotic cocktail, 0,5% 200X antibiotic cocktail, 2 g/L β-cyclodextrin and 5% of horse blood. Kanamycin antibody (20 μg/mL) was added during the petri preparation to selection of gene deleted colonies. In order to prepare plates, the Columbia agar was dissolved in water according to the proportions specified in the preparation instructions, then autoclaved and equilibrated in a water bath at 50° C for 1h. 200X and 1000X antibiotic mixtures and freshly prepared β-cyclodextrin were added to prevent the contamination. After adding the horse blood to the medium, the medium poured into petri dishes. The culture was grown under microaerophilic conditions by using Anaerobic Jars (Don Whitley Scientific) at 37°C for 3-4 days.

The liquid bacteria culture was grown in Brucella Broth including 1X vancomycin and 10% FBS to induce survival. Kanamycin antibody (20 μg/mL) was an addition to the liquid medium of gene deleted strain (ΔoipA-G27). The liquid culture of *H. pylori* was grown under microaerophilic conditions by using Anaerobic Jars (Don Whitley Scientific) at 37°C with shaking at 200 rpm for overnight.

The bacterial shape and purity were checked by gram staining (Nova Lab, Belgium) in every passage by following the kit's instructions. The growth and motility were observed under a light microscope.

The bacterial stock was prepared after liquid cultivation of *H. pylori* at overnight. The 10 mL of culture was centrifuged at 3000 rpm for 10 min. The pellet was resuspended with 1 mL freezing medium in cryopreservation vial and stored at -80°C.

3.2.1.2 *oipA* gene deletion by homologous recombination system

3.2.1.2.1 Synthesis of DNA cassette with SOE-PCR

The homologous recombination method was used for the *oipA* gene deletion. The DNA cassette required for this method, which is performed by replacing the naturally occurring allele in the genome with the allele containing the mutation, was prepared with the 'splicing by overlap extension PCR (SOE PCR)' technique. For this polymerase chain reaction, which is used to assemble different DNA fragments, primers are specific to the region desired to be deleted and they were designed by using the National Center for Biotechnology Information (NCBI) database.

The DNA cassette to be replaced by the *oipA* gene was designed as three different parts; a selective antibiotic site Kanamycin gene K1-2, start part of *oipA* gene P1-2 fragment and P3-4 DNA fragment from the end part of the *oipA* gene as shown in Figure 3.

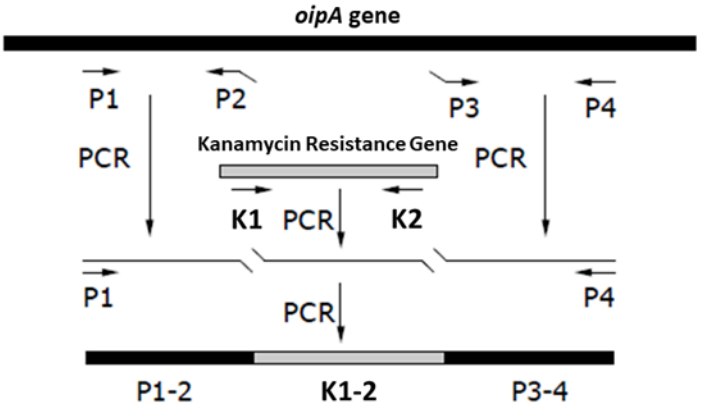

Figure 3. Design of DNA cassette carrying kanamycin resistance gene to be inserted into target gene region for deletion of *oipA* gene by homologous recombination method.

Plasmid pET His6-GST-TEV-LIC used as a kanamycin gene template and amplified by using K1 and K2 primers in PCR reaction. The P1-2 and P3-4 DNA fragments are amplified by *H. pylori* G27 gDNA, which was isolated from 30 ml liquid culture by using the gram-negative bacteria-specific protocol proposed by the

Bacteria Genomic DNA Purification Kit (GenemarkBio, Taiwan). The primers' annealing temperature was optimized by performing a gradient PCR Phusion™ High-Fidelity PCR Master Mix (Thermo Scientific) PCR kit, which was used in cloning and gene mutation experiments with high accuracy, was used in all PCR reactions for gene silencing experiments. The reaction mixture was 1µl of gDNA and 1 pmol from each primer pairs in a total of 10 µl reaction mixture. Gradient PCR thermal cycler conditions are specified as 30 sec at 98°C for initial denaturation; followed by 35 cycles of 10 sec at 98°C for denaturation, 10 sec at 55˚C to 68 ˚C gradient for annealing, 30 sec at 72 ˚C for extension; 5 min at 72˚C for final extension. The PCR products were loaded onto 1,5% agarose gel by using 6X loading dye and 10X Sybr Gold dye. Samples were run at 100V for 50 minutes. Bands were visualized under UV with ChemiDoc (ThermoScientific). The optimized reaction conditions were selected based on those results and the DNA fragments K1-2, P1-2 and P3-4 were amplified by setting annealing temperatures at 55˚C, 66˚C and 63˚C respectively and the reaction volume was increased to 50 µl. Then the PCR products were purified by using a Clean & Concentrator- Kit (Zymo Research, Orange, CA) according to the manufacturer's instructions. The amount of the purified DNA samples was quantified by NanoDrop™.

SOE PCR is a two-step PCR method. The first stage involves the annealing of regions that are complementary via the temperature change. The second step is to integrate the fused DNA fragments with polymerase activity in the presence of external primers (P1 and P4). K1-2, P1-2 and P3-4 DNA fragments whose concentrations were measured for the first step, were mixed in PCR solution to a final concentration of 0.5 pmol (in 25 µl total volume) and placed in the PCR device for annealing. The first step reaction conditions; 30 sec at 98°C for initial denaturation; followed by 10 cycles of 10 sec at 98°C for denaturation, 30 sec at 55˚C for annealing, 20 sec at 72 ˚C for extension. At the end of the final cycle of the SOE PCR's first reaction, the temperature of the samples was waited to drop to the binding temperature of the outer primers, when the temperature decreased to 59˚C the outer primers P1 and P2 were added to reaction tubes at 0.5 pmol final concentration and the new reaction was started. The second step reaction conditions;

30 sec at 98°C for initial denaturation; followed by 30 cycles of 10 sec at 98°C for denaturation, 15 sec at 59˚C for annealing, and 22 sec at 72 ˚C for extension. After the SOE PCR reactions were completed, obtained PCR products were controlled by an agarose gel electrophoresis. The samples were loaded in a 1.5% agarose gel with Sybr gold dye and electrophoresis at 100V for 50 min. *H. pylori* G27 DNA was used as positive control while the water was used as a negative control for all PCR experiments.

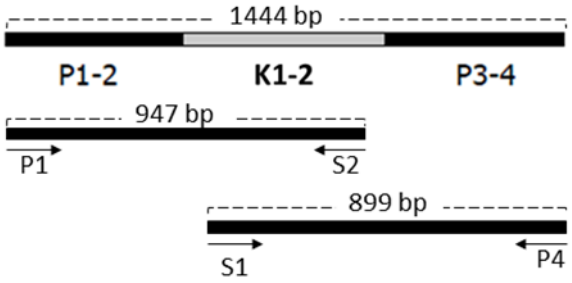

Figure 4. Schematic representation of the working mechanism of sequencing primers S1 and S2 with the P1 and P4 primers.

Since the reaction mixture of the SOE PCR contains lots of ingredients, the target band of the PCR product is cut and purified from the agarose gel after being visualized under UV. The purified DNA sample was subjected to one more PCR reaction which is a repeat of the second reaction step of SOE-PCR to elicit more and purer sample. The final PCR product was purified and quantified by NanoDrop™.

The constructed DNA fragment's sequence was analyzed before natural transfection. Primers S1 and S2 were designed to work together with primers P1 and P2 to form two overlapping fragments to cover the constructed DNA fragment as schematized in Figure 4. The amplified PCR products were sequenced in Eurofins Genomics laboratories in Germany, and the data was blasted to designed DNA sequence (1444 bp). Sanger sequenced data was analyzed by using BioEdit sequence alignment editor program and the aligned fragments were blasted with designed DNA fragment sequenced as query at NCBI page.

3.2.1.2.2 Natural transformation

The DNA fragment constructed by SOE PCR was transfected into *H. pylori* G27 strain by natural transfection method which was performed on an agar surface. *H. pylori* G27 bacteria that grew on an agar plate for 36 hours were collected in 200 µl of Brucella Broth (BB). 100 µl of bacteria solution was plated at high density on the agar plate, as areas of 8-1O mm in diameter and incubated for 5 h. After incubation, approximately 2 µg of SOE PCR-created DNA cassette solution was spread over the incubated culture and the culture was left to incubate for another 12 hours. The DNA-treated cells were scraped up with a loop in a small volume of BB and were then spread on 20µg/mL Kanamycin included CBA plate to select transformants. After one week of incubation, colonies were seen on the selective agar plate. Seen colonies were inoculated as single colonies separately on the medium for growth and prepared for transfection confirmation studies.

3.2.1.3 Confirmation studies for *oipA* gene deletion

3.2.1.3.1 PCR-based transfection check

Conventional PCR was the first step of the confirmation studies of the *oipA* gene replacement by kanamycin gene on the *H. pylori* G27 genome. DNA isolations were made from the grown transfected cultures by using Bacteria Genomic DNA Purification Kit (GenemarkBio, Taiwan). SOE PCR's start-end primers, P1 and P4 were used for the confirmation of transfection because of the expectation of DNA size difference between the transfected (1444 bp) and wild type's target region of bacteria's genome (1093 bp). The PCR reaction conditions are specified as 30 sec at 98°C for initial denaturation; followed by 30 cycles of 10 sec at 98°C for denaturation, 10 sec at 60˚C for annealing, 15 sec at 72 ˚C for extension; 15 sec at 72˚C for final extension. The confirmation PCR products were loaded onto 1.2% agarose gel by using 6X loading dye and Sybr Gold dye. Samples were run at 100V for 50 minutes. Bands were visualized with ChemiDoc (ThermoScientific).

3.2.1.3.2 Whole genome sequencing of ΔoipA colony

Homolog recombination experiments which were chosen for the deletion of the *oipA* gene may cause a multiple recombination of DNA cassette into the donor genome. The final confirmation study was done by whole genome sequencing (WGS) which would reveal all the sequences and the mutation on the genome. Since the WGS is a very expensive technique, the sample to be sent for analysis was selected by a real-time polymerase chain reaction (RT-PCR). For this purpose, two different single colony (ΔoipA1 and ΔoipA2) were grown in liquid medium, the gDNAs was isolated and equal amount of DNA (10 ng from each sample) were added to reaction mixture. To determine relative expression levels of kanamycin gene in mutated *H. pylori* strains, *ureA* (urease A) was used as an endogenous control gene. Sybr Green I (GMBiolab) was used to detect PCR products and experiment was conducted in CFX96 (BioRad) RT-PCR machine. PCR conditions were as following: initial denaturation at 95°C for 2 min, 40 cycles for denaturation at 95°C for 20 sec, annealing at 60°C for 45 sec and extension at 72°C for 45 sec. Cycle threshold (Ct) values obtained after run and results were analyzed with $2^{-\Delta Ct}$ method. Bar graphs and statistical analysis was performed in GraphPad program.

After the selection of mutated strain, 4000 ng of gDNA sample of ΔoipA2 mutated strain was send to the whole genome sequencing analysis. The next generation sequencing (NGS) performed by using Illumina - INVIEW Resequencing technology in Eurofins Genomics laboratories in Germany. The sequenced data were analyzed by using GENEIOUS PRIME sequence analysis tool.

3.2.1.4 Growth curve analysis of *H. pylori*

H. pylori G27 and ΔoipA-G27 strains were inoculated with an initial optical density at 600 nm (OD600) of 0.1 in liquid growth medium and incubated with 200 rpm rotation and 37°C for up to 7 days. The OD600 values were measured at various time points and line graph was drawn using GraphPad program.

3.2.2 Construction of human gastric organoid (hGOs) models

3.2.2.1 Preparation of hGOs culture condition mediums

3D organoid cell culture systems require special mediums and growth factors to maintain the stem cell niche and provide stem cell differentiation. The most important component in gastric organoid growth is functional WNT and R-spondin1. In this study homemade conditioned mediums that contains these proteins are prepared to use in 3D organoid cell culture experiments.

3.2.2.1.1 WNT condition medium

Many of the patterning and growth events throughout embryonic development are regulated by the secreted glycoprotein encoded by the WNT gene. The WNT-3A condition medium was made using the L-WNT-3A (ATCC 2647) cell line.

L-WNT-3A cell line, was grown at high glucose DMEM medium containing 1 mM sodium pyruvate, 10% FBS and 1% Penicillin-Streptomycin in a 37˚C incubator with 5% CO_2. The start culture of the condition medium production, cells were cultured in T25 flask in culture medium. Since these cells were created by transfection of the Wnt-3A expression vector, once they became 50 % confluent G418 antibiotic was added to the culture medium to choose stable cells. After the cells became 70–80% confluent, they were split into 4 T75 culture flasks in a culture medium without G418 antibiotics. When the cells in the culture flasks became confluent (after 3–4 d), they were trypsinized for 2-3 min, resuspended, and pooled together in a 17 mL growth medium that included 12% FBS and DMEM. The cell suspension was plated in 17 T75 culture flasks (1 mL/flask) before adding 9 mL of growth medium per flask. The prepared flasks were incubated for seven days, at the end of the incubation, the medium was harvested by centrifugation for 5 min at 400 g and filtering through a 0.22 μm filter. Harvested condition medium aliquoted and stored at -20˚C to use within six months.

3.2.2.1.2 R-Spondin condition medium

R-Spondins positively regulate Wnt/beta-catenin signaling, induces proliferation of intestinal crypt epithelial cells, increase intestinal epithelial healing, and support intestinal epithelial stem cell renewal. For the stomach organoid culture, the stem cells are required a differentiation medium that contains 10 % R-Spondin condition medium. The Culturex HA-R-Spondin1-Fc 293T cell line was used as a source of the R-Spondin condition medium.

The HA-R-Spondin1-Fc 293T cells were cultured at high glucose DMEM medium containing 1X GlutaMAX, 10% FBS and 1% Penicillin-Streptomycin in a 37˚C incubator with 5% CO_2. The production of the R-Spondin condition medium procedure is the same as the WNT condition medium. The only difference in the creation of the two mediums is the selective antibiotic used. Zeocin is the antibiotic selective for the R-Spondin cell line and the cells were grown in a zeocin-containing medium for at least five days at the start of production.

Every batch of homemade WNT and R-Spondin mediums needs to be tested by an activity test.

3.2.2.1.3 Activity testing of condition mediums

Functional WNT and R-Spondin are the most critical factor for organoid growth. Every batch of homemade WNT3A-CM and RSPO1-CM mediums needs to be tested for activity and efficiency of the medium.

The TOP/FOP test is used for quantification of the condition medium's activity. The test is based on using the TOP, FOP, and Renilla luciferase (RL) plasmids. The TOP plasmid is containing a luciferase reporter gene that is responsive to the WNT signaling pathway. When the WNT pathway is triggered, the TOP plasmid is activated, resulting in an elevation in luciferase activity. On the other hand, the FOP plasmid is designed with mutations that make it unresponsive to WNT signaling and

serves as a negative control. Renilla luciferase plasmid is used to standardize each sample for transfection efficiency.

The TOP/FOP assay was carried out using HEK-293T cells, which are cultured in DMEM medium containing 10% FBS and 1% penicillin-streptomycin in a 37˚C incubator with 5% CO_2. To ensure optimal transfection efficiency, the cells needed to undergo at least two passages before transfection. When the cells were ready for transfection, processing began with preparing the plasmid mixtures, which are; TOP with RL (90 ng TOP-10 ng RL) and FOP with RL (90 ng FOP-10 ng RL) in 7.5 µL of DMEM without FBS. In another tube, 0.75 µL the transfection reagent PEI-MAX (1 mg/mL) was mixed with 7.5 µL of FBS per well. Then, 4 µL of this solution was added to the TOP and FOP plasmid DNA mixes, respectively, and incubated for 20 min at room temperature. During incubation, the HEK-293T cells were trypsinized for 3–4 minutes. After centrifugation and resuspension of the cells in DMEM medium, which contains 10% FBS, cells were counted and prepared with 40,000 cells per well. When the plasmid and PEI-MAX mixture incubation was complete, the mixture was mixed with the cell suspension (11.5 µL plasmid mixture per well with 88.5 µL containing 40,000 cells), seeded in a 96-well plate, and incubated for 48 hours. Finally, after the 48-hour incubation, the well medium was changed into the media to be tested and incubated for 24 hours.

After transfection, the transfected cells were treated with the following mediums: DMEM only, 40% DMEM/50% WNT/10% R-Spondin, 65% DMEM / 25% WNT /10%R-Spondin and as a positive control, 200, 100, 50 ng/mL human recombinant L-WNT protein (Proteintech- HumanKine® recombinant human Wnt3A protein). After 24 hours of incubation, the luciferase activity was measured using the Dual-Luciferase® Reporter Assay System (E1910, Promega) kit by following the manufacturer's instructions. The measurements were taken on a luminator and analyzed in Microsoft Excel.

3.2.2.2 Isolation of gastric glands

3.2.2.2.1 Collection of gastric tissue samples from HP negative patients

The creation of a gastric organoid model starts with a sufficient amount of the of gastric glands. Therefore, bariatric surgery patients without a history of *H. pylori* and with negative *H. pylori* test results were selected and included in the study. Samples were obtained from patients who agreed to participate in the study after reading the informed consent form in the Bariatric Surgery department of Maslak Acıbadem Hospital. Approximately 3 cm^2 of tissue from the corpus part of the stomach was taken, placed in Advanced DMEM/F12 solution containing 100 µg/mL Primocin antibiotic, and transported to the laboratory on ice.

To be used as a control tissue for the characterization studies of the three-dimensional gastric organoid culture, approximately 1 cm^2 of the collected tissue was flash-frozen using liquid nitrogen and stored at -80°C.

The remaining tissue, approximately 1 cm^2, was fixed in a 4% paraformaldehyde solution at +4°C overnight for paraffin embedding. After fixation, the tissue was placed in PBS at room temperature for another night of incubation. Following the incubation, manual tracking was performed on the tissue, and the tissue was subsequently embedded in paraffin blocks.

The remaining portion of the tissue was used for gastric gland isolation after the initial fixation and paraffin embedding process of the dissected tissue.

Within the scope of this study, gastric organoid models were created with tissues taken from two patients, and the models were named hGO-1 and hGO-2.

3.2.2.2.2 Gastric gland extraction

Gastric gland isolation was performed from the remaining tissue from flash freezing and paraffin embedding procedures, taken from the gastric corpus region. Within 4 hours of tissue collection, special precautions were taken to isolate the gastric gland. The sample was transported to the laboratory in an antibiotic-containing culture medium and placed in a clean petri dish containing a chelating solution for gastric gland isolation. This chelating solution, which prepared the tissue for gastric gland isolation, was prepared with 5.6 mM Na_2HPO_4, 8.0 mM KH_2PO_4, 96.2 mM NaCl, 1.6 mM KCl, 43.4 mM sucrose, 54.9 mM D-sorbitol, 0.5 mM DL-dithiothreitol, and distilled water. The samples were washed in the chelating solution with forceps, and the thin mucus layer on them was removed with the help of a scalpel. The washed tissues were transferred to a clean petri dish, cut into small pieces using scissors, and then transferred to a 50 mL falcon tube using forceps. Ten milliliters of chelating solution were added to the tissues using a serological pipette, and the tissues were washed by pipetting ten times. The tissues were allowed to settle by gravity, and the upper phase was discarded. This process was continued until the solution became transparent (approximately 80 mL of chelating solution was used during the procedure). Twenty milliliters of the chelating solution containing 10 mM EDTA was added to the washed tissues and left to incubate at room temperature for 10 minutes. During the incubation period, the falcon was gently mixed every 2 minutes.

The tissues were then transferred to a clean petri dish, and as much solution as possible was discarded. A sterile glass slide was placed on top of the tissues in the petri dish, and the tissues were observed under a microscope. The pressure method was applied using two thumbs to separate the gastric glands from the tissues. The tissue cluster was checked under a microscope to confirm whether the gastric glands were separated from the tissue, and the tissue was transferred to 30 mL of cold Advanced DMEM/F-12 culture medium. The tissue was allowed to settle in the falcon, the upper phase was collected in two clean 15 mL falcons and centrifuged at

4°C, 200 g for 5 minutes. The resulting pellet, which contained the isolated gastric glands, was stored on ice before being seeded.

3.2.2.3 Seeding of the gastric glands

The stomach glands were immediately immersed in the matrigel, which mimics the tissue basal matrix, once they had been isolated. The isolated gastric glands were resuspended by adding 30 µL of Matrigel, which was in liquid form in a cold environment. Then, 50 µL of Matrigel was added to five different 1.5 mL Eppendorf tubes, which were placed on ice, and 10 µL of gastric gland-matrigel solution was added to the first tube, followed by serial dilution. The mixtures that prepared by serial dilution were placed in 24-well plates in droplet form and incubated in a 37 °C and 5% CO_2 incubator for 15 minutes to allow the gel to polymerize. After the drop was formed as a dome, the plate was carefully transferred back to the cell culture hood and the drop is overlayed with the organoid culture medium which is supplemented with the following growth factors for human gastric organoids: 50 ng/ml EGF, 10% noggin-conditioned medium, 10% R-spondin1–conditioned medium, 50% Wnt-conditioned medium, 200 ng/ml FGF, 1 nM gastrin, and 2 µM TGF-β inhibitor and 10 µM rho-associated coiled coil forming protein serine/ threonine kinase inhibitor (RHOKi). The organoid medium was changed every 2-3 days, and RHOKi was only used in the medium that added on the first day of culture. The generated spheroids were examined under a microscope daily.

3.2.2.4 Cultivation of human gastric organoid culture

After the gastric gland seed in basal matrix, the glands were become sphere form and observed every day under inverted microscope. According to organoid development, the culture was passaged every 11^{th} to 14^{th} day. For the passaging the medium that covered the matrix dome was aspirated and the resuspended by cold Advanced DMEM/F12 medium, collected in a 15 mL falcon tube. The organoid structures were fractionated mechanically and the wash with cold medium by pipetting. The fractioned organoid was pellet by centrifugation at 4°C. The

supernatant was removed, and the pellet was resuspended with liquid basal matrix at a ratio of 1:3 to 1:6. The resuspended fractions were placed in 37 °C pre warm 24-well plate as one drop of 50 µl in the center of the well. After the dome formation complete in incubator for 15 min, the drop was overlayed with the organoid culture medium.

Every passage, one well of human gastric organoids (hGOs) was collected for cryopreservation. For the cryopreservation fractionated organoid pellet was resuspended with 1 mL of Recovery™ Cell Culture Freezing Medium (Thermo Scientific) and stocked using a freezing container for progressive cooling.

3.2.2.5 Characterization of constructed hGOs

Differentiation of epithelial cell types in the stomach was achieved by isolating the gastric glands and growing them in three-dimensional cell culture media with various growth factors. The characterization of the generated gastric organoids determined whether the stomach surface was accurately mimicked. Characterization studies were composed of two parts: gene level and structural.

3.2.2.5.1 Expression analysis of gastric-specific and epithelial-specific genes

Gene expression analyses were performed with real-time polymerase chain reaction (RT-PCR) for characterization studies at the gene level. Primers suitable for target genes were designed in the NCBI database and characterized by PCR using cDNAs, whether expressed in culture or not. In order to show that the organoid culture created has gastric tissue properties, LGR5 was used as a marker for stem cells, MUC5AC was used as a marker for gastric pit mucous cells, PGC was used as a marker for chief cells, SST was used as a marker for enteroendocrine cells, and MUC6 was used as a marker for gland mucous cells. Gastric TFF1 expression was also checked. Housekeeping gene β-actin was used as loading control. MUC2 is the marker of intestinal tissue and were used to control for tissue specificity.

DNA and RNA isolation were performed using the Quick-DNA/RNA Microprep Plus Kit (Zymo Research), which has the ability to isolate DNA and RNA simultaneously from the generated gastric organoid cultures. The isolation was carried out according to the kit instructions, and RNA and DNA samples were obtained by eluting with DNase/RNase-free water after washing steps. The purity and concentration of the isolated nucleic acids were measured using a NanoDrop™ 2000/2000c Spectrophotometer (Thermo Scientific). cDNA synthesis was performed using the High-Capacity cDNA Reverse Transcription Kit (Thermo Scientific) from the isolated RNA samples. After completing the reaction according to the kit instructions, a gradient PCR was performed to determine the appropriate working temperatures for the designed primers using cDNA obtained from the gastric tissue. PCR reactions were established for all primers at the optimized temperature. The reaction conditions were set to; 3 minutes of initial denaturation at 95°C, followed by 45 cycles of 35 seconds of intra-cycle denaturation at 95°C, 35 seconds of annealing step at 58°C, and 20 seconds of extension step at 72°C. Gene expressions of the samples were calculated based on the CT values obtained from RT-PCR using $2^{-\Delta\Delta CT}$ formula in Microsoft Excel and expression graph was prepared using GraphPad software The products obtained from the PCR were analyzed by 2% agarose gel electrophoresis with Sybr Gold staining.

After completing gene-level studies for the characterization of hGO-1 and hGO-2 cultures, structural analyses were initiated.

3.2.2.5.2 Morphological analysis of gastric organoid cell lines

Human gastric organoid models' structures were analyzed by paraffin blocks. The formation of the paraffin blocks was started by removing the medium from organoids and adding the 500 µL dispase solution onto the matrigel drops to dissociate the basal matrix. After 30 minutes of incubation, the organoids were collected in a 15 mL falcon tube, the organoids settled by gravity, and the supernatant was removed. The organoids were fixed in 1 mL of 2 % paraformaldehyde (PFA) and incubated for 20 min at room temperature. At the end

of the incubation, the supernatant was removed, and the organoids were dehydrated in 25 %, 50 %, and 70 % ethanol (in H_2O) for 15 min each and 96 % ethanol for 30 min. Dehydrated organoids were incubated in paraffin for 30 minutes, three times at 56°C, and embedded into paraffin after the incubations by using a metal mold.

Histological analysis of organoid cell lines and human gastric tissue sample

Paraffin embedded human gastric organoid and human gastric tissue specimens were cut with microtome into 2,5 µm slices. Sections were collected on object slides and dried at room temperature for overnight (ON). After rehydration of the slides by descending concentrations of ethanol the slides were incubated in Haematoxylin for 8 minutes to stain nuclei and 1 % Eosin for 1 minute to stain cytosolic proteins. Stained slices were dehydrated and embedded in mounting medium with cover glass and analysed under microscope.

Immunofluorescence staining and image analysis

The constructed human gastric organoid structurally characterized by fluorescently labelled with antibodies against the epithelial marker E-cadherin, the polarization marker β-catenin.

Paraffin embedded human gastric organoid and human gastric tissue specimens were cut with microtome into 2,5 µm slices. Sections were collected on object slides and dried at room temperature for ON. For de-waxing and antigen retrieval, paraffinized samples slides were washed twice with xylene for 10 minutes followed by a descending series of alcohols, 20 second each and followed by two washes with water. After, the slides were incubated for 30 minutes in target retrieval solution (Dako) at 95°C, 20 min at RT and 5 min under running water. Antigen retrieved slides were washed twice with PBS and incubated 2 hours with blocking solution which contain PBS, 1% bovine serum albumin, 2% FBS. At the end of the incubation the primary antibody was prepared in blocking solution and slides were incubated at 4°C for ON. After 3 washes with PBS, samples were incubated with fluorescently

labeled secondary antibodies in blocking solution for 2 hours in the dark at RT. Samples were washed three times with PBS, mounted in Prolong® Gold Antifade Reagent with DAPI and analyzed by confocal microscopy. Confocal microscopy (Zeiss LSM 700) Single channel images were merged with Photoshop program.

3.2.2.6 Transformation of 3D gastric organoid model to 2D planar gastric model

Actively cultured 3D hGO cultures were transformed into 2D planar cultures, which is an easier infection model to handle as compared with the labour-intensive injection method and provides reliable infection conditions.

Organoids were prepared with the same protocol used for passaging. Organoid cultures were mechanically dissociated from the matrigel and collected as following the hGO passage protocol for transition to planar culture on the fourth day. The dissociated organoids were incubated with TrypLE Express Enzyme (Thermo Scientific) at 37°C for 5 minutes to obtain single-cell suspensions by separating cell clusters from each other. Cells were counted after staining with Trypan blue and then seeded onto collagen-coated wells (collagen type 1; 10 mg/cm2). Cultures were kept at 37°C, 5% CO2 in a humidified incubator. The morphological structure was observed by microscopy.

Two different culture media (68,166) were tested from two different studies that had successfully transitioned organoids to planar cultures, and the optimal medium was selected based on gene expression analysis by RT-PCR of cultures grown in different mediums, labelled as 2S and 2D mediums. Gene expressions of the samples were calculated based on the CT values obtained from real-time PCR using $2^{-\Delta\Delta CT}$ formula in Microsoft Excel and expression graph was prepared using GraphPad software.

The mediums ingredients were listed in Table 10.

Table 10. 2D planar culture medium ingredients

	3D complete medium	2D-Medium	2S-Medium
Reagent Name			
Advanced DMEM/F12	+	+	+
HEPES	10 mmol/L	10 mmol/L	--
GlutaMAX-I	1X	1X	--
Promicin	100μg/mL	100μg/mL	100μg/mL
FBS	--	10%	10%
B27	1x	1x	1X
Murine recombinant EGF	50 ng/mL	50 ng/mL	50 ng/mL
[Leu15]-Gastrin	1 nM	1 nM	--
Human recombinant FGF10	200 ng/mL	200 ng/mL	--
N-Acetylcysteine	1 mM	1 mM	--
TGFβi A-83-01	2 μM	2 μM	2 μM
RHOKi Y-27632	10 μM	10 μM	10 μM
Recombinant Human Noggin	100 ng/mL	--	--
R-spondin1 conditioned medium	10%	--	--
WNT conditioned medium	50%	--	--

3.2.3 *H. pylori* G27 and ΔoipA-G27 infection on human gastric model and protein profiling

3.2.3.1 *H. pylori* infection on 2D human gastric planar gastric cell culture model

During *H. pylori* infection, it is known that the IL-8 ratio in the cell increases(51). In order to determine the incubation time of the bacteria with the cells, a preliminary study was designed to compare the expression of IL-8 in cells infected with different incubation times. The optimization study was initiated by following the protocol prepared for the transition from three-dimensional to two-dimensional culture. At a density of 350,000 cells per well, the cells were seeded onto collagen-coated 24-well plates, and 18 hours later, the two-dimensional culture media without FBS was added to the wells. The *H. pylori* G27 culture grown for infection was prepared in RPMI medium, and the bacterial solution was added to the cells 30 hours after cell seeding, with a multiplicity of infection (MOI) of 50, meaning that the number of bacteria added was 50 times the number of cells. After infection, cells were collected at 4, 8, and 24 hours by trypsinization, washed three times with PBS

solution, and then centrifuged. The live cells were counted using trypan blue dye. The counted cells were collected in the last wash step and pelletized. RNA isolation was performed from the pellets using the Quick-DNA/RNA Microprep Plus Kit (Zymo Research) following the manufacturer's instructions, and the filters were eluted with DNase/RNase-free water after washing.

The obtained RNA samples were prepared with High-Capacity cDNA Reverse Transcription Kit (Thermo Scientific) using 250 ng of RNA in each reaction and converted into cDNA. The synthesis reaction was carried out according to the kit instructions at 25°C for 10 min, 37°C for 120 min, and 85°C for 5 min. Real-time PCR was performed using IL-8 and GAPDH primers with the synthesized samples. The reaction conditions were set as 1 minute of initial denaturation at 95°C, 10 seconds of denaturation at 95°C within the cycle, 10 seconds of annealing at 63°C, and 15 seconds of extension at 72°C for 40 cycles. Gene expressions of the samples were calculated based on the CT values obtained from real-time PCR using $2^{-\Delta\Delta CT}$ formula in Microsoft Excel and expression graph was prepared using GraphPad software. During the infection study, the cell viability was analyzed along with the viability graph of the cells and the IL-8 gene expression values of the cells that were counted.

Infections with optimized conditions were performed in triplicates with *H. pylori* G27 and ΔoipA-G27 strains in planar cultures formed from both, hGO-1 and hGO-2, organoid cultures and uninfected control wells.

3.2.3.2 LC-MS/MS analysis

The infection experiments were carried out in four biological replicates and three technical replicates for each of the two human gastric organoid lines. After the infection, proteins were isolated from the cell pellets and subjected to LC-MS/MS.

Protein isolation

After infection experiments, cells were collected from each group to reach at least $1x10^6$ cells and protein isolation was performed. Cells were lysed in a solution containing 8M urea, 50mM NH_4CO_3 (Ambic), one tablet of phosphatase inhibitor, and one tablet of protease inhibitor without EDTA, the lysed solution was then centrifuged to obtain the supernatant which contain the proteins. Protein concentrations were prepared according to the instructions of the Bicinchoninic acid (BCA) assay kit and calculated after spectrophotometric measurement.

LC-MS/MS analysis

The mass spectrometry analyses for the prepared samples were performed by obtaining services from Koç University, KUTTAM OMICS laboratory. The protein samples were prepared for LC-MS/MS analysis by reduction with DTT and alkylation with iodoacetamide before analysis. Before adding trypsin, the samples were diluted 8-fold with 50 mM ammonium bicarbonate and incubated with trypsin overnight. The following morning, the reaction was stopped by acidification with 10% formic acid, and the salt of the trypsinized peptides was removed by solid-phase extraction (SPE).

The prepared peptides were analyzed using a C18 nanoflow reversed-phase HPLC (Dionex Ultimate 3000, 3500 RSLC nano, Thermo Scientific) with 90-minute gradients coupled to an orbitrap mass spectrometer (Q Exactive Orbitrap HF, Thermo Scientific). The scanning parameters for MS1 were 120,000 resolution, AGC 3e6, maximum injection time of 100 ms, and a scan range of 375–1400 m/z. For MS2, the parameters were 30,000 resolution, AGC 1e5, maximum injection time 60 ms, top 20 data-dependent acquisition, isolation window 1.2 m/z, and NCE 26. The raw files were analyzed using Thermo Scientific Proteome Discoverer 2.3 software with the Sequest search engine and the human Uniprot database Uniprot_Human_LastVersion_OK_MP_201616_20160320.fasta (Version 2019).

3.2.3.3 Bioinformatic analysis

The Thermo Scientific Proteome Discoverer 2.5 (PD) software was used for the analysis of proteins obtained by LC-MS/MS. Proteins were identified by creating a workflow by the instructions of the PD software, and False Discovery Rate (FDR) correction described by Benjamini-Hochberg was applied to correct for alpha errors. The resulting protein list was sorted according to the number of unique peptides specific to each protein. Normalization of proteins with two or more unique peptides was performed relative to the total amount of peptides analyzed by the software, and proteins, that has a p-value less than 0.05, were considered statistically significant. A Principal Component Analysis (PCA) was performed to observe the difference between the groups and the outlier situation within the group that is not compatible with the group profile. The GO analysis of the identified proteins molecular functions was analyzed using the Panther-Gene List Analysis software.

Proteins that were filtered based on normalization and the number of unique peptides were identified according to the groups they belong to, and proteins that showed differences between groups were shown in Venn diagrams. In addition to protein identification using the PD program, the amounts of identified proteins in the samples were quantified using the label-free quantification (LFQ) method. LFQ is a multidimensional LC-MS/MS data quantification method without isotopic labeling. Using this method, the amounts of identified proteins in the infection and control samples were determined and normalized using the total peptide amount. The values were transformed according to the logarithm of base 2. The protein differences between groups statistically calculated comparing the infection samples to the control samples and fold changes (FC) were determined. The resulting data set was filtered by ANOVA ($p < 0.05$, $q < 0.05$), and proteins with a change ratio of at least 1.3 according to the groups were considered to show significant variation.

The proteins that showed a significant FC between the groups were segregated based on whether their quantity increased or decreased in comparison to the control group. Later, the PANTHER software was utilized to conduct Go analyses. The

pathways in which the proteins belonging to the infection groups are included were analyzed in the Reactome pathway enrichment database, and the enriched pathways were listed.

Proteins affected only by the OipA protein were identified by analyzing the proteins that changed significantly in *H. pylori* G27 infection compared to both control and ΔoipA-G27 infections. Hierarchical Clustering (HC) analysis was performed to examine the similarities of the samples by grouping the similarities and differences between the expression levels for the identified proteins. The heatmap was created with the following parameters: rows centered, and unit variance scaling applied. Rows and columns were clustered by correlation distance and average linkage. Cluster groups were created automatically by the SRplot software.

Cytoscape software (3.8.2) was used to create and visualize the protein-protein interaction map and detect hub proteins via the STRING database. Hub proteins were revealed with the CytoNCA plug-in using the Local Average Junction-Based Method (LAC) and the CytoHubba plug-in using the Maximum Neighborhood Component Density (DMNC) method.

4 RESULTS

4.1 Construction of *H. pylori* ΔoipA-G27 Strain

4.1.1 *H. pylori* G27 cultivation

Helicobacter pylori G27 strain was grown on Columbia agar firstly and the grown bacteria was transferred to *H. pylori* liquid medium under optimized conditions. The bacterial shape and motility were observed under microscope and gram staining technique.

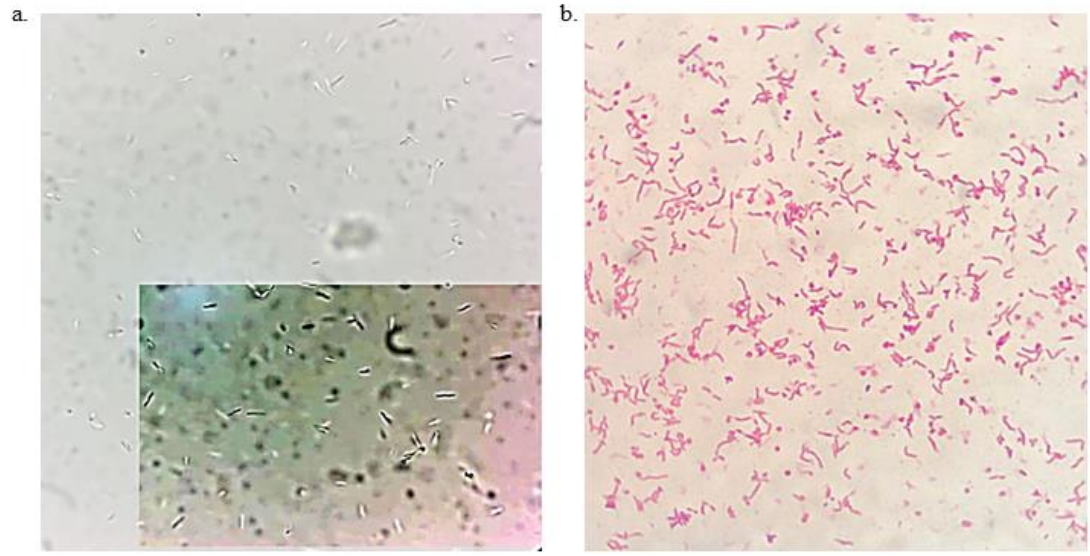

Figure 5. Morphology of *H. pylori* G27 bacteria. Bacterial motility and shape examination in liquid culture (a) and Gram-stained bacterial slide (b) under microscopy with a 1000X magnification.

4.1.2 *oipA* Gene Deletion by homologous recombination system

4.1.2.1 Amplification of K1-2, P1-2 and P3-4 DNA fragments

The *oipA* gene was deleted using a homologous recombination system, which provides the advantage of adding a selective antibiotic site to the deleted region of the genome. For this purpose, a DNA cassette was designed by fusion of three DNA fragments containing the upper and lower sequences of the *oipA* gene with a

kanamycin-resistant gene. DNA fragments K1-2, P1-2, and P3-4 were amplified by conventional PCR reactions. Primers' annealing temperatures were optimized by a gradient PCR reaction and the final products were analyzed by an agarose gel electrophoresis, results are presented in Figure 6.

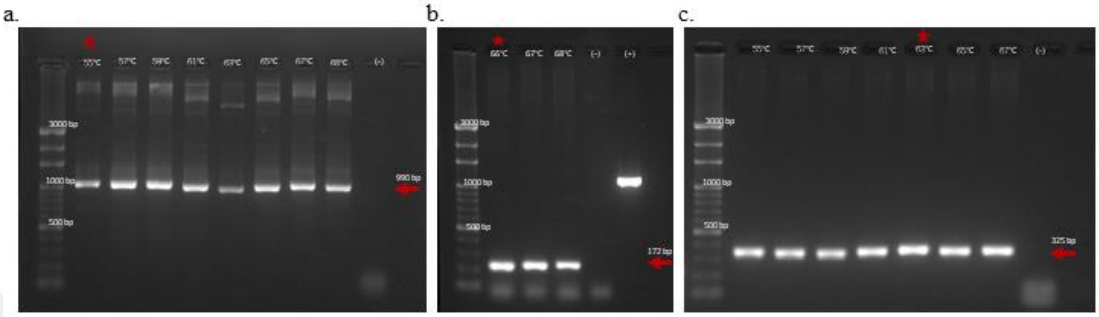

Figure 6. K1-2, P1-2 and P3-4 DNA fragment amplification PCR optimization studies. Gradient PCR for a. K1 and K2 primers (990 bp), b. P1 and P2 primers (172 bp) and c. P3 and P4 primer (325 bp).

After optimization experiments, DNA fragments were produced under optimized conditions and purified. Since the purified DNA fragments will be added in the SOE-PCR reaction at a certain molar ratio, they were measured with the Nanodrop. The results are shown in Table 11.

Table 11**.** Purified K1-2, P1-2 and P3-4 DNAs concentration results

Sample	Concentration ng/µL	A260/280	A260/230
K1-2	122.2	1.95	2.06
P1-2	60	2.01	2.08
P3-4	112.1	1.98	2.01
K1-2	122.2	1.95	2.06

4.1.2.2 SOE-PCR

Constructed DNA fragments (K1-2, P1-2 and P3-4) were aligned in the first step of the SOE-PCR and combined at the second step. The final product of this reaction was run on an agarose gel, since the SOE-PCR reaction buffer is including, unbounded DNA fragments the target band was cut out from the gel, purified, and subjected to a nested PCR (Figure 7)

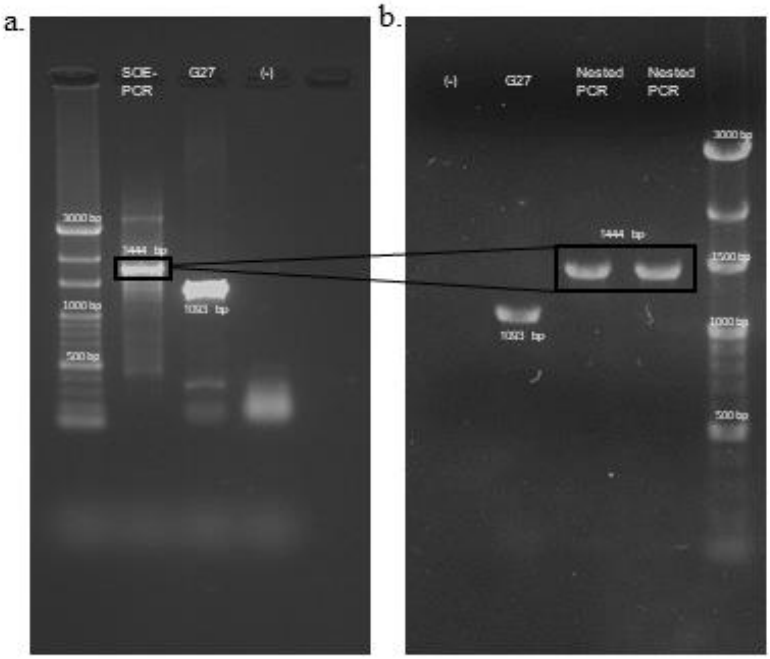

Figure 7. SOE-PCR (a) and nested PCR (b) products' agarose gel results. The P1 and P2 primers were used in both reaction and *H. pylori* G27 gDNA was used as a positive control (1093 bp). The purified target band from the SOE-PCR used as a template for the nested PCR.

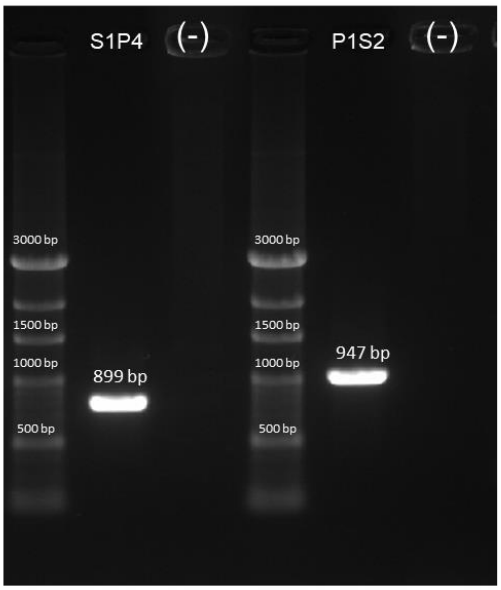

Figure 8. PCR study with sequencing primers of DNA fragments obtained by SOE-PCR method and amplified by nested PCR method. P1 and S2 primers covered the first 947 bp (P1S2) of the target gene, while the S1 and P4 primers amplified the last 899 bp (S1P4).

Although the DNA bands were observed to be in the correct places in the agarose gel results, the samples were sent for sanger sequencing to ensure the accuracy of the DNA sequence. The samples for sending to the sequencing process were amplified with the P1-S2 and S1-P4 primer pairs that specially prepared for the target sequence. Then the PCR products were analyzed by the agarose gel electrophoresis method and the results are presented in Figure 8. It was observed that the region was amplified correctly by blasting over the target sequence that was designed by combining three DNA fragments at the beginning of the study. Aligned and blasted DNA sequences are showed in Figure 9-10.

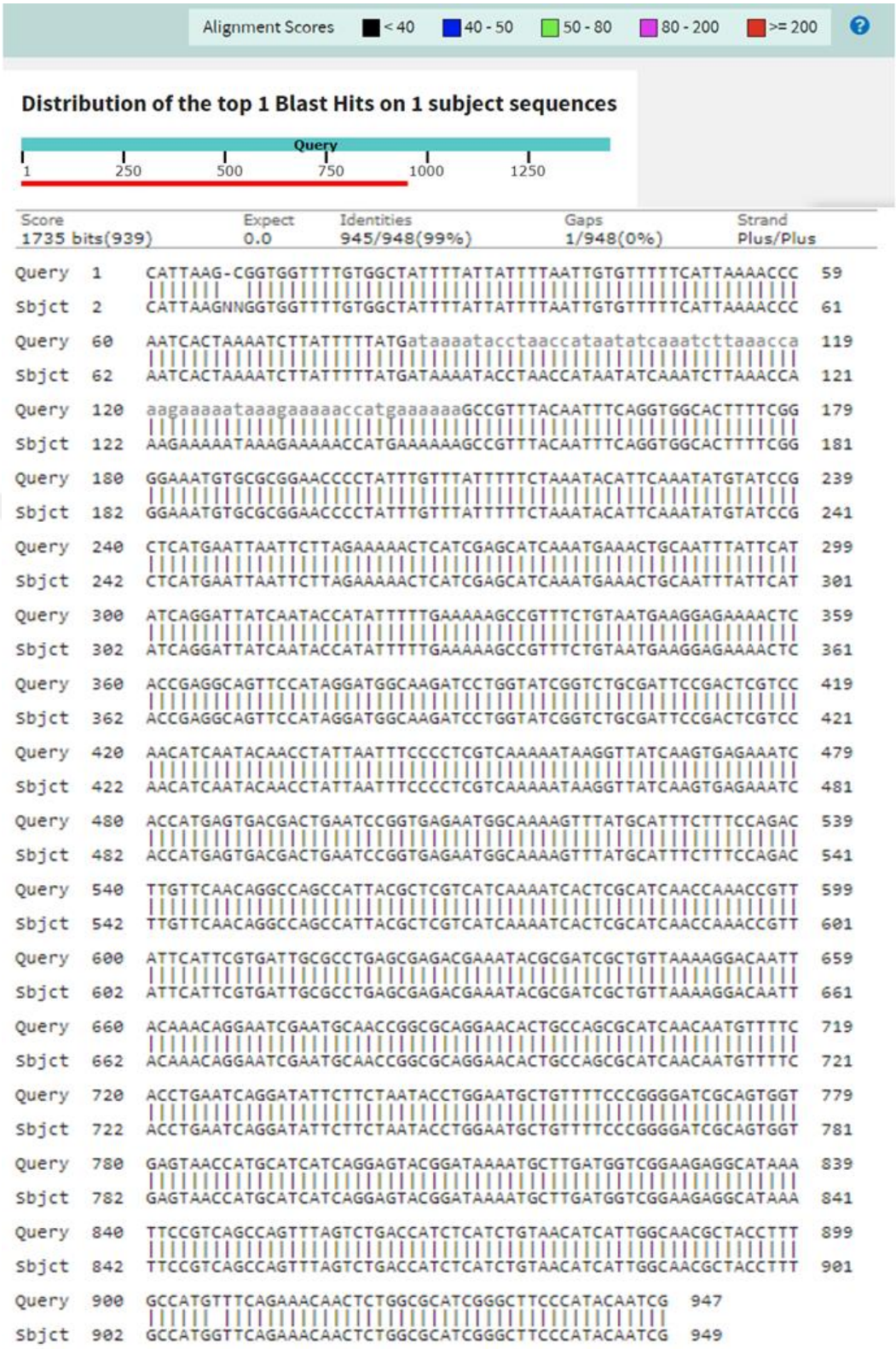

Figure 9. The P1S2 DNA fragment's blasting result. The blasting score was 99% identical with the query sequence.

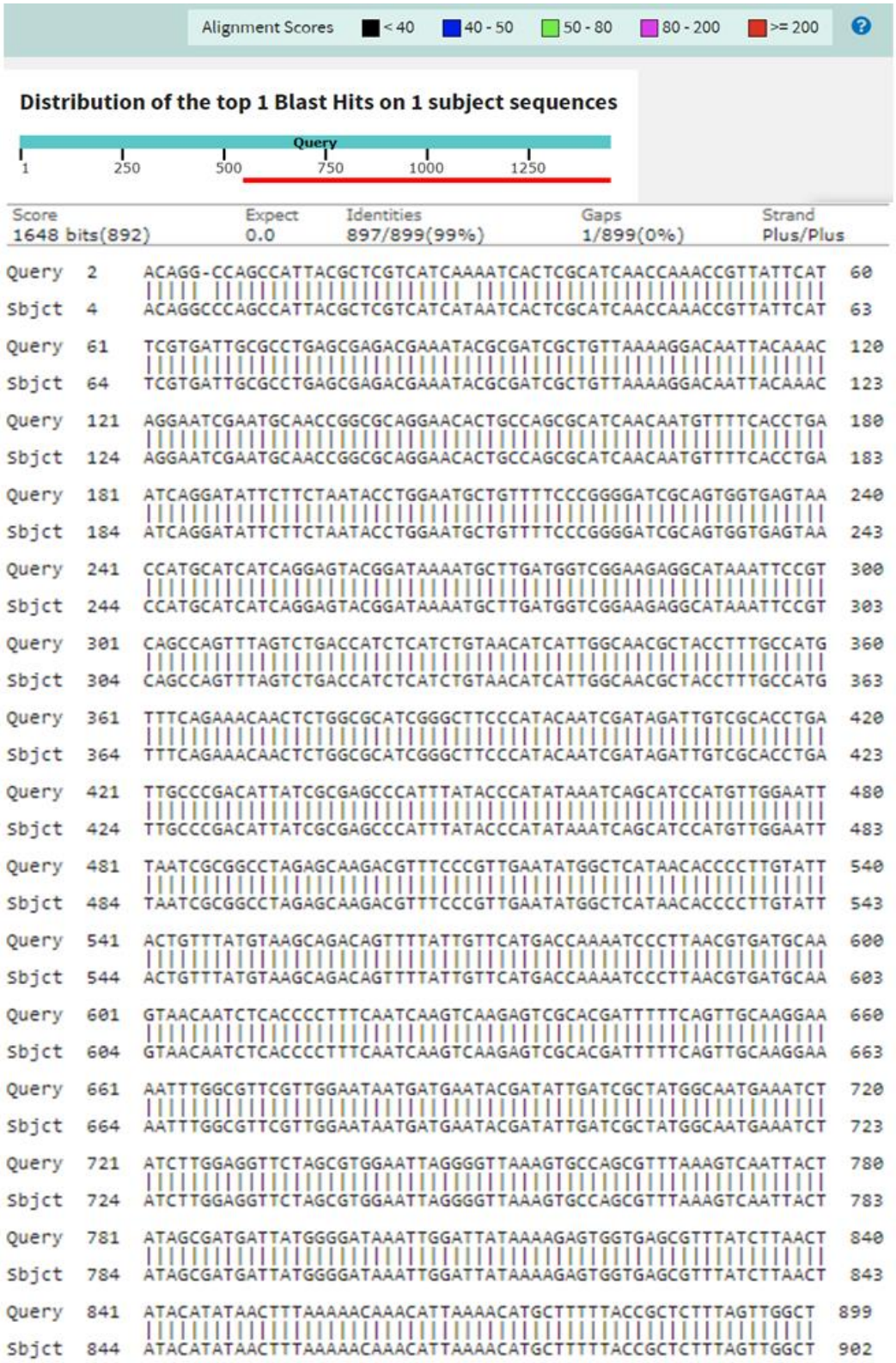

Figure 10. The S1P4 DNA fragment's blasting result. The blasting score was 99% identical with the query sequence.

4.1.3 *oipA* gene deletion confirmation studies

The DNA cassette designed and produced for the deletion of the *oipA* gene from the *H. pylori* G27 genome was sent to the sequencing process to ensure the accuracy of the sequence, and the sequence was observed to be correct as a result of the analysis. For the transfer of the formed DNA cassette into bacteria, the natural transformation process, which allows the desired DNA fragment to be easily taken up into the bacteria, was preferred in the deletion process. Due to transfection, performed on an agar plate, two colonies were observed on selective agar plates, and colonies were grown in the liquid medium as a single colony culture.

The transfection was firstly checked by a conventional PCR with P1 and P4 primers. These primers amplified different sized products between transfected and wild type *H. pylori* G27 bacteria. So, the gDNA samples were isolated from liquid culture and subjected to the PCR analysis. The results are shown in Figure 11.

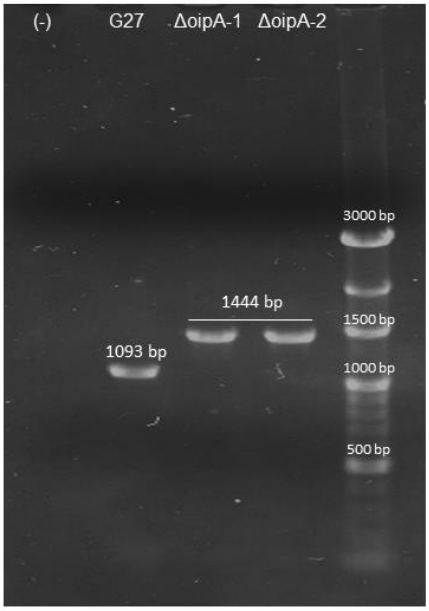

Figure 11. Conventional PCR based transfection confirmation study.

Homologous recombination, which allows insertion, deletion, or alteration of any sequence and has no regard for the location of restriction sites on the bacterial genome, was the gene deletion system that enabled *H. pylori* G27 to incorporate the

DNA fragment into its genome. Since the homologous system is not location dependent, the DNA cassette, to be sent to the bacterium, was designed to bind to the complementary regions of the target gene region. However, the localization of the DNA fragment after the genome integration should confirm to avoid any misplacement or placement into more than one place. For this purpose, after DNA isolation from cultures grown after transformation, samples were first subjected to RT-PCR to measure the amount of kanamycin resistance gene in their genomes relative to each other, and then, according to this RT-PCR result, the sample, which is thought to contain less kanamycin resistance genes, was sent to WGS process.

UreA and kanamycin resistant gene (KanR) expressions were assessed by RT-PCR analysis to compare the number of KanR gene between the colonies. UreA was used as an endogenous control. Gene expression analysis were shown KanR in bar graphs and the samples were analyzed, reaction implemented as duplicate (Figure 12).

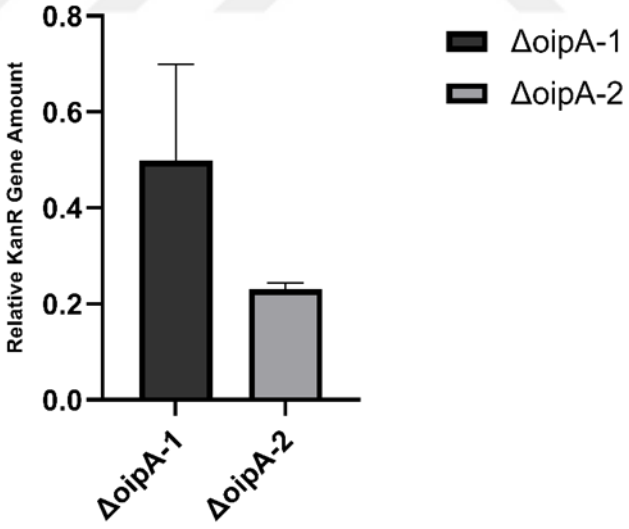

Figure 12. KanR gene number analysis of ΔoipA-1 and ΔoipA-2. The data was analyzed relative gene level of samples with $2^{-\Delta Ct}$ method and normalized by *ureA* gene results. Bar graphs were prepared with GraphPad Prism and shows the average of three independent experiment

Relatively less KanR level was detected in the ΔoipA-2 mutant strain and the isolated gDNA sample was sent to WGS analysis which is the final and most accurate confirmation study for *oipA* gene deletion on *H. pylori* G27 genome. After the sequencing step the mutated strain's genome sequence blasted over *H. pylori* G27 reference genome sequence and the differences were detected by using GENEIOUS PRIME sequence analysis tool (Figure 13-14).

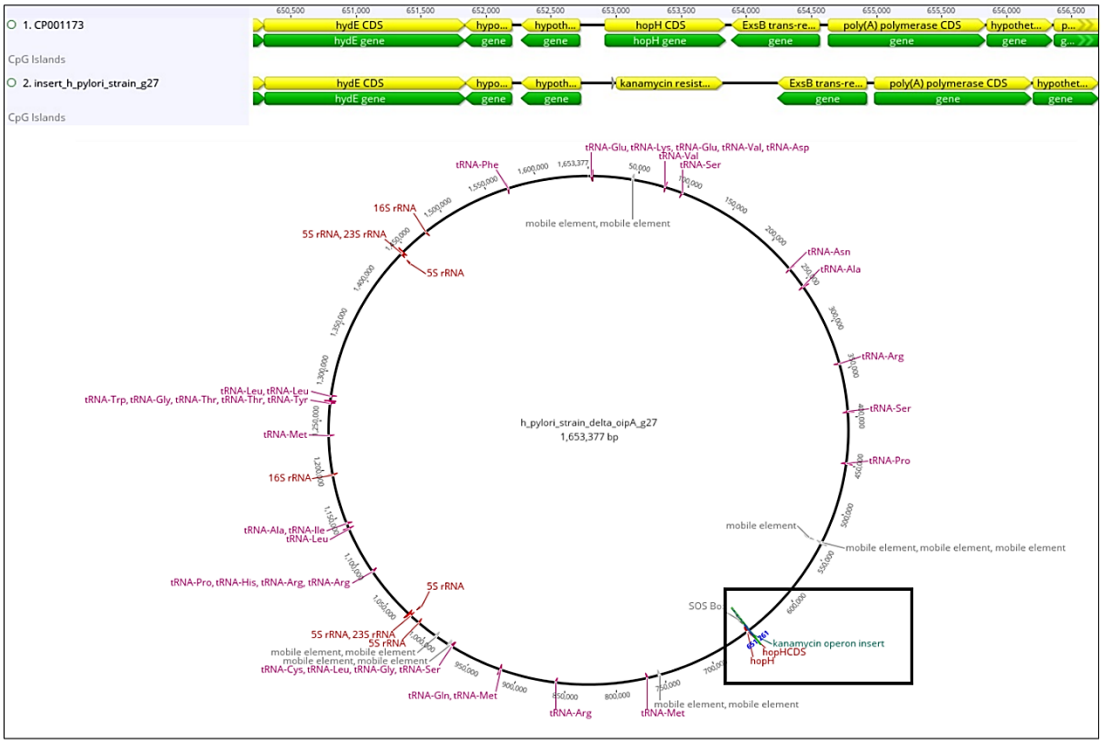

Figure 13. Comparison of the *H. pylori* ΔoipA G27 genome with the reference sequence in the analysis of the sequence sequenced by the Next Genome Sequencing-INVIEW Resequencing method with the Geneious Prime program and display of the kanamycin resistance gene (named insert_*h.pylori*_strain_g27) in the genome instead of the *oipA* (hopH) gene region in the reference sequence

Figure 14. WGS analysis result, the location of the DNA cassette transferred into the *H. pylori* G27 strain on the whole genome is displayed with the Geneious Prime program. The head and end regions of the *oipA* gene are shown in red and the inserted DNA cassette is shown in blue.

4.1.4 Growth curve analysis of *H. pylori* strains

The *H. pylori* G27 strain *oipA* gene was deleted using the homologous recombination method and the ΔoipA-2 was confirmed by the WGS method, the strain was labelled as ΔoipA-G27. It was seen in microscopic examinations that the *oipA* gene deleted from the genome did not affect the mobility and viability of the bacteria. The growth curve analysis of the ΔoipA-G27, as comparison of the growth chart between mutated and wild type was performed and the results are represented in Figure 15.

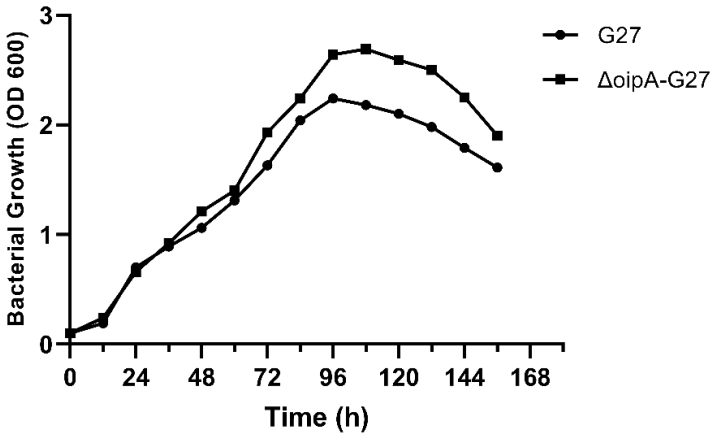

Figure 15. The growth curve of *H. pylori* G27 and ΔoipA-G27 strains. The growth data was obtained by making spectrometric (OD 600) measurements with 12h intervals.

4.2 Construction of Human Gastric Organoid (hGOs) Models

4.2.1 Preparation of hGOs culture condition mediums

The culture mediums containing factors that promote cell growth and differentiation in three-dimensional organoid culture, WNT and R-Spondin condition mediums, were prepared using L-Wnt-3a (ATCC-2647) and Culturex HA-R-Spondin1-Fc 293T (R&D Systems) cell lines (Figure 16).

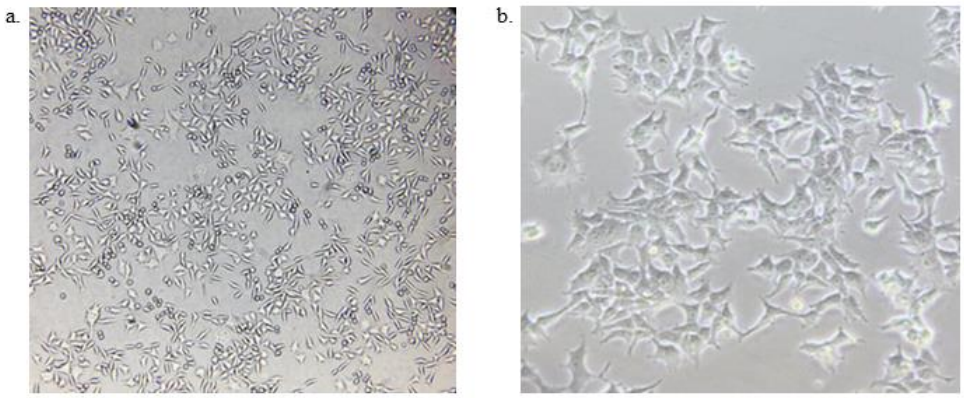

Figure 16. (a) L-WNT-3A cell image under inverted microscope, (b) HA-R-Spondin-FC 293T cell image under inverted microscope.

The cells were cultured under optimal conditions to facilitate the production of the conditioning medium. Following the production of the conditioning medium, the

TOP/FOP assay was employed to evaluate its activity. The activation level of the WNT signaling pathway was measured in the medium in which the cells were incubated, using specific plasmids that were transfected into HEK-293T cells. The TOP/FOP test of the first conditioning medium produced, recombinant L-Wnt-3A protein, was used as a positive control. Subsequently, the media used in gastric organoid culture and found to be effective were used as positive controls in the activity tests of the conditioning media produced. TOP/FOP test result of the produced medium is in Figure 17.

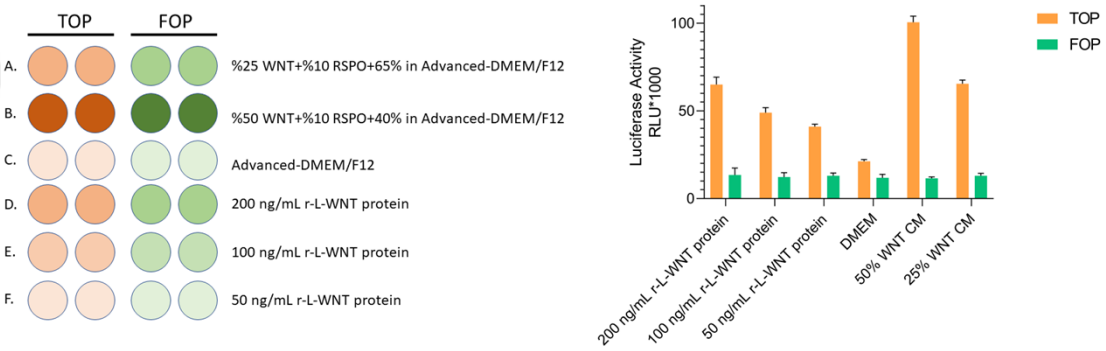

Figure 17. TOP/FOP assay analysis. Experiment template for cell cultivation, transfection, and incubation of media (left) and bar graph results generated by the values obtained after normalization with the luminescence results for the TOP and FOP plasmid (right)

The medium that tested with the TOP/FOP assay was used in gastric organoid culture and was found to be suitable for the culture.

4.2.2 Cultivation of the hGOs models

Isolation of gastric glands

Gastric gland isolation was successfully made from the remaining part of the tissue sample taken from the stomach corpus region, which was divided into equal parts for flash freezing and paraffin embedding. The isolated gastric glands were shown in Figure 18.

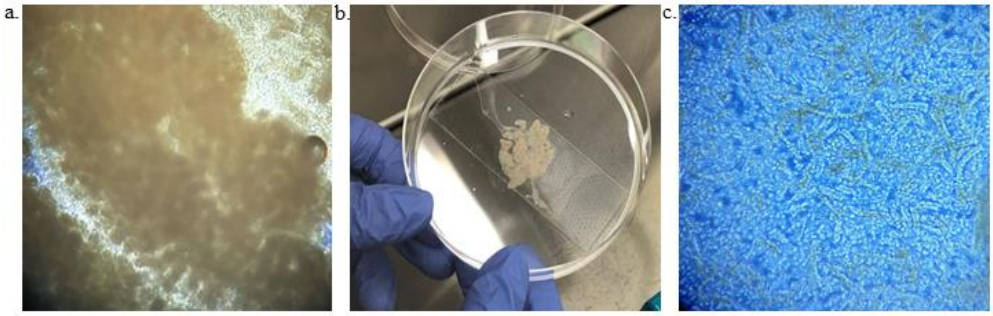

Figure 18. Gastric gland isolation images. The washed tissue, before the thumb pressure method, under microscope (a), the sample after the thumb pressure method (b), the washed tissue which covered by glass lam and observed under microscope, isolated gastric glands observed under microscope (c).

hGOs culture

After establishing the organoid cultures, they were observed daily under a microscope (Figure 19). Microscopic examinations showed the budding of spheroids from the fourth or fifth day cultures, indicating the transformation of the culture into a stomach organoid model. As the passages continued, it was observed that the cultures produced a more uniform and well-defined organoid line.

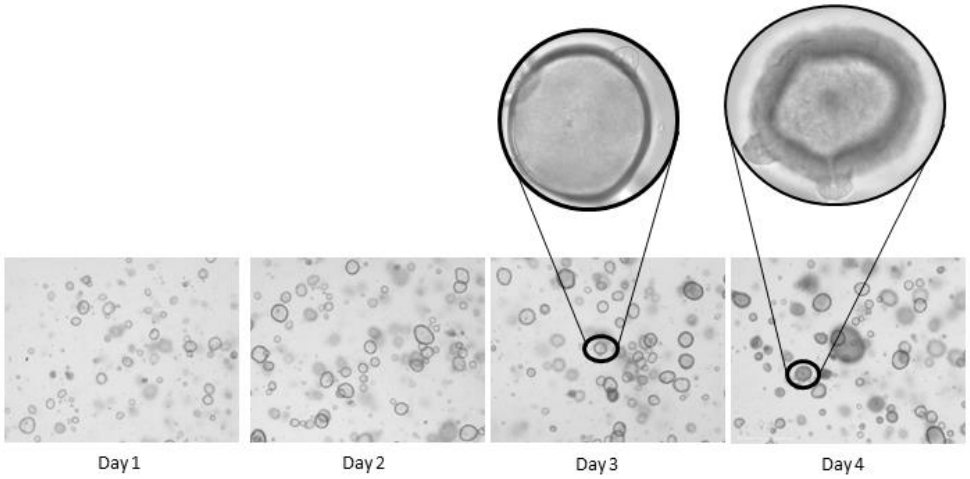

Figure 19. Microscopic examination of the constructed gastric organoid culture

4.2.3 Characterization of hGOs models

4.2.3.1 Expression analysis of gastric-specific and epithelial-specific genes

The gene expression of gastric-specific and epithelial-specific markers in organoid cultures was analyzed through RT-PCR. The expression levels of several genes, including EPCAM for epithelial cell adhesion, LGR5 as a stem cell marker, MUC5AC for gastric pit mucous cells, PGC for chief cells, SST for enteroendocrine cells, and MUC6 for gland mucous cells, were evaluated. Additionally, the expression of the TFF-1 marker for gastric cell differentiation was examined. The GAPDH gene was used as a loading control during analysis.

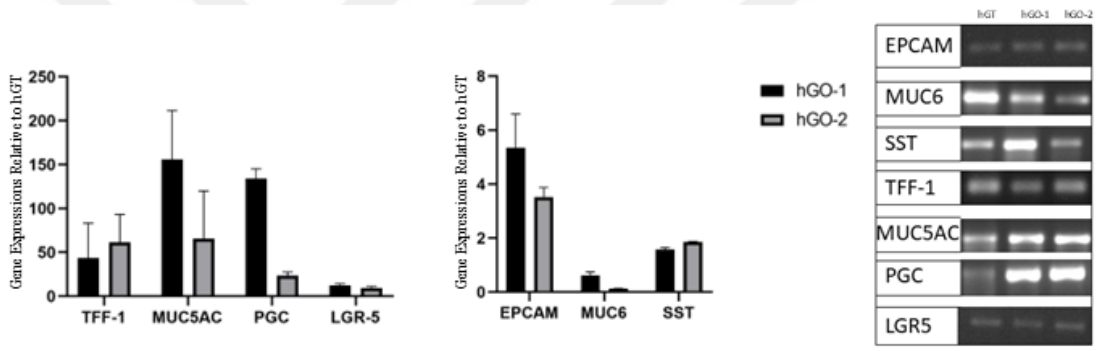

Figure 20**.** Gene expression analysis of hGO-1 and hGO-2 relative to human gastric tissue (hGT). Data were calculated with $2^{-\Delta\Delta CT}$ formula in Microsoft Excel and expression graph was prepared using GraphPad software

RT-PCR results indicated that the organoids expressed the stem cell marker LGR5 as well as the pit mucous cells, gland mucous cells, chief cells, and enteroendocrine cells. These gene expression results, which are in parallel with the studies in the literature (68,149), indicate that the gastric organoid model has been successfully created.

4.2.3.2 Morphological analysis of gastric organoid cell lines

Histological analysis of hGOs

Structural analyzes were started with Hematoxylin&Eosin (H&E) staining. Healthy gastric tissue was also added to the staining as a control. The results are given in Figure 21.

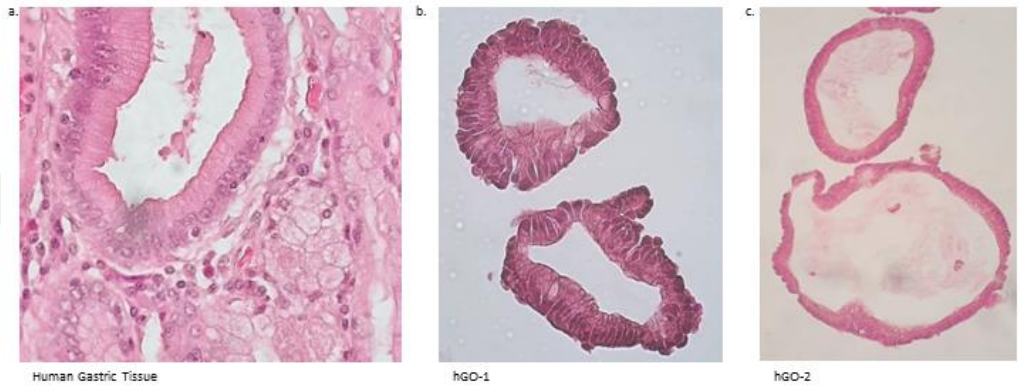

Figure 21. H&E staining results of hGO-1 and hGO-2 of paraffin sections. Healthy human gastric tissue sample (a) and human gastric organoid culture samples (b,c).

The H&E staining results indicates that the constructed human gastric organoids maintain similar characteristics in culture as natural gastric tissue.

Immunofluorescence staining and image analysis

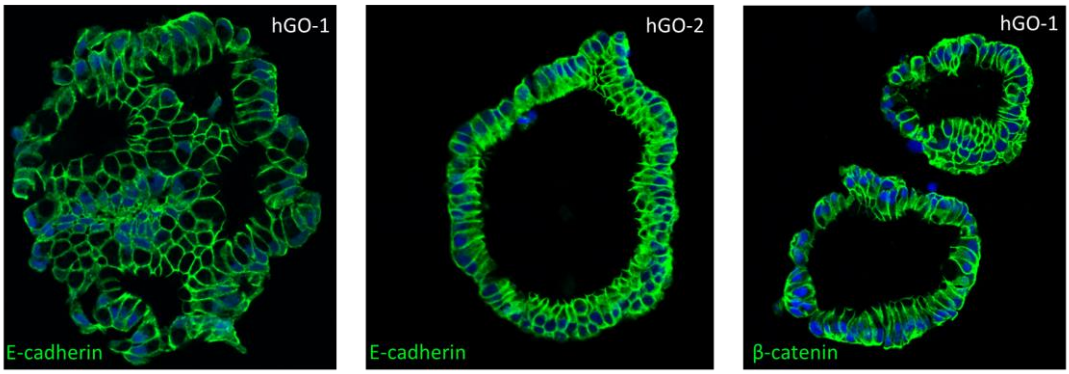

Figure 22. Confocal micrographs of human gastric organoids (cross sections), fluorescently labelled with antibodies against the epithelial marker E-cadherin (green), the polarisation marker β-catenin (green), Nuclei counterstained with DAPI (blue).

When the spheroids were stained with E-cadherin and -catenin, they were seen as hollow objects with a sealed lumen encircled by a single layer of cylindrical epithelial cells. There was no evidence of any unusual cell types in the spheroid epithelial cells, which clearly had a high level of polarization.

Confocal microscopy of human gastric organoids reveals that they are made up of a single layer of cylindrical, highly polarized epithelial cells, shown by the immunolabelling of E-cadherin and -catenin. The organoids display folded, gland-like features commonly seen in healthy stomach mucosa.

4.2.4 Transformation of 3D gastric organoid model to 2D planar gastric model

Characterized three-dimensional human gastric organoid models with observed growth and differentiation characteristics over time were transformed into two-dimensional planar cultures to obtain a more homogeneous infection result. When the development and differentiation times of the formed organoid lines were analyzed, it was noticed that the transition period to planar culture should be 4 days after the passage of the organoid.

In the formation of cultures prepared with the 2D planar culture protocol, two different media were tried and the expression differences of the cultures in the genes selected as gastric markers were analyzed by real-time PCR. In the relative gene expression graphs, the results of which are given in Figure X, GAPDH was used as a control gene and the expressions were calculated compared to the human gastric tissue sample. Student t test was used to compare gene levels between samples.

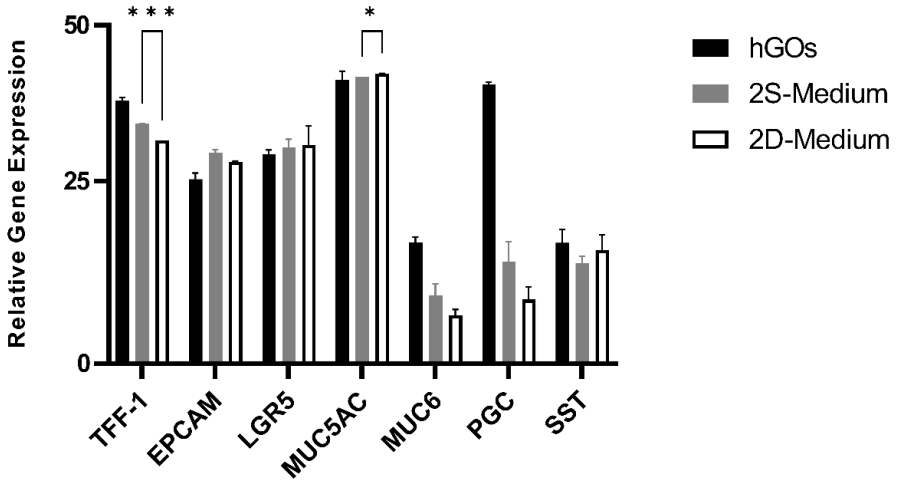

Figure 23. Gene expression analysis of 2D cultures which treated with 2S and 2D mediums. Data were calculated with 2-ΔΔCT formula in Microsoft Excel and expression graph was prepared using GraphPad software. Statistical analysis was performed with student t-test (* $p < 0.05$, *** $p<0.001$).

The effects of two different media used during the transition from a three-dimensional gastric culture to a two-dimensional culture were compared with the gene expression analyzes selected specifically for the gastric epithelium. Although there were no big differences between the two media, the experiments were continued using 2S-medium, since 2S-medium gave similar results to organoid culture in more genes.

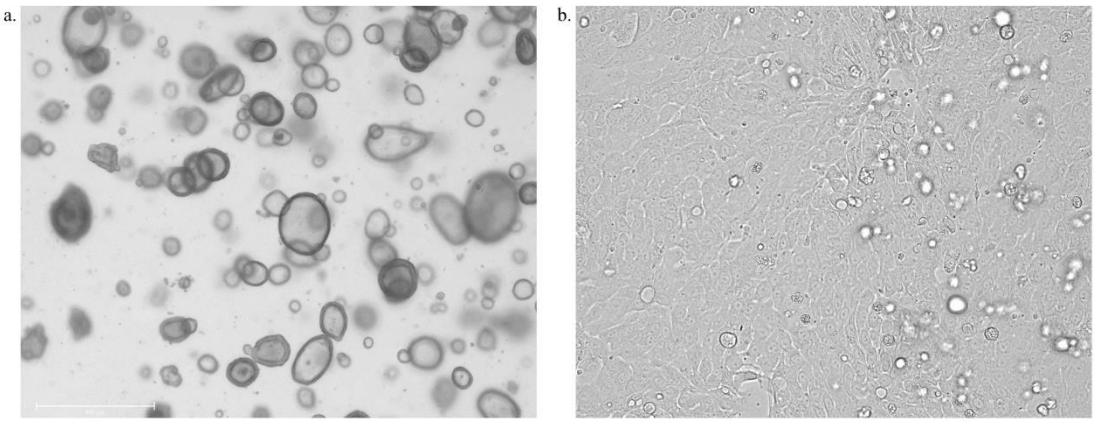

Figure 24. The human gastric 2D planar culture (b) from the gastric organoids (a).

4.3 *H. pylori* G27 And ΔoipA-G27 Infection on Human Gastric Model and Protein Profiling

4.3.1 *H. pylori* infection on 2D human planar gastric cell culture model

The number of hours of incubation for *H. pylori* infection in the created planar cultures was determined by a preliminary study. In the study, the IL-8 value in infected cells collected at different time intervals was examined by real-time PCR and analyzed by considering cell viability (Figure 26).

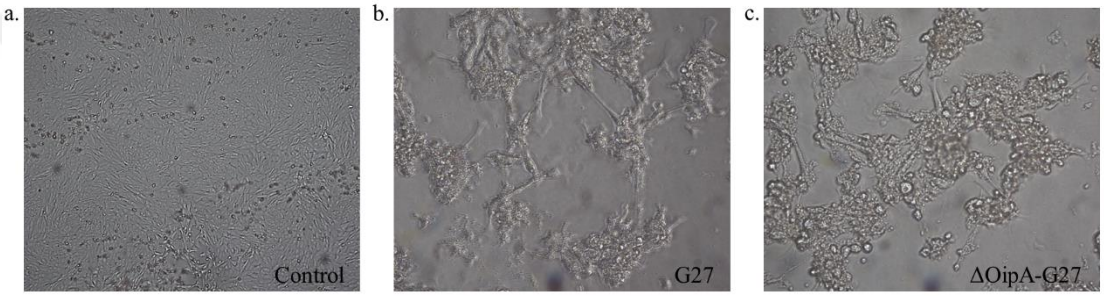

Figure 25. The *H. pylori* infection of 2D planar human gastric cells (a) control well, (b) G27 infected cells and, (c) ΔoipA-G27 infected cells.

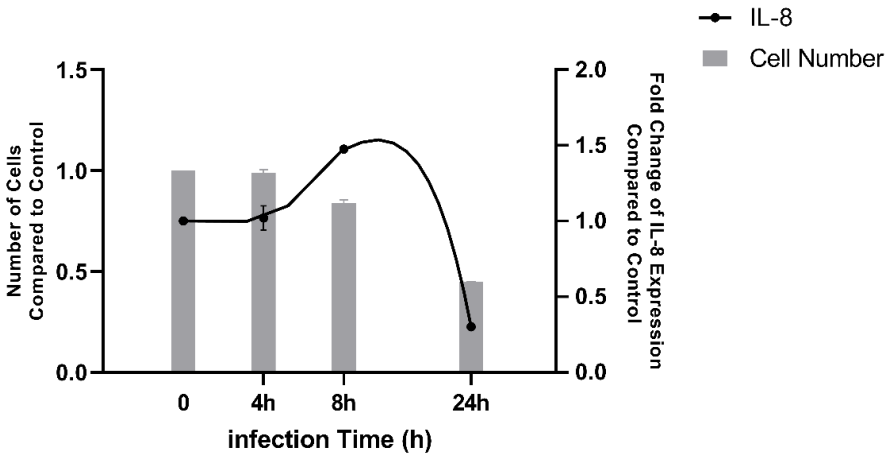

Figure 26**.** Incubation study for *H. pylori* infection. The bar graph is formed by the ratio of viable cell number to the number of viable cells in control wells in cells collected at different incubation times and a line graph indicating IL-8 gene expression in these cells at different incubation times. RT-PCR normalizations were performed using the GAPDH control gene. Analyzes were calculated according to the gene expression values of control cells with the formula $2^{-\Delta\Delta CT}$, and graphs were created using the GraphPad program.

As a result of optimization experiments, the incubation period of *H. pylori* infection was decided to be 8 hours considering cell viability. Infections were performed in triplicates with *H. pylori* G27 and ΔoipA-G27 strains in planar cultures formed from both organoid cultures and uninfected control wells.

4.3.2 LC-MS/MS analysis

Protein identifications

The analysis of the proteins obtained by LC-MS/MS was performed with Thermo Scientific Proteome Discoverer 2.5 (PD) software and identified peptides were searched in Sequest search engine for human database, 3650 proteins were identified. To correct alpha errors in identified proteins, the False Discovery Rate (FDR) correction described by Benjamini-Hochberg was applied, and the number of proteins was reduced to 2700. Samples were normalized to total peptide ion counts, and proteins with protein-specific peptide counts of 1 or less were filtered out. The number of proteins included in the analysis was thus reduced to 1921. PC1 and PC2 calculated by PCA analysis of infected and control samples, plotted by using ClustVis analyzing tool to show group classification and intra-group correlations. The identified proteins were categorized based on their respective groups, and a Venn diagram was used to illustrate the protein lists that were either common or unique to each group (Figure 27).

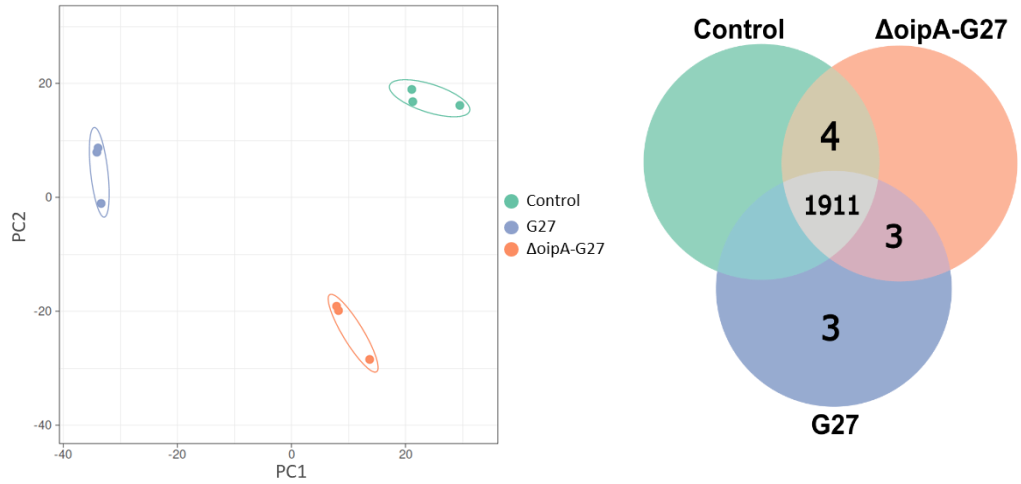

Figure 27. PC1 and PC2 calculated by PCA analysis of infected and control samples showed in left. Venn diagram of the proteins identified in the infection and control groups showed in right.

As a result of the venn diagram, it was seen that the *H. pylori* G27 infection group had some proteins that were unique to it and shared with ΔoipA-G27 infection group, also control and ΔoipA-G27 infection group have common proteins which are not present in the G27 infection group. These proteins are listed in table 12.

Table 12. The list of the identified proteins that are common or unique to groups

***H.pylori* G27 Infection**	***H.pylori* G27 and ΔoipA-G27 Infection**	**Control and *H.pylori* ΔoipA-G27 Infection**
P13674-Prolyl 4-hydroxylase subunit alpha-1, P4HA1	Q15063-Periostin	Q9BTY2-Plasma alpha-L-fucosidase, FUCA2
P49736-DNA replication licensing factor, MCM2	Q96JB2-Conserved oligomeric Golgi complex subunit3, COG3	Q8IWJ2-GRIP and coiled-coil domain-containing protein 2
O14773-Tripeptidyl-peptidase 1, TPP1	P04114-Apolipoprotein B-100, Apo B-100	Q9NSK0-Kinesin light chain 4, KLC 4
		Q9Y2V2-Calcium-regulated heat-stable protein 1

Panther-Gene List Analysis tool (http://www.pantherdb.org/) was used to group the discovered proteins based on molecular function and biological process of the proteins shown in Figures 28.

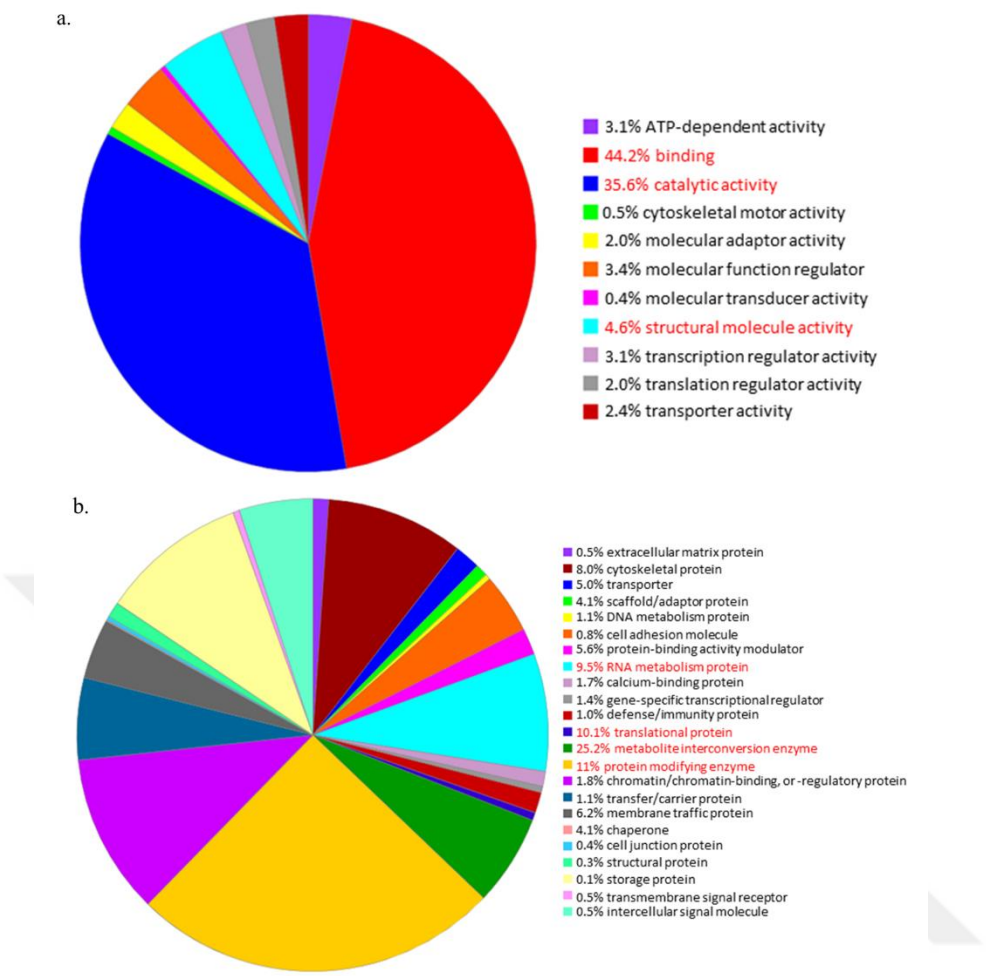

Figure 28. Proteins detected as a result of LC-MS/MS analysis; pie charts distribution showing based on (a) molecular function and, (b) biological process categories.

In protein classification, it was observed that proteins were divided into 23 groups according to their biological process, and 25.2% of the detected proteins were predominantly composed of enzymes that convert small molecules, 10% were translational proteins, and approximately 10% were proteins were RNA metabolism proteins. Proteins were divided into 11 groups according to their molecular functions and it was observed that approximately 44% was binding, approximately 36% was catalytic activity and 4.6% was structural protein.

Quantification and enrichment analysis

The amounts of the identified proteins in the sample were calculated using the label-free quantification (LFQ) method. Calculated values were transformed according to the logarithm base 2 and protein groups were determined by the ANAVO test, the amount of which decreased and increased between groups. As a result of the analysis, the changes of the proteins with a p value less than 0.05 were considered statistically significant. Protein differences between groups were analyzed by the ratio of infection samples to control and fold differences were determined (more or less than 1,3 fold). Volcano plots are used to summarize the results of up and down regulated proteins analysis by using GraphPad. GO-molecular function analyzes were performed using Panther-Gene List Analysis tool and plotted by using GraphPad (Figure 29).

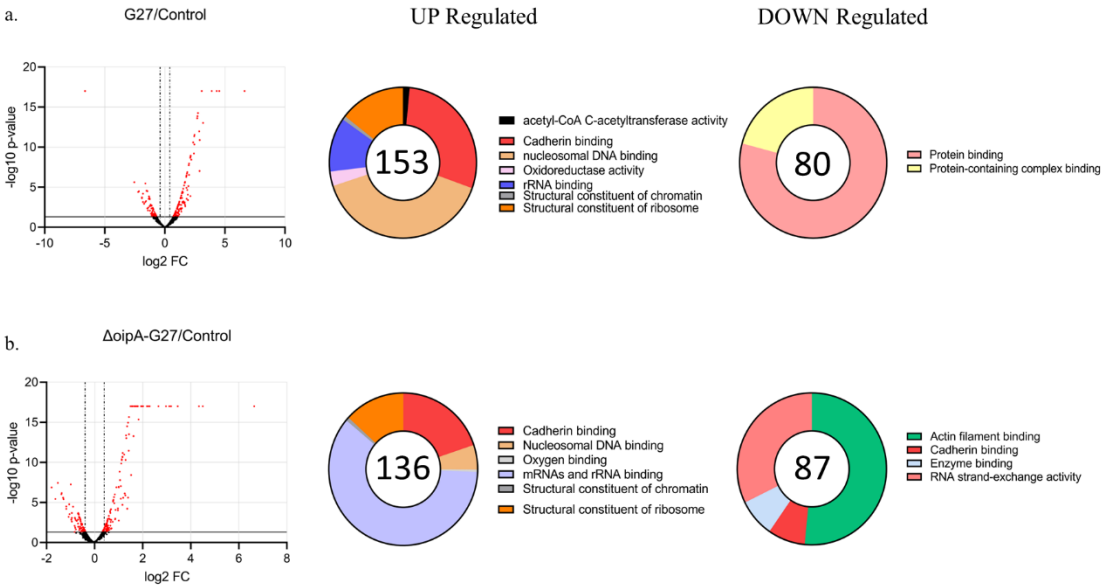

Figure 29. Proteins with different protein amounts compared to control in infection groups were classified based on the determination of up-regulated and down-regulated proteins and their GO analysis based on intracellular molecular functions.

After conducting the infection study, we analyzed the molecular functions of proteins that showed different expressions compared to the control using GO analysis. We further investigated the pathways in which these proteins were involved by performing the Reactome pathway analysis (reactome.org). Table 13 presents the

pathways that were common to both infections, as well as those that were specific to each infection.

Table 13. The pathway enrichment analysis results

	H. pylori G27 Infected Cells Pathway Enrichment Results			*H. pylori* ΔoipA-G27 Infected Cells Pathway Enrichment Results		
Reactome pathways	Gene Count	Fold Enrichment	FDR	Gene Count	Fold Enrichment	FDR
Peptide chain elongation	38	38.22	2.32E-41	47	49.88	2.31E-56
Viral mRNA Translation	38	38.22	1.74E-41	47	49.88	1.54E-56
Eukaryotic Translation Termination	39	37.54	8.44E-42	47	47.73	3.92E-56
Nonsense Mediated Decay (NMD) independent of the Exon Junction Complex (EJC)	39	36.75	8.27E-42	48	47.72	1.28E-56
Selenocysteine synthesis	38	36.58	4.48E-41	47	47.73	3.36E-56
Formation of a pool of free 40S subunits	38	33.68	3.48E-40	47	43.95	4.66E-55
Response of EIF2AK4 (GCN2) to amino acid deficiency	38	33.68	3.17E-40	47	43.95	4.27E-55
SRP-dependent cotranslational protein targeting to membrane	40	31.97	2.26E-41	48	40.48	5.48E-55
L13a-mediated translational silencing of Ceruloplasmin expression	39	31.45	3.01E-40	49	41.69	3.38E-56
GTP hydrolysis and joining of the 60S ribosomal subunit	39	31.17	3.57E-40	49	41.32	3.85E-56
Nonsense Mediated Decay (NMD) enhanced by the Exon Junction Complex	39	30.36	6.30E-40	X	X	X
Regulation of expression of SLITs and ROBOs	42	22.25	1.63E-38	50	27.94	7.01E-51
Apoptosis induced DNA fragmentation	3	20.66	3.48E-02	4	29.06	1.49E-03
Major pathway of rRNA processing in the nucleolus and cytosol	39	19.18	1.29E-33	50	25.95	1.47E-49
Formation of the ternary complex, and subsequently, the 43S complex	9	15.8	1.16E-06	14	25.93	2.92E-13
Ribosomal scanning and start codon recognition	10	15.43	2.43E-07	16	26.05	3.21E-15
Translation initiation complex formation	10	15.43	2.36E-07	16	26.05	3.12E-15
Cytoprotection by HMOX1	10	7.46	1.08E-04	X	X	X

Table 13 (cont'd). The pathway enrichment analysis results

Respiratory electron transport, ATP synthesis by chemiosmotic coupling, and heat production by uncoupling proteins.	7	4.97	3.57E-02	X	X	X
Neutrophil degranulation	19	3.57	1.62E-04	15	2.97	1.20E-02
LDL clearance	X	X	X	4	19.88	4.92E-03
Formation of Senescence-Associated Heterochromatin Foci (SAHF)	X	X	X	3	17.71	4.10E-02
RNA Polymerase II Transcription Termination	X	X	X	5	7.15	3.92E-02
Regulation of Insulin-like Growth Factor (IGF) transport and uptake by Insulin-like Growth Factor Binding Proteins (IGFBPs)	X	X	X	8	6.09	4.48E-03
COPI-mediated anterograde transport	X	X	X	6	5.56	4.04E-02
Diseases of signal transduction by growth factor receptors and second messengers	X	X	X	13	2.94	3.02E-02

As the only difference between the infection groups was the presence or absence of the *oipA* gene in one of the strains, further analysis was conducted on the proteins that varied based on the presence of the OipA protein. Proteins that were found to have similar amounts in the control and *H. pylori* ΔoipA-G27 infected groups, which differed in the G27 infection group, and those with different protein amounts in both infected groups, but with a significant change between G27 and ΔoipA-G27 were included in this group and 97 protein was detected. The list of proteins is shown in Appendix 1. HC analyzes of proteins are given in a heatmap shown in Figure 30.

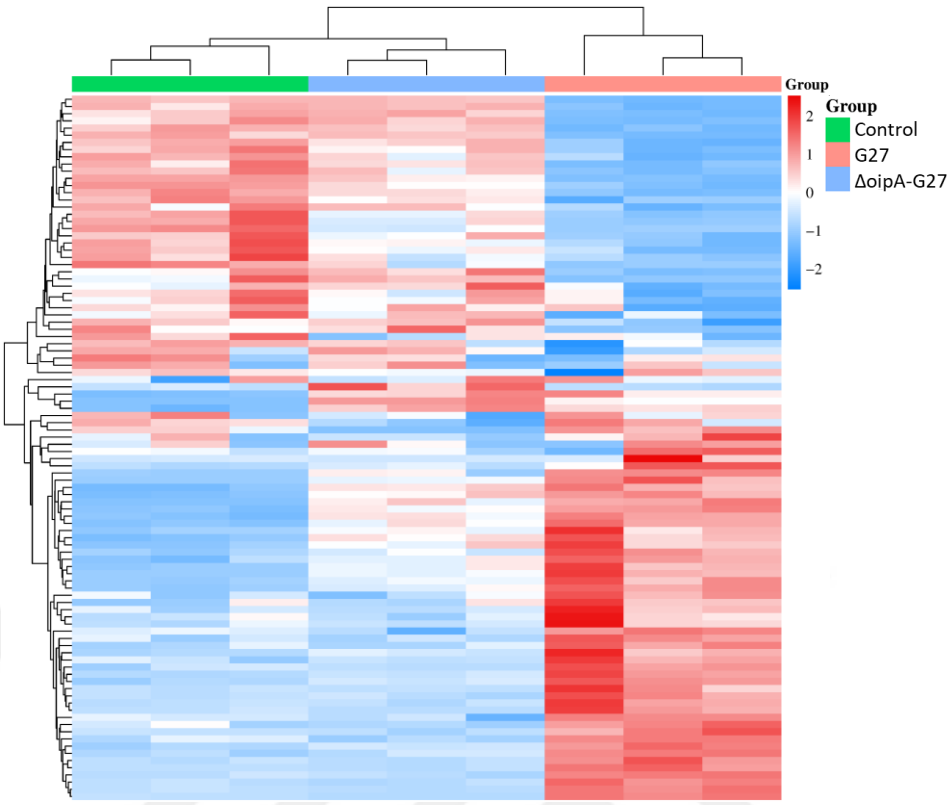

Figure 30. A heatmap was created by hierarchical clustering analysis of 97 proteins, whose expression differences were caused by the effect of the OipA protein on infection as a result of experiments.

Analysis of the proteomic data revealed that in the presence of OipA, 61 out of 97 proteins showed an increase in protein abundance, while 36 proteins showed a decrease. Protein-protein interaction analyzes were performed to analyze interactions between significantly altered proteins and to identify core regulatory genes. For this, proteins whose expression was significantly changed in *H. pylori* G27 infection were mapped and RPL21, PSMC5 and DRG1 were identified as the top 3 hub proteins (Figure 31).

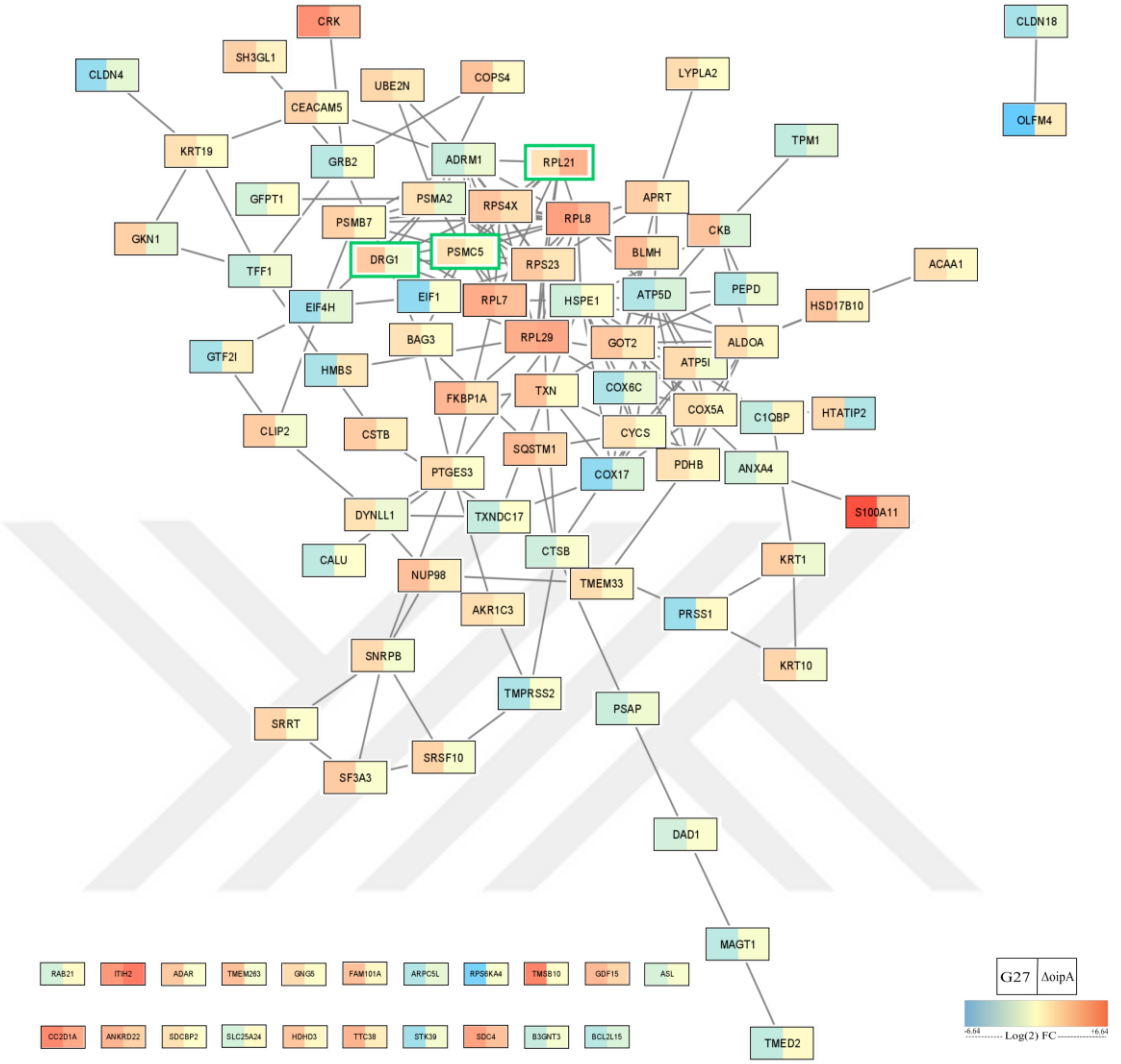

Figure 31. Protein-protein interaction map for the list where the presence of OipA causes variation. G27 and ΔoipA-G27 infections show significant changes in the expression of each protein compared to the control. A rectangle represents each protein, with G27 and ΔoipA-G27 representing the left and right sides of a rectangle, respectively. An increase in the expression of a protein is shown in red, a decrease in blue, and the lightness and darkness of the color gradually depend on the fold change (minimum: -6.64, maximum: 6.64). The yellow color indicates a closer expression of the protein to the control. The first three hub proteins are shown with a green border line.

In order to better understand the biological functions of these proteins and to correlate them with gastric infection, GO and Reactome pathway analyzes were performed and the results are presented in Figure 32-33.

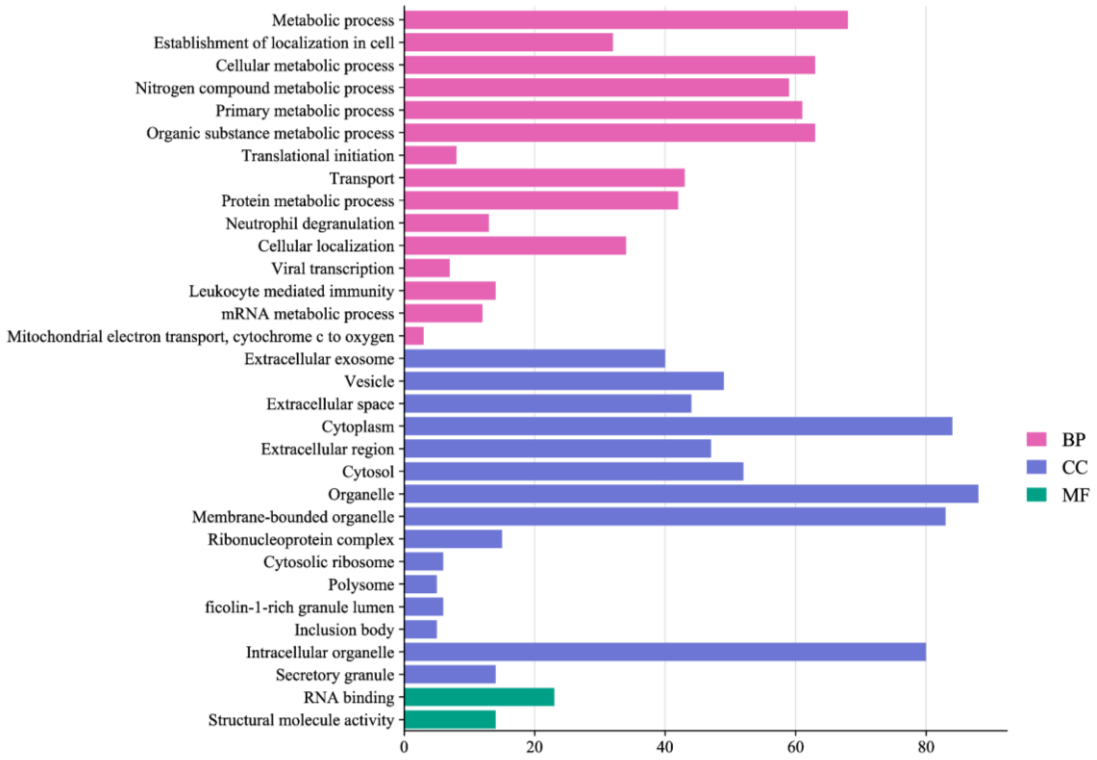

Figure 32. Bar graph display of GO analyzes of proteins that show significant change in the presence of OipA compared to the control. BP for biological process, CC for cellular component and MF for molecular function.

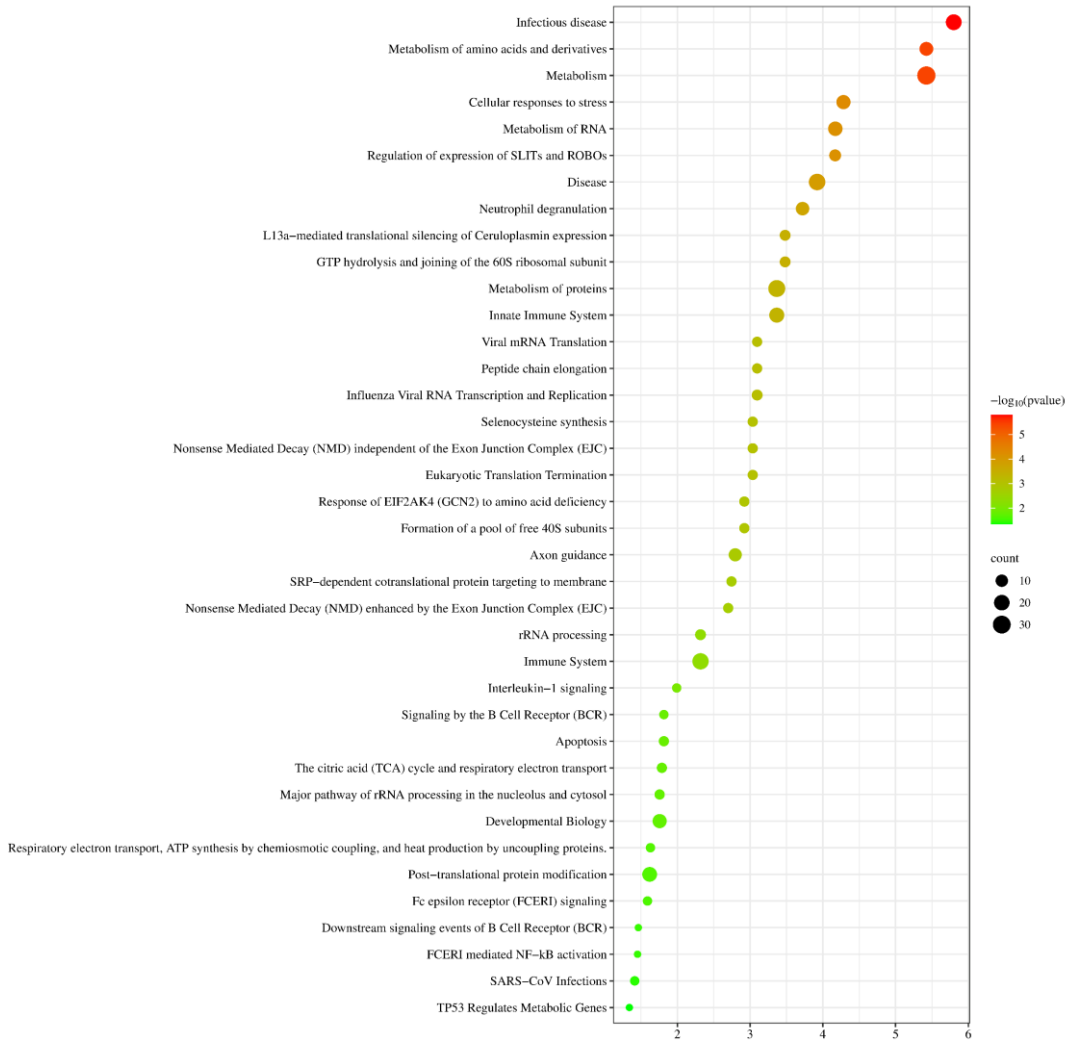

Figure 33. Bubble plot representation of pathways enriched in proteins that show significant change in the presence of OipA compared to control.

5 DISCUSSION

Helicobacter pylori is a gram-negative, microaerophilic bacterium that is an important human pathogen implicated in developing several gastrointestinal diseases, including chronic gastritis, peptic ulcer disease, and gastric cancer. Infecting more than half of the world's population, *H. pylori* was the first bacteria to be formally recognized as causing cancer. The pathogenesis of *H. pylori* infection involves a complex interplay between the bacterium and the host's immune system. The bacterium colonizes the stomach by adhering to the gastric epithelial cells, which triggers an immune response, responsible for much of the tissue damage that occurs in *H. pylori*-associated diseases.

H. pylori has several virulence factors that are believed to be significant contributors to its pathogenesis. These factors include urease, VacA toxin, CagA protein, and outer membrane proteins that are critical for the initial step of the pathogenesis. The outer membrane proteins of *H. pylori* play a crucial role in facilitating bacterial attachment to the stomach surface while providing protection against various cleaning mechanisms employed by the stomach. One of the outer membrane proteins of *H. pylori* is OipA, which is regulated by a phase variation mechanism within the CT dinucleotide repeat motif of the *oipA* gene.

The OipA protein is a key virulence factor that plays a significant role in the adherence and colonization of the bacterium within the gastric mucosa and the studies have shown that the presence of the *oipA* gene is associated with an increased risk of developing gastric cancer (167). OipA has also been shown to induce a stronger immune response in host cells and increase the infiltration of immune cells in the gastric mucosa (51). Additionally, studies suggest that there is a significant correlation between OipA virulence factors to antibiotic resistance to clarithromycin(168). Despite existing literature discussing the role of OipA in *H. pylori* infection, its precise function and mechanisms in the pathogenesis of the bacterium remain largely unknown. However, it is widely believed that OipA plays a significant role in developing *H. pylori*-related diseases and the host's immune

response to the bacterium. Further investigations are required to unravel the intricate details of OipA's involvement and its potential implications for understanding and managing *H. pylori* infections.

The objective of this study was to elucidate the impact of OipA on human cells during *H. pylori* infection by using human gastric organoid model as an infection model and conducting a comprehensive protein-profile analysis.

First of all, the *oipA* gene was deleted from Hp G27, followed by the construction of an organoid model and using the gastric organoid model as an infection model for the G27 and ΔoipA-G27 strains. Finally, post-infection protein profiling was performed using bioinformatic analysis to examine the effect of deletion of *oipA* on the host's response to *H. pylori* infection.

5.1 *H. pylori* OipA and Construction of the ΔoipA-G27 Strain

The targeted gene deletion strategy, which is frequently employed in the identification of the roles of proteins in the cell, was utilized in this investigation to examine the impact of the *H. pylori* OipA protein on infection. The G27 strain, recognized as a reference strain of *H. pylori*, was specifically chosen for deletion of the *oipA* gene due to its advantageous characteristics. These include its exceptional transformability through a natural transformation with exogenous DNA, possessing all well-established virulence factors associated with *H. pylori*, and the robust functionality of the pathogenicity island (PAI) (169). The deletion of the *oipA* gene was the first step of this study, and it was done by using the natural transformation of a pre-designed DNA fragment. Taking up foreign DNA from the environment is an advantage of gram-negative bacteria, and once it enters the bacteria, the homolog recombination system facilitates the integration of constructed DNA fragments into the bacterial genome (170). Since the homolog recombination mechanism has a risk of integrating the constructed DNA into other than the targeted gene region, the deletion of the *oipA* gene was checked by whole genome sequencing, which revealed the successful genome editing results.

5.2 Using Gastric Organoids as a *H. pylori* Infection Models

Previous in vitro studies on *H. pylori* have used cancer cell lines that are often derived from malignant tissue samples and have altered protein expression profiles. As a result, these cell lines may not be ideal for understanding the molecular effects of *H. pylori* infection. In previous studies on the impact of *oipA* on infected cells, the AGS cancer cell line was used to analyze the intracellular protein profiles of cancer cells infected with both *oipA* on and *oipA* deleted *H. pylori* strains (171). However, to address this, the current study employed human gastric organoid models that more closely mimic the natural structure and protein expression of healthy gastric tissue.

Gastric organoids, which have been used in personalized treatment models, cancer model formation, and infection models, can be formed by using induced pluripotent or adult stem cells. Adult stem cells were used in this study because of their fast organoid formation and availability from the source desired to be differentiated (138). Organoid cultures start by providing an environment that will support their transformation into target tissue cell types while ensuring the continuation of proliferation by mimicking the natural environment of stem cells. To provide the necessary conditions in the gastric organoid model, one of the requirements is the presence of a WNT signal. For this purpose, conditioned media were prepared from cells that support the production of WNT and R-Spondin. To prepare the conditioned media, protocols recommended by the companies that supply cell lines were first applied. However, it was observed that the organoid structure of the cultured gastric glands could not be maintained after their transformation into organoids using the obtained conditioned media. The problem was solved by a literature search and a different version of the condition medium protocol recommended by Dr. Sina Bartfield. She has also suggested an activation test, the TOP/FOP assay, which ensures that the quality of the medium can be controlled and optimized for culture. It was observed that the newly produced conditioning medium and activation tests resulted in a more densely populated culture of gastric organoids, similar to those reported in the literature.

The similarity of the gastric organoid model created in a three-dimensional culture to the natural tissue was characterized by analyzing the gene levels specific to gastric and epithelial cells and comparing them with the levels in the gastric tissue. The model we constructed using adult stem cells, parallel to the studies in the literature (149), was analyzed to contain the pit mucous cells, gland mucous cells, chief cells, and enteroendocrine cells, which are the four lineages of the stomach.

The morphology of the gastric organoids formed in this study was analyzed, and it was found that they have a hollow structure with a sealed lumen surrounded by a single layer of cylindrical epithelial cells, as expected. E-cadherin was used as a marker for epithelial cells, and β-catenin was used as a marker for cell polarization. The structural analysis revealed that the epithelial cells in the spheroids showed a high degree of polarization, and no abnormal cell types were observed.

After the characterization studies of gastric organoid culture, it was determined that it could be utilized as an infection model. There are two methods for *H. pylori* infection in gastric organoids: direct injection of bacteria into the organoids via microinjection or incubation with bacteria after transitioning from 3D organoid culture to 2D planar culture (68). For this particular study, the 3D gastric organoid model was converted into 2D planar cells to obtain a more rapid and uniform response to the infection.

5.3 Post-Infection Protein Profiling and Bioinformatic Analysis

The proteins obtained from gastric cells infected with *H. pylori* G27 and ΔoipA-G27 strains were analyzed by LC-MS/MS. The obtained data were analyzed in the Sequest database, and the proteins present in the samples were identified. The total number of identified proteins decreased from 3650 proteins to 1921 proteins after normalization and filtering.

In the analysis of samples obtained after *H. pylori* G27 infection, 3 group-specific proteins were identified; MCM2, TPP1 and P4HA1. While TPP1 and

P4HA1 proteins and *H. pylori* infection need further investigation, according to research in the literature, MCM2 is overexpressed in multiple types of cancer. Dysfunction of MCM2 has been linked to the progression of malignant tumors and poor prognoses (172). Studies have shown a significant negative correlation between the MCM2 gene and the p53 signaling pathway, which is known as the guardian of the genome (173). Additionally, the expression of MCM2 protein was significantly higher in tissue samples from patients with gastric cancer compared to normal gastric mucosa (174).

The proteins that are identified in both *H. pylori* G27 and ΔoipA-G27 infection groups are Periostin, COG3 and Apo B-100. A human cell attachment and adhesion protein Periostin is frequently overexpressed in various types of cancer, including gastric cancer, and is associated with cancer cell proliferation, invasion, the process of epithelial-mesenchymal transition, and the induction of angiogenesis (175). The studies also suggested that increased expression of periostin in gastric cancer cells leads to chemoresistance by activating the Akt pathway and thereby suppressing the expression of p53 (176). Research has demonstrated that *H. pylori* infection leads to the upregulation of cathepsin protease (177). As Periostin is an extracellular target protein for cathepsin proteases (178) and has an effect on gastric cancer formation, further investigation is needed to fully understand the mechanisms underlying the interaction between *H. pylori* and the Periostin protein. The second protein is COG3, which is a component of a protein complex known as the conserved oligomeric Golgi complex that regulates membrane trafficking and maintains Golgi homeostasis by facilitating retrograde vesicle trafficking within the Golgi (179). Research has suggested that the COG complex is involved in processes as viral entry, fusion, and egress for orthopoxviruses (180). The final protein is Apolipoprotein B-100, Apo-B100, that plays a role in moving cholesterol around our body. There is clinical research about the association between *H. pylori* infection and cardiovascular diseases, which indicates *H. pylori* infection-related disruption of lipid and lipoprotein metabolism in the host and results in an increment in the level of Apo-B proteins which can cause thrombogenesis and other cardiovascular diseases (181).

The last group-specific identified protein group is a group of common proteins that are in both the control and *H. pylori* ΔoipA-G27 infected groups: Plasma alpha-L-fucosidase (FUCA2), GRIP, and coiled-coil domain-containing protein 2 (GCC2), Kinesin light chain 4 (KLC 4), and Calcium-regulated heat-stable protein 1 (CARHSP1). The quantities of these four proteins, which were detected in both control and ΔoipA-G27-infected group, were quantified by LFQ method. The results of the quantification analysis revealed that the expression of the CARHSP1 protein was significantly down-regulated (1.55-fold) in the *H. pylori* ΔoipA-G27 infection group compared to the control group, with a p-value of 0.0165. Recently, CARHSP1 has been identified as a regulator of TNF-α mRNA stability in macrophages (182), and a biomarker for diabetic retinopathy. CARHSP1 may contribute to oxidative stress through the movement of stress granules and processing bodies (183,184). Although the post-transcriptional change and clinical significance of CARHSP1 are slowly coming to light, little is known about how it affects metabolism. According to our results, in the absence of OipA, the amount of this protein was found to be significantly reduced compared to the control group, and since the CARHPS1 protein is functioning through many mechanisms, its post-infection effect needs to be investigated.

After the initial identification of proteins, the amounts of proteins were quantified within each group using the LFQ method. GO-molecular function analysis was then performed on the proteins that showed a significant change of at least 1.3 times compared to the control. In the G27 infection group, 153 proteins were found to be upregulated while 80 proteins were downregulated. Similarly, in the ΔoipA-G27 infection group, 136 proteins were upregulated while 87 proteins were downregulated. The upregulated proteins in both groups were found to be involved in cadherin binding, nucleosomal DNA binding, RNA binding, structural constituents of the ribosome, and chromatin functions. However, the activity of acetyl-CoA C-acetyltransferase was found to increase specifically in the G27-infected group. Two of the proteins identified in our analysis, mitochondrial and cytosolic Acetyl-CoA acetyltransferase, both belonging to the acetyl-CoA C-acetyltransferase family, showed a significant increase (fold changes: +1.8 and +2, p-values: 0.0178 and

0.004, respectively) in G27-infected cells, while no change was observed in ΔoipA-G27 infected cells. These enzymes use acetyl-CoA as a substrate and produce CoA and acetoacetyl-CoA (a reversible reaction). Since acetyl CoA plays a crucial role in regulating various cellular processes by affecting enzyme activity, substrate availability, and protein acetylation (185), the effect of *H. pylori* infection and OipA on this pathway requires exploration more deeply.

After GO functional analysis, the proteins participating in pathways were determined by the Reactome pathway analysis database. Since no significant results were found in the intracellular pathways from the down-regulated protein lists in the separate analysis of up- and down-regulated groups, the proteins were included in the analysis without grouping them according to their quantities. After conducting pathway analysis, it was found that the G27 infection group participated in 22 pathways, while the ΔoipA-G27 infection group participated in 26 pathways. Of these pathways, 20 were found to be common to both infections, with two being specific to the G27 infection and six being specific to the ΔoipA-G27 infection.

G27 infection specific pathways

Cytoprotection by HMOX1 is one of the pathways specific to G27 infection, HMOX-1 is a stress-inducible enzyme that works as an anti-oxidative and cytoprotective agent and is involved in the response to inflammatory processes (186,187). The studies suggested a strong association between HMOX-1 expression and oxidative stress-mediated injury during *H. pylori* infection (188). The other G27 infection pathway was combined from three pathways; respiratory electron transport, ATP synthesis by chemiosmotic coupling, and heat production by uncoupling proteins, which are all involved in mitochondrial and ROS production pathways, which is not surprising since we know *H. pylori* infection has an effect on mitochondria (189).

ΔoipA-G27 infection specific pathways

LDL (low-density lipoprotein) clearance pathway is related to the lipoprotein effects of the infection. LDL are complexes of a single molecule of Apo-B100, which is identified in the common protein group for the G27 and ΔoipA infection groups. The second pathway is the formation of Senescence-Associated Heterochromatin Foci (SAHF), a process that results from DNA damage and telomere stress-induced senescence and plays a significant role in the permanent cell cycle exit, helping to inhibit genes that promote proliferation (190). Other pathways specific to the infection include the termination of RNA Polymerase II transcription, regulation of insulin-like growth factor (IGF) transport and uptake by insulin-like growth factor binding proteins (IGFBPs), membrane trafficking, and diseases of signal transduction by growth factor receptors.

The identified and quantified proteins were analyzed to determine changes in protein levels in the presence of OipA protein during infection. Ninety-seven proteins were found to be significantly affected by the presence of the OipA protein. Out of these proteins, 61 showed significant increases in their levels in the presence of OipA protein, while decreased levels were observed in 36 proteins. The molecular functions of these proteins were determined by performing Gene Ontology (GO) analysis. The analysis showed that 68 proteins were associated with metabolic processes, while 40 proteins were linked to extracellular exosomes. Additionally, molecular function analysis identified RNA binding functions among 23 proteins.

Pathway enrichment and protein interactions

Based on the analysis of 97 proteins, it was found that RNA binding is a molecular function affected by the presence of OipA. Further enrichment analysis revealed that the RNA metabolism pathway was significantly enriched, which included 16 proteins. The results showed that the presence of OipA led to up-regulation of proteins involved in the RNA metabolism pathway. Compared with the control group, proteins involved in this pathway were found to be significantly

upregulated in the presence of OipA. One of the proteins in this pathway is the central protein 26S proteasome regulatory subunit 8 (PSMC5), which is upregulated in G27 infection. It is a component of the 26S proteasome, which plays a crucial role in maintaining protein homeostasis by eliminating misfolded or damaged proteins that can damage cellular processes and is involved in the elimination of proteins whose functions are no longer needed. In addition, the proteasome is known to be involved in a wide variety of biological functions such as DNA damage repair, cell cycle progression, and apoptosis (191,192). Other than PSMC5 there are two more proteasome subunits in the OipA-affected protein list, which are Proteasome subunit alpha type-2 and type-7 (PSMA2 and PSMA7). Both subunits act as constituents of the 20S core proteasome complex which is responsible for the proteolytic breakdown of a majority of intracellular proteins. Within the cell, this complex assumes various crucial functions through its interaction with diverse regulatory particles. When combined with two 19S regulatory particles, it forms the 26S proteasome, enabling the ATP-dependent degradation of proteins marked with ubiquitin (193). Studies have proposed that the proteasome-enriched structures could regulate the gastric epithelium's inflammatory and proliferative responses (194,195).

Another mechanism by which the PSMC5 protein is involved is the activation of the Ras-Raf-MEK-ERK pathway to NF-κB via the RPS6KA protein. The OipA protein has a significant impact on RPS6KA6 protein expression; its levels were found to be lower in the presence of *oipA* compared to both the control and ΔoipA-G27 infection groups. RPS6KA6 plays a crucial role in cellular proliferation, survival, and differentiation through growth factor stimulation, which is regulated via phosphorylation (196). It has been demonstrated that RPS6KA6 can modulate the function of p53, and its downregulation leads to cellular evasion of p53-mediated cell death (197). Furthermore, a study reported a reduced expression of RPS6KA6 in colon cancer patients compared to healthy individuals (198).

Another important route that the OipA protein affects is the neutrophil degranulation pathway. One of the proteins in this pathway is olfactomedin-4 (OLFM4), a glycoprotein that promotes cell adhesion through interactions with

lectins and cadherin on the cell surface. Studies showed enhanced expression of the OLFM4 protein in the gastric mucosa of *H. pylori* infected patients and speculated that it actively confers a survival advantage to *H. pylori* by promoting gastric colonization (199). In a subsequent investigation conducted by the same team, it was discovered that OLFM4 is a protein found in neutrophil granules and has been established as a significant negative modulator of bacterial killing. This was demonstrated by experiments involving neutrophils obtained from mice that had undergone OLFM4 knockdown, which showed an increased ability to eliminate *S. aureus* and *E. coli* and became more resilient to systemic sepsis (200). The olfactomedin 4 (OLFM4) protein is known to be upregulated in several types of tumors, but it has also been observed to be downregulated in certain tumor types (201). For instance, in patients with lymph node metastases in early gastric cancer, OLFM4 expression is reduced. In vitro studies have demonstrated that knocking down OLFM4 results in the activation of the NF-κB/interleukin-8 axis, which promotes the migration of gastric cancer cells and a negative correlation between OLFM4, and interleukin-8 expression was observed in early gastric cancer tumor samples (202). In this study, the impact of OipA protein on *H. pylori* infection was explored, and the results demonstrated that the presence of OipA protein led to a reduction of over four-fold in the amount of OLFM4 protein following infection with the G27 strain. In contrast, an increase of more than 1.3-fold in the amount of OLFM4 protein was observed after infection with the ΔoipA-G27 strain compared to the control.

The S100A11 protein, identified in the neutrophil degranulation pathway that is enriched in determining the impact of OipA presence on infection, experiences a considerable increase in the presence of OipA protein during infection. In the literature, it has been demonstrated that the S100A11 protein amount increases in response to infection with strains that have *oipA* in the "on" status as compared to the "off" status (203). Additionally, research has shown that this protein is overexpressed in gastric cancer, supports lung carcinogenesis progression through regulating cell migration and proliferation, and inhibits apoptosis (204–206).

It has been shown in previous studies that OipA can bind to host gastric cells through an intrinsic mechanism, resulting in the initiation of toxic events and an apoptotic cascade. Our investigation into the effect of OipA also revealed significant enrichment in apoptotic pathways. HTATIP2 is one of the apoptotic pathway proteins that is an oxidoreductase, which is necessary for tumor suppression. Studies have revealed that it has antiangiogenic and antiapoptotic actions, is pro-apoptotic, and is a metastasis suppressor (207,208). Protein profiling studies have shown that the presence of OipA enhanced the quantity of HTATIP2 protein as compared to OipA absence.

The apoptotic pathway is frequently associated with mitochondria (209). The pro-apoptotic proteins located in the inter-membrane space are released into the cytosol when the mitochondrial outer membrane becomes permeable or ruptures. This mitochondrial protein release causes catabolic reactions that lead to cell death, and one of them is cytochrome c (CYCS), which is released from the mitochondria and activates the caspase 3/9 complex (210,211). As expected, in the infection study, the amount of CYCS increased approximately 1.7 times in the presence of oipA protein compared to the control, while it almost did not change in ΔoipA-G27 infection.

The significant alterations in the regulation of specific proteins within pathways known to be activated during *H. pylori* infection when OipA was present are analyzed. The observed changes in apoptosis and p53 pathways raise intriguing questions about the complex relationship between OipA and the molecular mechanisms underlying these pathways and the proteins identified in the study.

6 CONCLUSION

This study aimed to investigate the impact of the OipA protein on the host proteome during *H. pylori* infection. Firstly, a controlled and reliable strain was generated by specifically deleting the *oipA* gene from the genome of the G27 strain, a well-established reference strain of *H. pylori*. This allowed for a focused examination of the effects of the OipA protein.

Furthermore, a gastric organoid culture model was established as an infection model, exhibiting the characteristics of a complete-type culture containing four distinct lineages of gastric tissue. The organoid culture system offers numerous advantages, including its non-cancerous origin, ability to mimic the human model without the use of animals, and long-term culture potential. Consequently, it was developed as a valuable protocol and culture source for future scientific investigations.

In addition, a gastric planar model was devised to facilitate infection in a two-dimensional planar culture while preserving characteristic cell changes observed in a three-dimensional environment. This model enabled more convenient and homogeneous infection procedures without the loss of specific cell types. Utilizing this model, infections were conducted with both ΔoipA-G27 and wild type G27 strains, and subsequent proteome analyses were performed.

By quantifying proteins in pathways identified through pathway enrichment analysis, we gained insights into the molecular mechanisms and interactions between OipA and key cellular pathways. The altered regulation of proteins in pathways associated with *H. pylori* infection, in the presence of OipA, provides valuable insights into the potential impact of this virulence factor on host cells. Deeper molecular studies are warranted to elucidate the specific molecular interactions between OipA and proteins within the apoptosis and p53 pathways. Understanding these intricate mechanisms will enhance our understanding of the role of OipA in *H. pylori* infection and may offer potential therapeutic targets for combating this prevalent bacterial infection

7 REFERENCES

1. Fagoonee S, Pellicano R. *Helicobacter pylori*: molecular basis for colonization and survival in gastric environment and resistance to antibiotics. A short review. Infect Dis (Lond) [Internet]. 2019 Jun 3 [cited 2023 Apr 14];51(6):399–408. Available from: https://pubmed.ncbi.nlm.nih.gov/30907202/
2. Konturek SJ, Konturek PC, Brzozowski T, Konturek JW, Pawlik WW. FROM NERVES AND HORMONES TO BACTERIA IN THE STOMACH; NOBEL PRIZE FOR ACHIEVEMENTS IN GASTROLOGY DURING LAST CENTURY. JOURNAL OF PHYSIOLOGY AND PHARMACOLOGY [Internet]. 2005 [cited 2023 Apr 14];56:507–30. Available from: www.jpp.krakow.pl
3. Marshall BJ, Armstrong JA, McGechie DB, Glancy RJ. Attempt to fulfil Koch's postulates for pyloric Campylobacter. Medical Journal of Australia [Internet]. 1985 Apr 1 [cited 2023 Apr 14];142(8):436–9. Available from: https://onlinelibrary.wiley.com/doi/full/10.5694/j.1326-5377.1985.tb113443.x
4. Goodwin CS, Armstrong JA. Microbiological aspects of *Helicobacter pylori* (*Campylobacter pylori*). Eur J Clin Microbiol Infect Dis [Internet]. 1990 Jan [cited 2023 Apr 14];9(1):1–13. Available from: https://pubmed.ncbi.nlm.nih.gov/2406141/
5. The National Institutes of Health (NIH) Consensus Development Program: *Helicobacter Pylori*</i> in Peptic Ulcer Disease [Internet]. [cited 2023 Apr 14]. Available from: https://consensus.nih.gov/1994/1994helicobacterpyloriulcer094html.htm
6. Zhu HM, Li BY, Tang Z, She J, Liang XY, Dong LK, et al. Epidemiological investigation of *Helicobacter pylori* infection in elderly people in Beijing. World J Clin Cases [Internet]. 2020 Jun 6 [cited 2023 Apr 14];8(11):2173. Available from: /pmc/articles/PMC7281052/
7. Khalifa MM, Sharaf RR, Aziz RK. *Helicobacter pylori*: a poor man's gut pathogen? Gut Pathog [Internet]. 2010 [cited 2023 Apr 14];2(1). Available from: https://pubmed.ncbi.nlm.nih.gov/20356368/
8. Kayali S, Manfredi M, Gaiani F, Bianchi L, Bizzarri B, Leandro G, et al. *Helicobacter pylori*, transmission routes and recurrence of infection: state of the art. Acta Biomed [Internet]. 2018 [cited 2023 Apr 14];89(8-S):72–6. Available from: https://pubmed.ncbi.nlm.nih.gov/30561421/
9. Wroblewski LE, Peek RM, Wilson KT. *Helicobacter pylori* and gastric cancer: factors that modulate disease risk. Clin Microbiol Rev [Internet]. 2010 Oct [cited 2023 Apr 14];23(4):713–39. Available from: https://pubmed.ncbi.nlm.nih.gov/20930071/
10. List of Classifications – IARC Monographs on the Identification of Carcinogenic Hazards to Humans [Internet]. [cited 2023 Apr 14]. Available from: https://monographs.iarc.who.int/list-of-classifications/

11. Amieva M, Peek RM. Pathobiology of *Helicobacter pylori*–Induced Gastric Cancer. Gastroenterology [Internet]. 2016 Jan 1 [cited 2023 Apr 15];150(1):64–78. Available from: http://www.gastrojournal.org/article/S0016508515013128/fulltext
12. Asaka M, Sepulveda AR, Sugiyama T, Graham DY. Gastric Cancer. *Helicobacter pylori*: Physiology and Genetics [Internet]. 2001 [cited 2023 Apr 15]; Available from: https://www.ncbi.nlm.nih.gov/books/NBK2445/
13. Pellicano R, Ianiro G, Fagoonee S, Settanni CR, Gasbarrini A. Review: Extragastric diseases and *Helicobacter pylori*. Helicobacter [Internet]. 2020 Sep 1 [cited 2023 Apr 15];25(S1):e12741. Available from: https://onlinelibrary.wiley.com/doi/full/10.1111/hel.12741
14. Gravina AG, Zagari RM, De Musis C, Romano L, Loguercio C, Romano M. *Helicobacter pylori* and extragastric diseases: A review. World J Gastroenterol [Internet]. 2018 Aug 8 [cited 2023 Apr 15];24(29):3204. Available from: /pmc/articles/PMC6079286/
15. Wang YK, Kuo FC, Liu CJ, Wu MC, Shih HY, Wang SSW, et al. Diagnosis of *Helicobacter pylori* infection: Current options and developments. World Journal of Gastroenterology : WJG [Internet]. 2015 Oct 10 [cited 2023 Apr 15];21(40):11221. Available from: /pmc/articles/PMC4616200/
16. Takashima T, Fujiwara Y, Watanabe T, Tominaga K, Oshitani N, Higuchi K, et al. Current concepts in the management of *Helicobacter pylori* infection--the Maastricht 2-2000 Consensus Report. Aliment Pharmacol Ther [Internet]. 2002 Apr [cited 2023 Apr 16];16(2):167–73. Available from: https://pubmed.ncbi.nlm.nih.gov/11860399/
17. Garza-González E, Perez-Perez GI, Maldonado-Garza HJ, Bosques-Padilla FJ. A review of *Helicobacter pylori* diagnosis, treatment, and methods to detect eradication. World J Gastroenterol [Internet]. 2014 Feb 14 [cited 2023 Apr 16];20(6):1438–49. Available from: https://pubmed.ncbi.nlm.nih.gov/24587620/
18. WHO publishes list of bacteria for which new antibiotics are urgently needed [Internet]. [cited 2023 Apr 16]. Available from: https://www.who.int/news/item/27-02-2017-who-publishes-list-of-bacteria-for-which-new-antibiotics-are-urgently-needed
19. Kao CY, Sheu BS, Wu JJ. *Helicobacter pylori* infection: An overview of bacterial virulence factors and pathogenesis. Biomed J. 2016 Feb 1;39(1):14–23.
20. Cletus Sharndama H, Elibe Mba I. *Helicobacter pylori*: an up-to-date overview on the virulence and pathogenesis mechanisms. Brazilian Journal of Microbiology [Internet]. 2022 [cited 2023 Apr 16];1:3. Available from: https://doi.org/10.1007/s42770-021-00675-0
21. Matsumoto Y, Marusawa H, Kinoshita K, Endo Y, Kou T, Morisawa T, et al. *Helicobacter pylori* infection triggers aberrant expression of activation-induced cytidine deaminase in gastric epithelium. Nature Medicine 2007 13:4 [Internet]. 2007 Apr 1 [cited 2023 Apr 17];13(4):470–6. Available from: https://www.nature.com/articles/nm1566
22. Cheok YY, Lee CYQ, Cheong HC, Vadivelu J, Looi CY, Abdullah S, et al. An Overview of *Helicobacter pylori* Survival Tactics in the Hostile Human Stomach Environment.

Microorganisms 2021, Vol 9, Page 2502 [Internet]. 2021 Dec 3 [cited 2023 Apr 25];9(12):2502. Available from: https://www.mdpi.com/2076-2607/9/12/2502/htm

23. Skouloubris S, Thiberge JM, Labigne A, De Reuse H. The *Helicobacter pylori* UreI protein is not involved in urease activity but is essential for bacterial survival in vivo. Infect Immun [Internet]. 1998 [cited 2023 Apr 17];66(9):4517–21. Available from: https://journals.asm.org/journal/iai
24. Ghalehnoei H, Ahmadzadeh A, Farzi N, Alebouyeh M, Aghdaei HA, Azimzadeh P, et al. Relationship between ureB sequence diversity, urease activity and genotypic variations of different *Helicobacter pylori* strains in patients with gastric disorders. Pol J Microbiol. 2016;65(2):153–9.
25. Yamaoka Y, Graham DY. *Helicobacter pylori* virulence and cancer pathogenesis. Future Oncol [Internet]. 2014 [cited 2023 Apr 18];10(8):1487. Available from: /pmc/articles/PMC4197059/
26. Tegtmeyer N, Wessler S, Backert S. Role of the cag-pathogenicity island encoded type IV secretion system in *Helicobacter pylori* pathogenesis. FEBS J [Internet]. 2011 Apr [cited 2023 Apr 18];278(8):1190–202. Available from: https://pubmed.ncbi.nlm.nih.gov/21352489/
27. Kwok T, Zabler D, Urman S, Rohde M, Hartig R, Wessler S, et al. Helicobacter exploits integrin for type IV secretion and kinase activation.
28. Chang CC, Kuo WS, Chen YC, Perng CL, Lin HJ, Ou YH. Fragmentation of CagA Reduces Hummingbird Phenotype Induction by *Helicobactor pylori*. PLoS One [Internet]. 2016 Mar 1 [cited 2023 Apr 18];11(3). Available from: /pmc/articles/PMC4775065/
29. Gorrell RJ, Guan J, Xin Y, Tafreshi MA, Hutton ML, Mcguckin MA, et al. A novel NOD1- and CagA-independent pathway of interleukin-8 induction mediated by the *Helicobacter pylori* type IV secretion system. Cell Microbiol [Internet]. 2013 Apr 1 [cited 2023 Apr 18];15(4):554–70. Available from: https://onlinelibrary.wiley.com/doi/full/10.1111/cmi.12055
30. Lamb A, Yang XD, Tsang YHN, Li JD, Higashi H, Hatakeyama M, et al. *Helicobacter pylori* CagA activates NF-kappaB by targeting TAK1 for TRAF6-mediated Lys 63 ubiquitination. EMBO Rep [Internet]. 2009 [cited 2023 Apr 18];10(11):1242–9. Available from: https://pubmed.ncbi.nlm.nih.gov/19820695/
31. Mashima H, Suzuki J, Hirayama T, Yoshikumi Y, Ohno H, Ohnishi H, et al. Involvement of vesicle-associated membrane protein 7 in human gastric epithelial cell vacuolation induced by *Helicobacter pylori*-produced VacA. Infect Immun [Internet]. 2008 Jun [cited 2023 Apr 18];76(6):2296–303. Available from: https://pubmed.ncbi.nlm.nih.gov/18362137/
32. Boncristiano M, Paccani SR, Barone S, Ulivieri C, Patrussi L, Ilver D, et al. The *Helicobacter pylori* vacuolating toxin inhibits T cell activation by two independent mechanisms. J Exp Med [Internet]. 2003 Dec 15 [cited 2023 Apr 18];198(12):1887–97. Available from: https://pubmed.ncbi.nlm.nih.gov/14676300/
33. Zheng PY, Jones NL. *Helicobacter pylori* strains expressing the vacuolating cytotoxin interrupt phagosome maturation in macrophages by recruiting and retaining TACO (coronin

1) protein. Cell Microbiol [Internet]. 2003 Jan 1 [cited 2023 Apr 18];5(1):25–40. Available from: https://pubmed.ncbi.nlm.nih.gov/12542468/

34. Papini E, Satin B, Norais N, De Bernard M, Telford JL, Rappuoli R, et al. Selective increase of the permeability of polarized epithelial cell monolayers by *Helicobacter pylori* vacuolating toxin. J Clin Invest [Internet]. 1998 Aug 15 [cited 2023 Apr 18];102(4):813–20. Available from: https://pubmed.ncbi.nlm.nih.gov/9710450/

35. Yamasaki E, Wada A, Kumatori A, Nakagawa I, Funao J, Nakayama M, et al. *Helicobacter pylori* vacuolating cytotoxin induces activation of the proapoptotic proteins Bax and Bak, leading to cytochrome c release and cell death, independent of vacuolation. J Biol Chem [Internet]. 2006 Apr 21 [cited 2023 Apr 18];281(16):11250–9. Available from: https://pubmed.ncbi.nlm.nih.gov/16436379/

36. Galmiche A, Rassow J, Doye A, Cagnol S, Chambard JC, Contamin S, et al. The N-terminal 34 kDa fragment of *Helicobacter pylori* vacuolating cytotoxin targets mitochondria and induces cytochrome c release. EMBO J [Internet]. 2000 Dec 1 [cited 2023 Apr 18];19(23):6361–70. Available from: https://pubmed.ncbi.nlm.nih.gov/11101509/

37. Yamaoka Y. Mechanisms of disease: *Helicobacter pylori* virulence factors. Nat Rev Gastroenterol Hepatol [Internet]. 2010 Nov [cited 2023 Apr 18];7(11):629–41. Available from: https://pubmed.ncbi.nlm.nih.gov/20938460/

38. Yokoyama K, Higashi H, Ishikawa S, Fujii Y, Kondo S, Kato H, et al. Functional antagonism between *Helicobacter pylori* CagA and vacuolating toxin VacA in control of the NFAT signaling pathway in gastric epithelial cells. Proc Natl Acad Sci U S A [Internet]. 2005 Jul 5 [cited 2023 Apr 18];102(27):9661–6. Available from: https://pubmed.ncbi.nlm.nih.gov/15980153/

39. Argent RH, Thomas RJ, Letley DP, Rittig MG, Hardie KR, Atherton JC. Functional association between the *Helicobacter pylori* virulence factors VacA and CagA. J Med Microbiol [Internet]. 2008 Feb [cited 2023 Apr 18];57(Pt 2):145–50. Available from: https://pubmed.ncbi.nlm.nih.gov/18201978/

40. Jang S, Jones KR, Olsen CH, Joo YM, Yoo YJ, Chung IS, et al. Epidemiological link between gastric disease and polymorphisms in VacA and CagA. J Clin Microbiol [Internet]. 2010 Feb [cited 2023 Apr 18];48(2):559–67. Available from: https://pubmed.ncbi.nlm.nih.gov/19955279/

41. Oleastro M, Ménard A. The Role of *Helicobacter pylori* Outer Membrane Proteins in Adherence and Pathogenesis. Biology 2013, Vol 2, Pages 1110-1134 [Internet]. 2013 Aug 27 [cited 2023 Apr 25];2(3):1110–34. Available from: https://www.mdpi.com/2079-7737/2/3/1110/htm

42. Sijmons D, Guy AJ, Walduck AK, Ramsland PA. *Helicobacter pylori* and the Role of Lipopolysaccharide Variation in Innate Immune Evasion. Front Immunol. 2022 May 13;13:1943.

43. Ansari S, Yamaoka Y. *Helicobacter pylori* BabA in adaptation for gastric colonization. World J Gastroenterol [Internet]. 2017 Jun 21 [cited 2023 Apr 18];23(23):4158–69. Available from: https://pubmed.ncbi.nlm.nih.gov/28694656/
44. Benktander J, Ångström J, Breimer ME, Teneberg S. Redefinition of the carbohydrate binding specificity of *Helicobacter pylori* BabA adhesin. J Biol Chem [Internet]. 2012 Sep 14 [cited 2023 Apr 18];287(38):31712–24. Available from: https://pubmed.ncbi.nlm.nih.gov/22822069/
45. Sáenz JB, Vargas N, Mills JC. Tropism for Spasmolytic Polypeptide-Expressing Metaplasia Allows *Helicobacter pylori* to Expand Its Intragastric Niche. Gastroenterology [Internet]. 2019 Jan 1 [cited 2023 Apr 18];156(1):160-174.e7. Available from: http://www.gastrojournal.org/article/S0016508518350819/fulltext
46. Sheu BS, Odenbreit S, Hung KH, Liu CP, Sheu SM, Yang HB, et al. Interaction Between Host Gastric Sialyl-Lewis X and H. pylor... : Official journal of the American College of Gastroenterology | ACG. American Journal of Gastroenterology [Internet]. 2006 [cited 2023 Apr 18];101(1):36–44. Available from: https://journals.lww.com/ajg/Abstract/2006/01000/Interaction_Between_Host_Gastric_Sialyl_Lewis_X.9.aspx
47. Yanai A, Maeda S, Hikiba Y, Shibata W, Ohmae T, Hirata Y, et al. Clinical relevance of *Helicobacter pylori* sabA genotype in Japanese clinical isolates. J Gastroenterol Hepatol [Internet]. 2007 Dec 1 [cited 2023 Apr 18];22(12):2228–32. Available from: https://onlinelibrary.wiley.com/doi/full/10.1111/j.1440-1746.2007.04831.x
48. Kato S, Osaki T, Kamiya S, Zhang XS, Blaser MJ. *Helicobacter pylori* sabA gene is associated with iron deficiency anemia in childhood and adolescence. PLoS One [Internet]. 2017 Aug 1 [cited 2023 Apr 18];12(8):e0184046. Available from: https://journals.plos.org/plosone/article?id=10.1371/journal.pone.0184046
49. Su YL, Huang HL, Huang BS, Chen PC, Chen CS, Wang HL, et al. Combination of OipA, BabA, and SabA as candidate biomarkers for predicting *Helicobacter pylori*-related gastric cancer. Sci Rep [Internet]. 2016 Nov 7 [cited 2023 Apr 18];6. Available from: https://pubmed.ncbi.nlm.nih.gov/27819260/
50. Yamaoka Y, Kwon DH, Graham DY. A Mr 34,000 proinflammatory outer membrane protein (oipA) of *Helicobacter pylori*. Proc Natl Acad Sci U S A [Internet]. 2000 Jun 20 [cited 2023 Apr 18];97(13):7533–8. Available from: https://www.pnas.org/doi/abs/10.1073/pnas.130079797
51. Yamaoka Y, Kikuchi S, ElZimaity HMT, Gutierrez O, Osato MS, Graham DY. Importance of *Helicobacter pylori* oipA in clinical presentation, gastric inflammation, and mucosal interleukin 8 production. Gastroenterology [Internet]. 2002 [cited 2023 Apr 18];123(2):414–24. Available from: https://pubmed.ncbi.nlm.nih.gov/12145793/
52. Tabassam FH, Graham DY, Yamaoka Y. OipA plays a role in *Helicobacter pylori*-induced focal adhesion kinase activation and cytoskeletal re-organization. Cell Microbiol [Internet].

2008 Apr [cited 2023 Apr 18];10(4):1008–20. Available from: https://pubmed.ncbi.nlm.nih.gov/18067607/

53. Yang ZM, Chen WW, Wang YF. Gene Expression Profiling in Gastric Mucosa from *Helicobacter pylori*-Infected and Uninfected Patients Undergoing Chronic Superficial Gastritis. PLoS One [Internet]. 2012 Mar 16 [cited 2023 Apr 18];7(3):e33030. Available from: https://journals.plos.org/plosone/article?id=10.1371/journal.pone.0033030

54. Horridge DN, Begley AA, Kim J, Aravindan N, Fan K, Forsyth MH. Outer inflammatory protein a (OipA) of *Helicobacter pylori* is regulated by host cell contact and mediates CagA translocation and interleukin-8 response only in the presence of a functional cag pathogenicity island type IV secretion system. Pathog Dis [Internet]. 2017 Nov 30 [cited 2023 Apr 18];75(8). Available from: https://academic.oup.com/femspd/article/75/8/ftx113/4494363

55. Zhang J, Qian J, Zhang X, Zou Q. Outer membrane inflammatory protein A, a new virulence factor involved in the pathogenesis of *Helicobacter pylori*. Mol Biol Rep [Internet]. 2014 Dec 1 [cited 2023 Apr 18];41(12):7807–14. Available from: https://link.springer.com/article/10.1007/s11033-014-3673-9

56. Zhao Q, Yin W, Zhao R, Wang Y, Song C, Wang H, et al. Outer inflammatory protein of *Helicobacter pylori* impacts IL-8 expression, adherence, cell apoptosis and cell cycle of gastric cells independent of its copy number. Med Microbiol Immunol [Internet]. 2020 Oct 1 [cited 2023 Apr 18];209(5):621–30. Available from: https://link.springer.com/article/10.1007/s00430-020-00688-w

57. Sugimoto M, Ohno T, Graham DY, Yamaoka Y. Gastric mucosal interleukin-17 and -18 mRNA expression in *Helicobacter pylori*-induced Mongolian gerbils. Cancer Sci [Internet]. 2009 Nov [cited 2023 Apr 18];100(11):2152–9. Available from: https://pubmed.ncbi.nlm.nih.gov/19694753/

58. Sakurai Y, Otani Y, Kameyama K, Hosoda Y, Okazaki I, Kubota T, et al. Expression of interstitial collagenase (matrix metalloproteinase-1) in gastric cancers. Jpn J Cancer Res [Internet]. 1997 [cited 2023 Apr 18];88(4):401–6. Available from: https://pubmed.ncbi.nlm.nih.gov/9197533/

59. Teymournejad O, Mobarez AM, Hassan ZM, Moazzeni SM, Ahmadabad HN. In Vitro Suppression of Dendritic Cells by *Helicobacter pylori* OipA. Helicobacter. 2014;19(2):136–43.

60. M. Calvino-Fernández, T. Parra-Cid. *H. pylori* and mitochondrial changes in epithelial cells. The role of oxidative stress. 2010.

61. Ashktorab H, Dashwood RH, Dashwood MM, Zaidi SI, Hewitt SM, Green WR, et al. *H. pylori*-Induced Apoptosis in Human Gastric Cancer Cells Mediated via the Release of Apoptosis-Inducing Factor from Mitochondria. 2008;

62. Capurro MI, Greenfield LK, Prashar A, Xia S, Abdullah M, Wong H, et al. VacA generates a protective intracellular reservoir for *Helicobacter pylori* that is eliminated by activation of the lysosomal calcium channel TRPML1. Nat Microbiol. 2019 Aug 1;4(8):1411–23.
63. Teymournejad O, Mobarez AM, Hassan ZM, Talebi Bezmin Abadi A. Binding of the *Helicobacter pylori* OipA causes apoptosis of host cells via modulation of Bax/Bcl-2 levels. Scientific Reports 2017 7:1 [Internet]. 2017 Aug 14 [cited 2023 Apr 18];7(1):1–8. Available from: https://www.nature.com/articles/s41598-017-08176-7
64. De Bruyne E, Ducatelle R, Foss D, Sanchez M, Joosten M, Zhang G, et al. Oral glutathione supplementation drastically reduces Helicobacter-induced gastric pathologies. Scientific Reports 2016 6:1 [Internet]. 2016 Feb 2 [cited 2023 Apr 19];6(1):1–13. Available from: https://www.nature.com/articles/srep20169
65. Amagase K, Nakamura E, Kato S, Takeuchi K. [Prophylactic effect of glutamate on gastrointestinal damage]. Yakugaku Zasshi [Internet]. 2011 [cited 2023 Apr 19];131(12):1711–9. Available from: https://pubmed.ncbi.nlm.nih.gov/22129864/
66. Du J, Li XH, Liu F, Li WQ, Gong ZC, Li YJ. Role of the Outer Inflammatory Protein A/Cystine-Glutamate Transporter Pathway in Gastric Mucosal Injury Induced by *Helicobacter pylori*. Clin Transl Gastroenterol. 2020 May 26;11(5):E00178.
67. Evonuk KS, Baker BJ, Doyle RE, Moseley CE, Sestero CM, Johnston BP, et al. Inhibition of System Xc(-) Transporter Attenuates Autoimmune Inflammatory Demyelination. J Immunol [Internet]. 2015 Jul 15 [cited 2023 Apr 19];195(2):450–63. Available from: https://pubmed.ncbi.nlm.nih.gov/26071560/
68. Schlaermann P, Toelle B, Berger H, Schmidt SC, Glanemann M, Ordemann J, et al. A novel human gastric primary cell culture system for modelling *Helicobacter pylori* infection in vitro. Gut [Internet]. 2016 Feb 1 [cited 2023 Apr 19];65(2):202–13. Available from: https://gut.bmj.com/content/65/2/202
69. Zakrzewski W, Dobrzyński M, Szymonowicz M, Rybak Z. Stem cells: Past, present, and future. Stem Cell Res Ther [Internet]. 2019 Feb 26 [cited 2023 Apr 19];10(1):1–22. Available from: https://stemcellres.biomedcentral.com/articles/10.1186/s13287-019-1165-5
70. Pennings S, Liu KJ, Qian H. The Stem Cell Niche: Interactions between Stem Cells and Their Environment. Stem Cells Int [Internet]. 2018 [cited 2023 Apr 19];2018. Available from: /pmc/articles/PMC6204189/
71. Orkin RW, Gehron P, McGoodwin EB, Martin GR, Valentine T, Swarm R. A murine tumor producing a matrix of basement membrane. J Exp Med [Internet]. 1977 Jan 1 [cited 2023 Apr 19];145(1):204–20. Available from: https://pubmed.ncbi.nlm.nih.gov/830788/
72. Li ML, Aggeler J, Farson DA, Hatier C, Hassell J, Bissell MJ. Influence of a reconstituted basement membrane and its components on casein gene expression and secretion in mouse mammary epithelial cells. Proc Natl Acad Sci U S A [Internet]. 1987 [cited 2023 Apr 19];84(1):136. Available from: /pmc/articles/PMC304157/?report=abstract

73. Sato T, Vries RG, Snippert HJ, Van De Wetering M, Barker N, Stange DE, et al. Single Lgr5 stem cells build crypt-villus structures in vitro without a mesenchymal niche. Nature. 2009;
74. Barker N, Van Es JH, Kuipers J, Kujala P, Van Den Born M, Cozijnsen M, et al. Identification of stem cells in small intestine and colon by marker gene Lgr5. Nature [Internet]. 2007 Oct 25 [cited 2023 Apr 19];449(7165):1003–7. Available from: https://pubmed.ncbi.nlm.nih.gov/17934449/
75. Fatehullah A, Tan SH, Barker N. Organoids as an in vitro model of human development and disease. Nat Cell Biol [Internet]. 2016 Feb 25 [cited 2023 Apr 19];18(3):246–54. Available from: https://pubmed.ncbi.nlm.nih.gov/26911908/
76. Clevers H. Modeling Development and Disease with Organoids. Cell [Internet]. 2016 Jun 16 [cited 2023 Apr 19];165(7):1586–97. Available from: https://pubmed.ncbi.nlm.nih.gov/27315476/
77. Barker N, Huch M, Kujala P, van de Wetering M, Snippert HJ, van Es JH, et al. Lgr5+ve Stem Cells Drive Self-Renewal in the Stomach and Build Long-Lived Gastric Units In Vitro. Cell Stem Cell [Internet]. 2010 Jan 8 [cited 2023 Apr 20];6(1):25–36. Available from: http://www.cell.com/article/S1934590909006183/fulltext
78. Huch M, Gehart H, Van Boxtel R, Hamer K, Blokzijl F, Verstegen MMA, et al. Long-Term Culture of Genome-Stable Bipotent Stem Cells from Adult Human Liver. Cell [Internet]. 2015 Jan 1 [cited 2023 Apr 20];160(1–2):299. Available from: /pmc/articles/PMC4313365/
79. Lancaster MA, Renner M, Martin CA, Wenzel D, Bicknell LS, Hurles ME, et al. Cerebral organoids model human brain development and microcephaly. Nature 2013 501:7467 [Internet]. 2013 Aug 28 [cited 2023 Apr 20];501(7467):373–9. Available from: https://www.nature.com/articles/nature12517
80. Morizane R, Lam AQ, Freedman BS, Kishi S, Valerius MT, Bonventre J V. Nephron organoids derived from human pluripotent stem cells model kidney development and injury. Nat Biotechnol [Internet]. 2015 Oct 6 [cited 2023 Apr 20];33(11):1193–200. Available from: https://pubmed.ncbi.nlm.nih.gov/26458176/
81. Driehuis E, Gracanin A, Vries RGJ, Clevers H, Boj SF. Establishment of Pancreatic Organoids from Normal Tissue and Tumors. STAR Protoc. 2020 Dec 18;1(3):100192.
82. Zhao Z, Chen X, Dowbaj AM, Sljukic A, Bratlie K, Lin L, et al. Organoids. Nature Reviews Methods Primers 2022 2:1 [Internet]. 2022 Dec 1 [cited 2023 Apr 20];2(1):1–21. Available from: https://www.nature.com/articles/s43586-022-00174-y
83. Sato T, Stange DE, Ferrante M, Vries RGJ, Van Es JH, Van Den Brink S, et al. Long-term expansion of epithelial organoids from human colon, adenoma, adenocarcinoma, and Barrett's epithelium. Gastroenterology [Internet]. 2011 [cited 2023 Apr 20];141(5):1762–72. Available from: https://pubmed.ncbi.nlm.nih.gov/21889923/
84. Cruz-Acuña R, Quirós M, Farkas AE, Dedhia PH, Huang S, Siuda D, et al. Synthetic hydrogels for human intestinal organoid generation and colonic wound repair. Nat Cell Biol

[Internet]. 2017 Nov 1 [cited 2023 Apr 20];19(11):1326–35. Available from: https://pubmed.ncbi.nlm.nih.gov/29058719/

85. Ladoux B, Mège RM. Mechanobiology of collective cell behaviours. Nature Reviews Molecular Cell Biology 2017 18:12 [Internet]. 2017 Nov 8 [cited 2023 Apr 20];18(12):743–57. Available from: https://www.nature.com/articles/nrm.2017.98
86. Karzbrun E, Khankhel AH, Megale HC, Glasauer SMK, Wyle Y, Britton G, et al. Human neural tube morphogenesis in vitro by geometric constraints. Nature [Internet]. 2021 Nov 11 [cited 2023 Apr 20];599(7884):268–72. Available from: https://pubmed.ncbi.nlm.nih.gov/34707290/
87. Peng H, Poovaiah N, Forrester M, Cochran E, Wang Q. Ex Vivo Culture of Primary Intestinal Stem Cells in Collagen Gels and Foams. ACS Biomater Sci Eng [Internet]. 2015 Dec 14 [cited 2023 Apr 20];1(1):37–42. Available from: https://pubs.acs.org/doi/abs/10.1021/ab500041d
88. Goonoo N, Bhaw-Luximon A. Mimicking growth factors: role of small molecule scaffold additives in promoting tissue regeneration and repair. RSC Adv [Internet]. 2019 Jun 10 [cited 2023 Apr 20];9(32):18124–46. Available from: https://pubs.rsc.org/en/content/articlehtml/2019/ra/c9ra02765c
89. Siller R, Greenhough S, Naumovska E, Sullivan GJ. Small-molecule-driven hepatocyte differentiation of human pluripotent stem cells. Stem Cell Reports [Internet]. 2015 May 12 [cited 2023 Apr 20];4(5):939–52. Available from: https://pubmed.ncbi.nlm.nih.gov/25937370/
90. Janda CY, Dang LT, You C, Chang J, Lau W De, Zhong ZA, et al. Surrogate Wnt agonists that phenocopy canonical Wnt and β-catenin signalling. Nature 2017 545:7653 [Internet]. 2017 May 3 [cited 2023 Apr 20];545(7653):234–7. Available from: https://www.nature.com/articles/nature22306
91. Miao Y, Ha A, de Lau W, Yuki K, Santos AJM, You C, et al. Next-Generation Surrogate Wnts Support Organoid Growth and Deconvolute Frizzled Pleiotropy In Vivo. Cell Stem Cell [Internet]. 2020 Nov 5 [cited 2023 Apr 20];27(5):840-851.e6. Available from: https://pubmed.ncbi.nlm.nih.gov/32818433/
92. Below CR, Kelly J, Brown A, Humphries JD, Hutton C, Xu J, et al. A microenvironment-inspired synthetic three-dimensional model for pancreatic ductal adenocarcinoma organoids. Nature Materials 2021 21:1 [Internet]. 2021 Sep 13 [cited 2023 Apr 20];21(1):110–9. Available from: https://www.nature.com/articles/s41563-021-01085-1
93. Homan KA, Gupta N, Kroll KT, Kolesky DB, Skylar-Scott M, Miyoshi T, et al. Flow-enhanced vascularization and maturation of kidney organoids in vitro. Nature Methods 2019 16:3 [Internet]. 2019 Feb 11 [cited 2023 Apr 20];16(3):255–62. Available from: https://www.nature.com/articles/s41592-019-0325-y
94. Rimland CA, Tilson SG, Morell CM, Tomaz RA, Lu WY, Adams SE, et al. Regional Differences in Human Biliary Tissues and Corresponding In Vitro-Derived Organoids.

Hepatology [Internet]. 2021 Jan 1 [cited 2023 Apr 20];73(1):247–67. Available from: https://pubmed.ncbi.nlm.nih.gov/32222998/

95. Marx V. Cell-line authentication demystified. Nat Methods [Internet]. 2014 [cited 2023 Apr 20];11(5):483–8. Available from: https://pubmed.ncbi.nlm.nih.gov/24781320/

96. Masters JR, Stacey GN. Changing medium and passaging cell lines. Nat Protoc [Internet]. 2007 Sep [cited 2023 Apr 20];2(9):2276–84. Available from: https://pubmed.ncbi.nlm.nih.gov/17853884/

97. Al Shihabi A, Davarifar A, Lam Nguyen HT, Tavanaie N, Nelson SD, Yanagawa J, et al. Personalized chordoma organoids for drug discovery studies. Sci Adv [Internet]. 2022 Feb 1 [cited 2023 Apr 20];8(7). Available from: https://pubmed.ncbi.nlm.nih.gov/35171675/

98. Tebon PJ, Wang B, Markowitz AL, Davarifar A, Krawczuk P, Murray G, et al. Drug screening at single-organoid resolution via bioprinting and interferometry. bioRxiv [Internet]. 2022 Apr 20 [cited 2023 Apr 20];2021.10.03.462896. Available from: https://www.biorxiv.org/content/10.1101/2021.10.03.462896v2

99. Phan N, Hong JJ, Tofig B, Mapua M, Elashoff D, Moatamed NA, et al. A simple high-throughput approach identifies actionable drug sensitivities in patient-derived tumor organoids. Commun Biol [Internet]. 2019 Dec 1 [cited 2023 Apr 20];2(1). Available from: https://pubmed.ncbi.nlm.nih.gov/30820473/

100. Chen J, Zhao L, Peng H, Dai S, Quan Y, Wang M, et al. An organoid-based drug screening identified a menin-MLL inhibitor for endometrial cancer through regulating the HIF pathway. Cancer Gene Ther [Internet]. 2021 Feb 1 [cited 2023 Apr 20];28(1–2):112–25. Available from: https://pubmed.ncbi.nlm.nih.gov/32632269/

101. Verissimo CS, Overmeer RM, Ponsioen B, Drost J, Mertens S, Verlaan-Klink I, et al. Targeting mutant RAS in patient-derived colorectal cancer organoids by combinatorial drug screening. Elife [Internet]. 2016 Nov 15 [cited 2023 Apr 20];5(NOVEMBER2016). Available from: https://pubmed.ncbi.nlm.nih.gov/27845624/

102. Nuciforo S, Fofana I, Matter MS, Blumer T, Calabrese D, Boldanova T, et al. Organoid Models of Human Liver Cancers Derived from Tumor Needle Biopsies. Cell Rep [Internet]. 2018 Jul 31 [cited 2023 Apr 20];24(5):1363–76. Available from: https://pubmed.ncbi.nlm.nih.gov/30067989/

103. Schnalzger TE, Groot MH, Zhang C, Mosa MH, Michels BE, Röder J, et al. 3D model for CAR-mediated cytotoxicity using patient-derived colorectal cancer organoids. EMBO J [Internet]. 2019 Jun 17 [cited 2023 Apr 20];38(12). Available from: https://pubmed.ncbi.nlm.nih.gov/31036555/

104. Neal JT, Li X, Zhu J, Giangarra V, Grzeskowiak CL, Ju J, et al. Organoid Modeling of the Tumor Immune Microenvironment. Cell [Internet]. 2018 Dec 13 [cited 2023 Apr 20];175(7):1972-1988.e16. Available from: https://pubmed.ncbi.nlm.nih.gov/30550791/

105. Yui S, Nakamura T, Sato T, Nemoto Y, Mizutani T, Zheng X, et al. Functional engraftment of colon epithelium expanded in vitro from a single adult $Lgr5^+$ stem cell. Nat Med [Internet].

2012 Apr [cited 2023 Apr 21];18(4):618–23. Available from: https://pubmed.ncbi.nlm.nih.gov/22406745/

106. Hu H, Gehart H, Artegiani B, LÖpez-Iglesias C, Dekkers F, Basak O, et al. Long-Term Expansion of Functional Mouse and Human Hepatocytes as 3D Organoids. Cell [Internet]. 2018 Nov 29 [cited 2023 Apr 21];175(6):1591-1606.e19. Available from: https://pubmed.ncbi.nlm.nih.gov/30500538/

107. Peng WC, Logan CY, Fish M, Anbarchian T, Aguisanda F, Álvarez-Varela A, et al. Inflammatory Cytokine TNFα Promotes the Long-Term Expansion of Primary Hepatocytes in 3D Culture. Cell [Internet]. 2018 Nov 29 [cited 2023 Apr 21];175(6):1607-1619.e15. Available from: https://pubmed.ncbi.nlm.nih.gov/30500539/

108. Loomans CJM, Williams Giuliani N, Balak J, Ringnalda F, van Gurp L, Huch M, et al. Expansion of Adult Human Pancreatic Tissue Yields Organoids Harboring Progenitor Cells with Endocrine Differentiation Potential. Stem Cell Reports [Internet]. 2018 Mar 13 [cited 2023 Apr 21];10(3):712–24. Available from: https://pubmed.ncbi.nlm.nih.gov/29539434/

109. Georgakopoulos N, Prior N, Angres B, Mastrogiovanni G, Cagan A, Harrison D, et al. Long-term expansion, genomic stability and in vivo safety of adult human pancreas organoids. BMC Dev Biol [Internet]. 2020 Feb 26 [cited 2023 Apr 21];20(1). Available from: /pmc/articles/PMC7043048/

110. Elizondo DM, Brandy NZD, da Silva RLL, de Moura TR, Ali J, Yang D, et al. Pancreatic islets seeded in a novel bioscaffold forms an organoid to rescue insulin production and reverse hyperglycemia in models of type 1 diabetes. Scientific Reports 2020 10:1 [Internet]. 2020 Mar 9 [cited 2023 Apr 21];10(1):1–11. Available from: https://www.nature.com/articles/s41598-020-60947-x

111. Huch M, Dorrell C, Boj SF, Van Es JH, Li VSW, Van De Wetering M, et al. In vitro expansion of single Lgr5+ liver stem cells induced by Wnt-driven regeneration. Nature 2013 494:7436 [Internet]. 2013 Jan 27 [cited 2023 Apr 21];494(7436):247–50. Available from: https://www.nature.com/articles/nature11826

112. Vives J, Batlle-Morera L. The challenge of developing human 3D organoids into medicines. Stem Cell Res Ther [Internet]. 2020 Mar 4 [cited 2023 Apr 21];11(1):1–4. Available from: https://stemcellres.biomedcentral.com/articles/10.1186/s13287-020-1586-1

113. Fujii M, Shimokawa M, Date S, Takano A, Matano M, Nanki K, et al. A Colorectal Tumor Organoid Library Demonstrates Progressive Loss of Niche Factor Requirements during Tumorigenesis. Cell Stem Cell [Internet]. 2016 Jun 2 [cited 2023 Apr 21];18(6):827–38. Available from: https://pubmed.ncbi.nlm.nih.gov/27212702/

114. Kim M, Mun H, Sung CO, Cho EJ, Jeon HJ, Chun SM, et al. Patient-derived lung cancer organoids as in vitro cancer models for therapeutic screening. Nat Commun [Internet]. 2019 Dec 1 [cited 2023 Apr 21];10(1). Available from: https://pubmed.ncbi.nlm.nih.gov/31488816/

115. Lõhmussaar K, Oka R, Espejo Valle-Inclan J, Smits MHH, Wardak H, Korving J, et al. Patient-derived organoids model cervical tissue dynamics and viral oncogenesis in cervical

cancer. Cell Stem Cell [Internet]. 2021 Aug 5 [cited 2023 Apr 21];28(8):1380-1396.e6. Available from: https://pubmed.ncbi.nlm.nih.gov/33852917/

116. Hubert CG, Rivera M, Spangler LC, Wu Q, Mack SC, Prager BC, et al. A Three-Dimensional Organoid Culture System Derived from Human Glioblastomas Recapitulates the Hypoxic Gradients and Cancer Stem Cell Heterogeneity of Tumors Found In Vivo. Cancer Res [Internet]. 2016 Apr 15 [cited 2023 Apr 21];76(8):2465–77. Available from: https://pubmed.ncbi.nlm.nih.gov/26896279/
117. Zhou Z, Cong L, Cong X. Patient-Derived Organoids in Precision Medicine: Drug Screening, Organoid-on-a-Chip and Living Organoid Biobank. Front Oncol. 2021 Dec 30;11:5625.
118. Bose S, Clevers H, Shen X. Promises and Challenges of Organoid-Guided Precision Medicine. Med (N Y) [Internet]. 2021 Sep 9 [cited 2023 Apr 23];2(9):1011. Available from: /pmc/articles/PMC8492003/
119. Guillen KP, Fujita M, Butterfield AJ, Scherer SD, Bailey MH, Chu Z, et al. A human breast cancer-derived xenograft and organoid platform for drug discovery and precision oncology. Nature Cancer 2022 3:2 [Internet]. 2022 Feb 24 [cited 2023 Apr 23];3(2):232–50. Available from: https://www.nature.com/articles/s43018-022-00337-6
120. Sachs N, de Ligt J, Kopper O, Gogola E, Bounova G, Weeber F, et al. A Living Biobank of Breast Cancer Organoids Captures Disease Heterogeneity. Cell [Internet]. 2018 Jan 11 [cited 2023 Apr 23];172(1–2):373-386.e10. Available from: https://pubmed.ncbi.nlm.nih.gov/29224780/
121. Driehuis E, Van Hoeck A, Moore K, Kolders S, Francies HE, Gulersonmez MC, et al. Pancreatic cancer organoids recapitulate disease and allow personalized drug screening. Proc Natl Acad Sci U S A [Internet]. 2019 Dec 26 [cited 2023 Apr 23];116(52):26580–90. Available from: https://www.pnas.org/doi/abs/10.1073/pnas.1911273116
122. Jacob F, Salinas RD, Zhang DY, Nguyen PTT, Schnoll JG, Wong SZH, et al. A Patient-Derived Glioblastoma Organoid Model and Biobank Recapitulates Inter- and Intra-tumoral Heterogeneity. Cell [Internet]. 2020 Jan 9 [cited 2023 Apr 23];180(1):188-204.e22. Available from: https://pubmed.ncbi.nlm.nih.gov/31883794/
123. Seidlitz T, Koo BK, Stange DE. Gastric organoids—an in vitro model system for the study of gastric development and road to personalized medicine. Cell Death & Differentiation 2020 28:1 [Internet]. 2020 Nov 22 [cited 2023 Apr 23];28(1):68–83. Available from: https://www.nature.com/articles/s41418-020-00662-2
124. Broutier L, Mastrogiovanni G, Verstegen MMA, Francies HE, Gavarró LM, Bradshaw CR, et al. Human primary liver cancer–derived organoid cultures for disease modeling and drug screening. Nature Medicine 2017 23:12 [Internet]. 2017 Nov 13 [cited 2023 Apr 23];23(12):1424–35. Available from: https://www.nature.com/articles/nm.4438
125. Verstegen MMA, Roos FJM, Burka K, Gehart H, Jager M, De Wolf M, et al. Human extrahepatic and intrahepatic cholangiocyte organoids show region-specific differentiation

potential and model cystic fibrosis-related bile duct disease. Sci Rep [Internet]. 2020 [cited 2023 Apr 24]; Available from: https://doi.org/10.1038/s41598-020-79082-8

126. Dekkers JF, Berkers G, Kruisselbrink E, Vonk A, De Jonge HR, Janssens HM, et al. Characterizing responses to CFTR-modulating drugs using rectal organoids derived from subjects with cystic fibrosis. Sci Transl Med [Internet]. 2016 Jun 22 [cited 2023 Apr 24];8(344). Available from: https://www.science.org/doi/10.1126/scitranslmed.aad8278
127. Brewington JJ, Filbrandt ET, LaRosa FJ, Ostmann AJ, Strecker LM, Szczesniak RD, et al. Detection of CFTR function and modulation in primary human nasal cell spheroids. J Cyst Fibros [Internet]. 2018 Jan 1 [cited 2023 Apr 24];17(1):26. Available from: /pmc/articles/PMC5868354/
128. Schwank G, Koo BK, Sasselli V, Dekkers JF, Heo I, Demircan T, et al. Functional repair of CFTR by CRISPR/Cas9 in intestinal stem cell organoids of cystic fibrosis patients. Cell Stem Cell [Internet]. 2013 Dec 5 [cited 2023 Apr 24];13(6):653–8. Available from: https://pubmed.ncbi.nlm.nih.gov/24315439/
129. Huch M, Gehart H, Van Boxtel R, Hamer K, Blokzijl F, Verstegen MMA, et al. Long-term culture of genome-stable bipotent stem cells from adult human liver. Cell [Internet]. 2015 Jan 15 [cited 2023 Apr 24];160(1–2):299–312. Available from: https://pubmed.ncbi.nlm.nih.gov/25533785/
130. Soroka CJ, Assis DN, Alrabadi LS, Roberts S, Cusack L, Jaffe AB, et al. Bile-Derived Organoids From Patients With Primary Sclerosing Cholangitis Recapitulate Their Inflammatory Immune Profile. Hepatology [Internet]. 2019 Sep 1 [cited 2023 Apr 24];70(3):871–82. Available from: https://pubmed.ncbi.nlm.nih.gov/30561836/
131. Heydari Z, Moeinvaziri F, Agarwal T, Pooyan P, Shpichka A, Maiti TK, et al. Organoids: a novel modality in disease modeling. Biodes Manuf [Internet]. 2021 Dec 1 [cited 2023 Apr 24];4(4):689–716. Available from: https://pubmed.ncbi.nlm.nih.gov/34395032/
132. Ettayebi K, Crawford SE, Murakami K, Broughman JR, Karandikar U, Tenge VR, et al. Replication of human noroviruses in stem cell-derived human enteroids. Science [Internet]. 2016 Sep 23 [cited 2023 Apr 24];353(6306):1387–93. Available from: https://pubmed.ncbi.nlm.nih.gov/27562956/
133. Chen S, Li P, Wang Y, Yin Y, de Ruiter PE, Verstegen MMA, et al. Rotavirus Infection and Cytopathogenesis in Human Biliary Organoids Potentially Recapitulate Biliary Atresia Development. mBio [Internet]. 2020 Jul 1 [cited 2023 Apr 24];11(4):1–6. Available from: https://pubmed.ncbi.nlm.nih.gov/32843549/
134. Sachs N, Papaspyropoulos A, Zomer-van Ommen DD, Heo I, Böttinger L, Klay D, et al. Long-term expanding human airway organoids for disease modeling. EMBO J [Internet]. 2019 Feb 15 [cited 2023 Apr 24];38(4). Available from: https://pubmed.ncbi.nlm.nih.gov/30643021/
135. Driehuis E, Kolders S, Spelier S, Lõhmussaar K, Willems SM, Devriese LA, et al. Oral Mucosal Organoids as a Potential Platform for Personalized Cancer Therapy. Cancer Discov

[Internet]. 2019 Jul 1 [cited 2023 Apr 24];9(7):852–71. Available from: https://pubmed.ncbi.nlm.nih.gov/31053628/

136. Wroblewski LE, Piazuelo MB, Chaturvedi R, Schumacher M, Aihara E, Feng R, et al. *Helicobacter pylori* targets cancer-associated apical-junctional constituents in gastroids and gastric epithelial cells. Gut [Internet]. 2015 Apr 9 [cited 2023 Apr 24];64(5):720–30. Available from: https://pubmed.ncbi.nlm.nih.gov/25123931/

137. Heo I, Dutta D, Schaefer DA, Iakobachvili N, Artegiani B, Sachs N, et al. Modeling Cryptosporidium infection in human small intestinal and lung organoids. Nat Microbiol [Internet]. 2018 Jul 1 [cited 2023 Apr 24];3(7):814. Available from: /pmc/articles/PMC6027984/

138. Pompaiah M, Bartfeld S. Gastric organoids: An emerging model system to study *Helicobacter pylori* pathogenesis. Curr Top Microbiol Immunol [Internet]. 2017 Jan 1 [cited 2023 Apr 24];400:149–68. Available from: https://link.springer.com/chapter/10.1007/978-3-319-50520-6_7

139. Karam SM, Leblond CP. Dynamics of epithelial cells in the corpus of the mouse stomach. II. Outward migration of pit cells. Anat Rec [Internet]. 1993 Jun 1 [cited 2023 Apr 24];236(2):280–96. Available from: https://onlinelibrary.wiley.com/doi/full/10.1002/ar.1092360203

140. Karam SM, Leblond CP. Dynamics of epithelial cells in the corpus of the mouse stomach. III. Inward migration of neck cells followed by progressive transformation into zymogenic cells. Anat Rec [Internet]. 1993 Jun 1 [cited 2023 Apr 24];236(2):297–313. Available from: https://onlinelibrary.wiley.com/doi/full/10.1002/ar.1092360204

141. Karam SM. Dynamics of epithelial cells in the corpus of the mouse stomach. IV. Bidirectional migration of parietal cells ending in their gradual degeneration and loss. Anat Rec [Internet]. 1993 Jun 1 [cited 2023 Apr 24];236(2):314–32. Available from: https://onlinelibrary.wiley.com/doi/full/10.1002/ar.1092360205

142. Lee ER, Leblond CP. Dynamic histology of the antral epithelium in the mouse stomach: II. Ultrastructure and renewal of isthmal cells. American Journal of Anatomy [Internet]. 1985 Mar 1 [cited 2023 Apr 24];172(3):205–24. Available from: https://onlinelibrary.wiley.com/doi/full/10.1002/aja.1001720304

143. Kretzschmar K, Watt FM. Lineage Tracing. Cell [Internet]. 2012 Jan 20 [cited 2023 Apr 24];148(1):33–45. Available from: http://www.cell.com/article/S0092867412000037/fulltext

144. Qiao XT, Ziel JW, McKimpson W, Madison BB, Todisco A, Merchant JL, et al. Prospective Identification of a Multilineage Progenitor in Murine Stomach Epithelium. Gastroenterology [Internet]. 2007 Dec 1 [cited 2023 Apr 24];133(6):1989-1998.e3. Available from: http://www.gastrojournal.org/article/S0016508507017416/fulltext

145. Arnold K, Sarkar A, Yram MA, Polo JM, Bronson R, Sengupta S, et al. Sox2 + adult stem and progenitor cells are important for tissue regeneration and survival of mice. Cell Stem Cell

[Internet]. 2011 Oct 4 [cited 2023 Apr 24];9(4):317–29. Available from: http://www.cell.com/article/S1934590911004322/fulltext

146. Hayakawa Y, Jin G, Wang H, Chen X, Westphalen CB, Asfaha S, et al. CCK2R identifies and regulates gastric antral stem cell states and carcinogenesis. Gut [Internet]. 2015 Apr 1 [cited 2023 Apr 24];64(4):544–53. Available from: https://gut.bmj.com/content/64/4/544
147. Hayakawa Y, Ariyama H, Stancikova J, Sakitani K, Asfaha S, Renz BW, et al. Mist1 Expressing Gastric Stem Cells Maintain the Normal and Neoplastic Gastric Epithelium and Are Supported by a Perivascular Stem Cell Niche. Cancer Cell [Internet]. 2015 Dec 14 [cited 2023 Apr 24];28(6):800–14. Available from: http://www.cell.com/article/S1535610815003803/fulltext
148. McCracken KW, Catá EM, Crawford CM, Sinagoga KL, Schumacher M, Rockich BE, et al. Modelling human development and disease in pluripotent stem-cell-derived gastric organoids. Nature 2014 516:7531 [Internet]. 2014 Oct 29 [cited 2023 Apr 24];516(7531):400–4. Available from: https://www.nature.com/articles/nature13863
149. Bartfeld S, Bayram T, Van De Wetering M, Huch M, Begthel H, Kujala P, et al. In vitro expansion of human gastric epithelial stem cells and their responses to bacterial infection. Gastroenterology [Internet]. 2015 Jan 1 [cited 2023 Apr 24];148(1):126-136.e6. Available from: http://www.gastrojournal.org/article/S0016508514012037/fulltext
150. Schwank G, Andersson-Rolf A, Koo BK, Sasaki N, Clevers H. Generation of BAC Transgenic Epithelial Organoids. PLoS One [Internet]. 2013 Oct 18 [cited 2023 Apr 24];8(10):e76871. Available from: https://journals.plos.org/plosone/article?id=10.1371/journal.pone.0076871
151. Li VSW, Ng SS, Boersema PJ, Low TY, Karthaus WR, Gerlach JP, et al. Wnt Signaling through Inhibition of β-Catenin Degradation in an Intact Axin1 Complex. Cell [Internet]. 2012 Jun 8 [cited 2023 Apr 24];149(6):1245–56. Available from: http://www.cell.com/article/S0092867412005302/fulltext
152. Koo BK, Stange DE, Sato T, Karthaus W, Farin HF, Huch M, et al. Controlled gene expression in primary Lgr5 organoid cultures. Nature Methods 2011 9:1 [Internet]. 2011 Dec 4 [cited 2023 Apr 24];9(1):81–3. Available from: https://www.nature.com/articles/nmeth.1802
153. Pang MJ, Burclaff JR, Jin R, Adkins-Threats M, Osaki LH, Han Y, et al. Gastric Organoids: Progress and Remaining Challenges. Cell Mol Gastroenterol Hepatol [Internet]. 2022 Jan 1 [cited 2023 Apr 24];13(1):19–33. Available from: https://pubmed.ncbi.nlm.nih.gov/34547535/
154. Idowu Sulaimon, Bertrand Paul P., Walduck Anna K. Gastric organoids: Advancing the study of H. pylori pathogenesis and inflammation. Helicobacter. 2022;228–39.
155. Boccellato F, Woelffling S, Imai-Matsushima A, Sanchez G, Goosmann C, Schmid M, et al. Polarised epithelial monolayers of the gastric mucosa reveal insights into mucosal homeostasis and defence against infection. Gut [Internet]. 2019 Mar 1 [cited 2023 Apr 25];68(3):400–13. Available from: https://gut.bmj.com/content/68/3/400

156. Huang JY, Sweeney EG, Sigal M, Zhang HC, Remington SJ, Cantrell MA, et al. Chemodetection and destruction of host urea allows Helicobacter pylori to locate the epithelium. Cell Host Microbe [Internet]. 2015 Aug 12 [cited 2023 Apr 25];18(2):147–56. Available from: http://www.cell.com/article/S1931312815002942/fulltext

157. Backert S, Naumann M. What a disorder: Proinflammatory signaling pathways induced by Helicobacter pylori. Trends Microbiol [Internet]. 2010 Nov 1 [cited 2023 Apr 25];18(11):479–86. Available from: http://www.cell.com/article/S0966842X1000140X/fulltext

158. Miehlke S, Hackelsberger A, Meining A, Hatz R, Lehn N, Malfertheiner P, et al. Severe expression of corpus gastritis is characteristic in gastric cancer patients infected with Helicobacter pylori. Br J Cancer [Internet]. 1998 [cited 2023 Apr 25];78(2):263. Available from: /pmc/articles/PMC2062894/?report=abstract

159. Brandt S, Kwok T, Hartig R, König W, Backert S. NF-κB activation and potentiation of proinflammatory responses by the Helicobacter pylori CagA protein. Proc Natl Acad Sci U S A [Internet]. 2005 Jun 6 [cited 2023 Apr 25];102(26):9300. Available from: /pmc/articles/PMC1166591/

160. Uotani T, Murakami K, Uchida T, Tanaka S, Nagashima H, Zeng XL, et al. Changes of tight junction and interleukin-8 expression using a human gastroid monolayer model of Helicobacter pylori infection. Helicobacter [Internet]. 2019 Jun 1 [cited 2023 Apr 25];24(3):e12583. Available from: https://onlinelibrary.wiley.com/doi/full/10.1111/hel.12583

161. Kayisoglu Ö, Schlegel N, Bartfeld S. Gastrointestinal epithelial innate immunity—regionalization and organoids as new model. J Mol Med [Internet]. 2021 Apr 1 [cited 2023 Apr 25];99(4):517–30. Available from: https://link.springer.com/article/10.1007/s00109-021-02043-9

162. Morey P, Pfannkuch L, Pang E, Boccellato F, Sigal M, Imai-Matsushima A, et al. Helicobacter pylori Depletes Cholesterol in Gastric Glands to Prevent Interferon Gamma Signaling and Escape the Inflammatory Response. Gastroenterology [Internet]. 2018 Apr 1 [cited 2023 Apr 25];154(5):1391-1404.e9. Available from: http://www.gastrojournal.org/article/S0016508517367124/fulltext

163. Chakraborty A, Wakamiya M, Venkova-Canova T, Pandita RK, Aguilera-Aguirre L, Sarker AH, et al. Neil2-null mice accumulate oxidized DNA bases in the transcriptionally active sequences of the genome and are susceptible to innate inflammation. Journal of Biological Chemistry [Internet]. 2015 Oct 9 [cited 2023 Apr 25];290(41):24636–48. Available from: http://www.jbc.org/article/S0021925820445922/fulltext

164. Sayed IM, Sahan AZ, Venkova T, Chakraborty A, Mukhopadhyay D, Bimczok D, et al. Helicobacter pylori infection downregulates the DNA glycosylase NEIL2, resulting in increased genome damage and inflammation in gastric epithelial cells. Journal of Biological Chemistry [Internet]. 2020 Aug 7 [cited 2023 Apr 25];295(32):11082–98. Available from: http://www.jbc.org/article/S0021925817492052/fulltext

165. Bauer M, Nascakova Z, Mihai AI, Cheng PF, Levesque MP, Lampart S, et al. The ALPK1/TIFA/NF-κB axis links a bacterial carcinogen to R-loop-induced replication stress. Nature Communications 2020 11:1 [Internet]. 2020 Oct 9 [cited 2023 Apr 25];11(1):1–16. Available from: https://www.nature.com/articles/s41467-020-18857-z
166. Abugomaa A, Elbadawy M, Yamanaka M, Goto Y, Hayashi K, Mori T, et al. Establishment of 2.5D organoid culture model using 3D bladder cancer organoid culture. Sci Rep [Internet]. 2020 Dec 1 [cited 2023 Apr 27];10(1). Available from: https://pubmed.ncbi.nlm.nih.gov/32523078/
167. Dabiri H, Maleknejad P, Yamaoka Y, Feizabadi MM, Jafari F, Rezadehbashi M, et al. Distribution of Helicobacter pylori cagA, cagE, oipA and vacA in different major ethnic groups in Tehran, Iran. J Gastroenterol Hepatol [Internet]. 2009 Aug 1 [cited 2023 May 10];24(8):1380–6. Available from: https://onlinelibrary.wiley.com/doi/full/10.1111/j.1440-1746.2009.05876.x
168. Hosseini RS, Rahimian G, Shafigh MH, Validi M, Khaledi M, Gholipour A. Correlation between clarithromycin resistance, virulence factors and clinical characteristics of the disease in Helicobacter pylori infected patients in Shahrekord, Southwest Iran. AMB Express [Internet]. 2021 Dec 1 [cited 2023 May 3];11(1). Available from: /pmc/articles/PMC8566624/
169. Baldwin DN, Shepherd B, Kraemer P, Hall MK, Sycuro LK, Pinto-Santini DM, et al. Identification of Helicobacter pylori genes that contribute to stomach colonization. Infect Immun [Internet]. 2007 Feb [cited 2023 May 3];75(2):1005–16. Available from: https://pubmed.ncbi.nlm.nih.gov/17101654/
170. Wang Y, Roos KP, Taylor DE. Transformation of Helicobacter pylori by chromosomal metronidazole resistance and by a plasmid with a selectable chloramphenicol resistance marker. J Gen Microbiol [Internet]. 1993 [cited 2023 May 3];139(10):2485–93. Available from: https://pubmed.ncbi.nlm.nih.gov/8254319/
171. Al-Maleki AR, Loke MF, Lui SY, Ramli NSK, Khosravi Y, Ng CG, et al. Helicobacter pylori outer inflammatory protein A (OipA) suppresses apoptosis of AGS gastric cells in vitro. Cell Microbiol [Internet]. 2017 Dec 1 [cited 2023 May 3];19(12). Available from: https://pubmed.ncbi.nlm.nih.gov/28776327/
172. Sun Y, Cheng Z, Liu S. MCM2 in human cancer: functions, mechanisms, and clinical significance. Mol Med [Internet]. 2022 Dec 1 [cited 2023 May 5];28(1). Available from: https://pubmed.ncbi.nlm.nih.gov/36303105/
173. Wang CL, Liu XY, Wang YH, Zhang Z, Wang ZD, Zhou GQ. MCM2 promotes the proliferation, migration and invasion of cholangiocarcinoma cells by reducing the p53 signaling pathway. Yi Chuan [Internet]. 2022 Mar 20 [cited 2023 May 5];44(3):230–44. Available from: https://pubmed.ncbi.nlm.nih.gov/35307646/
174. Yang C, Wen Y, Li H, Zhang D, Zhang N, Shi X, et al. Overexpression of minichromosome maintenance 2 predicts poor prognosis in patients with gastric cancer. Oncol Rep [Internet].

2012 Jan [cited 2023 May 5];27(1):135–42. Available from: https://pubmed.ncbi.nlm.nih.gov/21947329/

175. Qiu F, Shi C hua, Zheng J, Liu Y bin. Periostin Mediates the Increased Pro-Angiogenic Activity of Gastric Cancer Cells under Hypoxic Conditions. J Biochem Mol Toxicol [Internet]. 2013 Jul 1 [cited 2023 May 5];27(7):364–9. Available from: https://onlinelibrary.wiley.com/doi/full/10.1002/jbt.21498

176. Li B, Wang L, Chi B. Upregulation of periostin prevents P53-mediated apoptosis in SGC-7901 gastric cancer cells. Mol Biol Rep [Internet]. 2013 Feb 19 [cited 2023 May 5];40(2):1677–83. Available from: https://link.springer.com/article/10.1007/s11033-012-2218-3

177. Krueger S, Kalinski T, Hundertmark T, Wex T, Küster D, Peitz U, et al. Up-regulation of cathepsin X in Helicobacter pylori gastritis and gastric cancer. J Pathol [Internet]. 2005 Sep [cited 2023 May 5];207(1):32–42. Available from: https://pubmed.ncbi.nlm.nih.gov/16025436/

178. Soond SM, Zamyatnin AA. Helicobacter pylori and gastric cancer: a lysosomal protease perspective. Gastric Cancer [Internet]. 2022 Mar 1 [cited 2023 May 5];25(2):306–24. Available from: https://pubmed.ncbi.nlm.nih.gov/34918208/

179. Blackburn JB, Kudlyk T, Pokrovskaya I, Lupashin V V. More than just sugars: Conserved oligomeric Golgi complex deficiency causes glycosylation-independent cellular defects. Traffic [Internet]. 2018 Jun 1 [cited 2023 May 5];19(6):463–80. Available from: https://onlinelibrary.wiley.com/doi/full/10.1111/tra.12564

180. Realegeno S, Priyamvada L, Kumar A, Blackburn JB, Hartloge C, Puschnik AS, et al. Conserved Oligomeric Golgi (COG) Complex Proteins Facilitate Orthopoxvirus Entry, Fusion and Spread. Viruses [Internet]. 2020 Jul 1 [cited 2023 May 5];12(7). Available from: /pmc/articles/PMC7411930/

181. Maciej Serda, Becker FG, Cleary M, Team RM, Holtermann H, The D, et al. Effect of Helicobacter pylori infection on the lipid, lipoproteins, apolipoprotein-A1, Lipoprotein (a) and Apolipoprotein-B in patients with gastritis. G. Balint, Antala B, Carty C, Mabieme JMA, Amar IB, Kaplanova A, editors. Afr J Microbiol Res [Internet]. 2010 [cited 2023 May 5];4(2):343–54. Available from: https://avesis.ogu.edu.tr/yayin/84131f73-1fce-460a-93f9-5ba2002f6bc9/effect-of-helicobacter-pylori-infection-on-the-lipid-lipoproteins-apolipoprotein-a1-lipoprotein-a-and-apolipoprotein-b-in-patients-with-gastritis

182. Pfeiffer JR, McAvoy BL, Fecteau RE, Deleault KM, Brooks SA. CARHSP1 is required for effective tumor necrosis factor alpha mRNA stabilization and localizes to processing bodies and exosomes. Mol Cell Biol [Internet]. 2011 Jan 1 [cited 2023 May 6];31(2):277–86. Available from: https://pubmed.ncbi.nlm.nih.gov/21078874/

183. Nishioka K, Daidoji T, Nakaya T. Downregulation of calcium-regulated heat stable protein 1 expression by low-temperature stimulation causes reduction of interferon-β expression and

sensitivity to influenza viral infection. Virus Res [Internet]. 2022 Feb 1 [cited 2023 May 6];309. Available from: https://pubmed.ncbi.nlm.nih.gov/34929215/

184. Fort PE, Losiewicz MK, Reiter CEN, Singh RSJ, Nakamura M, Abcouwer SF, et al. Differential Roles of Hyperglycemia and Hypoinsulinemia in Diabetes Induced Retinal Cell Death: Evidence for Retinal Insulin Resistance. PLoS One [Internet]. 2011 [cited 2023 May 6];6(10):e26498. Available from: https://www.academia.edu/en/27752316/Differential_Roles_of_Hyperglycemia_and_Hypoinsulinemia_in_Diabetes_Induced_Retinal_Cell_Death_Evidence_for_Retinal_Insulin_Resistance

185. Pietrocola F, Galluzzi L, Bravo-San Pedro JM, Madeo F, Kroemer G. Acetyl Coenzyme A: A Central Metabolite and Second Messenger. Cell Metab. 2015 Jun 2;21(6):805–21.

186. Gobert AP, Verriere T, Asim M, Barry DP, Piazuelo MB, de Sablet T, et al. Heme Oxygenase-1 Dysregulates Macrophage Polarization and the Immune Response to Helicobacter pylori. The Journal of Immunology [Internet]. 2014 Sep 15 [cited 2023 May 6];193(6):3013–22. Available from: https://journals.aai.org/jimmunol/article/193/6/3013/98299/Heme-Oxygenase-1-Dysregulates-Macrophage

187. Puentes-Pardo JD, Moreno-Sanjuan S, Carazo Á, León J. Heme Oxygenase-1 in Gastrointestinal Tract Health and Disease. Antioxidants [Internet]. 2020 Dec 1 [cited 2023 May 6];9(12):1–30. Available from: /pmc/articles/PMC7760122/

188. Ameriso SF, Villamil AR, Zedda C, Parodi JC, Garrido S, Sarchi MI, et al. Heme oxygenase-1 is expressed in carotid atherosclerotic plaques infected by Helicobacter pylori and is more prevalent in asymptomatic subjects. Stroke [Internet]. 2005 Sep [cited 2023 May 6];36(9):1896–900. Available from: http://ahajournals.org

189. Galmiche A, Rassow J. Targeting of Helicobacter pylori VacA to mitochondria. Gut Microbes [Internet]. 2010 Nov [cited 2023 May 6];1(6):392–5. Available from: https://pubmed.ncbi.nlm.nih.gov/21468222/

190. Aird KM, Zhang R. Detection of senescence-associated heterochromatin foci (SAHF). Methods Mol Biol [Internet]. 2013 [cited 2023 May 6];965:185. Available from: /pmc/articles/PMC3552318/

191. Chaithongyot S, Naumann · Michael. Helicobacter pylori-induced reactive oxygen species direct turnover of CSN-associated STAMBPL1 and augment apoptotic cell death. Cellular and Molecular Life Sciences [Internet]. 2022 [cited 2023 May 8];79:86. Available from: https://doi.org/10.1007/s00018-022-04135-2

192. Zhao Y, Zhang J, Cheng ASL, Yu J, To KF, Kang W. Gastric cancer: genome damaged by bugs. Oncogene 2020 39:17 [Internet]. 2020 Mar 2 [cited 2023 May 8];39(17):3427–42. Available from: https://www.nature.com/articles/s41388-020-1241-4

193. Rut W, Drag M. Human 20S proteasome activity towards fluorogenic peptides of various chain lengths. Biol Chem [Internet]. 2016 Sep 1 [cited 2023 May 11];397(9):921–6. Available from: https://pubmed.ncbi.nlm.nih.gov/27176742/

194. Coombs N, Sompallae R, Olbermann P, Gastaldello S, Göppel D, Masucci MG, et al. Helicobacter pylori affects the cellular deubiquitinase USP7 and ubiquitin-regulated components TRAF6 and the tumour suppressor p53. Int J Med Microbiol [Internet]. 2011 Mar [cited 2023 May 11];301(3):213–24. Available from: https://pubmed.ncbi.nlm.nih.gov/21131231/

195. Necchi V, Sommi P, Ricci V, Solcia E. In vivo accumulation of Helicobacter pylori products, NOD1, ubiquitinated proteins and proteasome in a novel cytoplasmic structure. PLoS One [Internet]. 2010 [cited 2023 May 11];5(3). Available from: https://pubmed.ncbi.nlm.nih.gov/20300534/

196. Dümmler BA, Hauge C, Silber J, Yntema HG, Kruse LS, Kofoed B, et al. Functional characterization of human RSK4, a new 90-kDa ribosomal S6 kinase, reveals constitutive activation in most cell types. J Biol Chem [Internet]. 2005 Apr 8 [cited 2023 May 8];280(14):13304–14. Available from: https://pubmed.ncbi.nlm.nih.gov/15632195/

197. Berns K, Hijmans EM, Mullenders J, Brummelkamp TR, Velds A, Heimerikx M, et al. A large-scale RNAi screen in human cells identifies new components of the p53 pathway. Nature [Internet]. 2004 Mar 25 [cited 2023 May 8];428(6981):431–7. Available from: https://pubmed.ncbi.nlm.nih.gov/15042092/

198. LLeonart ME, Vidal F, Gallardo D, Diaz-Fuertes M, Rojo F, Cuatrecasas M, et al. New p53 related genes in human tumors: Significant downregulation in colon and lung carcinomas. Oncol Rep [Internet]. 2006 Sep 1 [cited 2023 May 8];16(3):603–8. Available from: http://www.spandidos-publications.com/10.3892/or.16.3.603/abstract

199. Liu W, Yan M, Liu Y, Wang R, Li C, Deng C, et al. Olfactomedin 4 down-regulates innate immunity against Helicobacter pylori infection. Proc Natl Acad Sci U S A [Internet]. 2010 Jun 15 [cited 2023 May 8];107(24):11056–61. Available from: https://pubmed.ncbi.nlm.nih.gov/20534456/

200. Liu W, Yan M, Liu Y, Mcleish KR, Coleman WG, Rodgers GP. Olfactomedin 4 Inhibits Cathepsin C-Mediated Protease Activities, Thereby Modulating Neutrophil Killing of Staphylococcus aureus and Escherichia coli in Mice. The Journal of Immunology. 2012;189:2460–7.

201. Li H, Kim C, Liu W, Zhu J, Chin K, Rodriguez-Canales J, et al. Olfactomedin 4 downregulation is associated with tumor initiation, growth and progression in human prostate cancer. Int J Cancer [Internet]. 2020 Mar 1 [cited 2023 May 8];146(5):1346–58. Available from: https://onlinelibrary.wiley.com/doi/full/10.1002/ijc.32535

202. Zhao J, Shu P, Duan F, Wang X, Min L, Shen Z, et al. Loss of OLFM4 promotes tumor migration through inducing interleukin-8 expression and predicts lymph node metastasis in

early gastric cancer. Oncogenesis 2016 5:6 [Internet]. 2016 Jun 13 [cited 2023 May 8];5(6):e234–e234. Available from: https://www.nature.com/articles/oncsis201642

203. Al-Maleki AR, Loke MF, Lui SY, Ramli NSK, Khosravi Y, Ng CG, et al. Helicobacter pylori outer inflammatory protein A (OipA) suppresses apoptosis of AGS gastric cells in vitro. Cell Microbiol [Internet]. 2017 Dec 1 [cited 2023 May 8];19(12):e12771. Available from: https://onlinelibrary.wiley.com/doi/full/10.1111/cmi.12771
204. Foertsch F, Teichmann N, Kob R, Hentschel J, Laubscher U, Melle C. S100A11 is involved in the regulation of the stability of cell cycle regulator p21(CIP1/WAF1) in human keratinocyte HaCaT cells. FEBS J [Internet]. 2013 Aug [cited 2023 May 8];280(16):3840–53. Available from: https://pubmed.ncbi.nlm.nih.gov/23745637/
205. Matsubara D, Niki T, Ishikawa S, Goto A, Ohara E, Yokomizo T, et al. Differential expression of S100A2 and S100A4 in lung adenocarcinomas: clinicopathological significance, relationship to p53 and identification of their target genes. Cancer Sci [Internet]. 2005 Dec [cited 2023 May 8];96(12):844–57. Available from: https://pubmed.ncbi.nlm.nih.gov/16367903/
206. Oue N, Hamai Y, Mitani Y, Matsumura S, Oshimo Y, Aung PP, et al. Gene expression profile of gastric carcinoma: identification of genes and tags potentially involved in invasion, metastasis, and carcinogenesis by serial analysis of gene expression. Cancer Res [Internet]. 2004 Apr 1 [cited 2023 May 8];64(7):2397–405. Available from: https://pubmed.ncbi.nlm.nih.gov/15059891/
207. Whitman S, Wang X, Shalaby R, Shtivelman E. Alternatively spliced products CC3 and TC3 have opposing effects on apoptosis. Mol Cell Biol [Internet]. 2000 Jan 15 [cited 2023 May 8];20(2):583–93. Available from: https://pubmed.ncbi.nlm.nih.gov/10611237/
208. Shtivelman E. A link between metastasis and resistance to apoptosis of variant small cell lung carcinoma. Oncogene [Internet]. 1997 [cited 2023 May 8];14(18):2167–73. Available from: https://pubmed.ncbi.nlm.nih.gov/9174052/
209. DR G, JC R. Mitochondria and apoptosis. Science [Internet]. 1998 [cited 2023 May 9];281(5381):118. Available from: https://pubmed.ncbi.nlm.nih.gov/9721092/
210. Green DR, Amarante-Mendes GP. The point of no return: mitochondria, caspases, and the commitment to cell death. Results Probl Cell Differ [Internet]. 1998 [cited 2023 May 9];24:45–61. Available from: https://pubmed.ncbi.nlm.nih.gov/9949831/
211. Patterson SD, Spahr CS, Daugas E, Susin SA, Irinopoulou T, Koehler C, et al. Mass spectrometric identification of proteins released from mitochondria undergoing permeability transition. Cell Death Differ [Internet]. 2000 [cited 2023 May 9];7(2):137–44. Available from: https://pubmed.ncbi.nlm.nih.gov/10713728/

8 APPENDIX

APPENDIX 1

Table 14. List of proteins whose quantification changes significantly in the presence of oipA protein in infection compared to control

Uniprot Accession	Gene Symbol	Description	q-value	UP	ΔoipA-G27 Infected Grıup FC	G27 Infected Grıup FC	P-value
O14493	CLDN4	Claudin-4 [OS=Homo sapiens]	0	2	0.747424624	0.301451957	0.001153543
O15393	TMPRSS2	Transmembrane protease serine 2 [OS=Homo sapiens]	0	4	0.946057647	0.400534939	0.00013889
O43852	CALU	Calumenin [OS=Homo sapiens]	0	9	0.993092495	0.473028823	0.001906697
O75494	SRSF10	Serine/arginine-rich splicing factor 10 [OS=Homo sapiens]	0	2	0.920187651	2.188587403	0.012149128
O75676	RPS6KA4	Ribosomal protein S6 kinase alpha-4 [OS=Homo sapiens]	0	2	0.920187651	0.214641359	3.9123E-05
O95372	LYPLA2	Acyl-protein thioesterase 2 [OS=Homo sapiens]	0	4	1.021012126	1.853176124	0.013945706
O95817	BAG3	BAG family molecular chaperone regulator 3 [OS=Homo sapiens]	0	3	1.035264924	1.658639092	0.040203105
P00505	GOT2	Aspartate aminotransferase, mitochondrial [OS=Homo sapiens]	0	15	1.443929196	2.694467154	5.7335E-05
P04075	ALDOA	Fructose-bisphosphate aldolase A [OS=Homo sapiens]	0	26	1.109569472	1.853176124	0.01228518
P04080	CSTB	Cystatin-B [OS=Homo sapiens]	0	2	1.301341855	2.514026749	0.00018554
P04155	TFF1	Trefoil factor 1 [OS=Homo sapiens]	0	3	0.852634892	0.510506063	0.005006279
P04264	KRT1	Keratin, type II cytoskeletal 1 [OS=Homo sapiens]	0	7	0.817902059	2.37841423	0.001527935
P04424	ASL	Argininosuccinate lyase [OS=Homo sapiens]	0	7	0.926588062	0.624165274	0.049612722
P06731	CEACAM5	Carcinoembryonic antigen-related cell adhesion molecule 5 [OS=Homo sapiens]	0	3	0.993092495	2.158456473	0.001772313
P07477	PRSS1	Serine protease 1 [OS=Homo sapiens]	0	3	1.094293701	0.325335464	3.38779E-06
P07602	PSAP	Prosaposin [OS=Homo sapiens]	0	14	0.840896415	0.543367431	0.011343768
P07741	APRT	Adenine phosphoribosyltransferase [OS=Homo sapiens]	0	6	1.189207115	2.329467173	0.000623844
P07858	CTSB	Cathepsin B [OS=Homo sapiens]	0	5	0.939522749	0.574349177	0.019737671
P08397	HMBS	Porphobilinogen deaminase [OS=Homo sapiens]	0.002	2	1.505246747	0.378929142	0.007663807
P08727	KRT19	Keratin, type I cytoskeletal 19 [OS=Homo sapiens]	0	28	1.035264924	1.717130873	0.028244889
P09110	ACAA1	3-ketoacyl-CoA thiolase, peroxisomal [OS=Homo sapiens]	0	9	1.125058485	1.765405993	0.020169848
P09493	TPM1	Tropomyosin alpha-1 chain [OS=Homo sapiens]	0	14	0.732042848	0.496546248	0.00359668
P09525	ANXA4	Annexin A4 [OS=Homo sapiens]	0	15	0.901250463	0.582366793	0.0237422
P09669	COX6C	Cytochrome c oxidase subunit 6C [OS=Homo sapiens]	0	3	0.801069878	0.395020656	0.000286061
P10599	TXN	Thioredoxin [OS=Homo sapiens]	0	3	1.064370182	3.031433133	6.00766E-06
P11177	PDHB	Pyruvate dehydrogenase E1 component subunit beta, mitochondrial [OS=Homo sapiens]	0	6	1.156688184	1.670175839	0.037526676
P12277	CKB	Creatine kinase B-type [OS=Homo sapiens]	0	3	0.664342907	2.887858391	1.57071E-05
P12955	PEPD	Xaa-Pro dipeptidase [OS=Homo sapiens]	0	2	0.829319546	0.420448208	0.00031584

Table 14 (cont'd). List of proteins whose quantification changes significantly in the presence of oipA protein in infection compared to control

P13645	**KRT10**	**Keratin, type I cytoskeletal 10 [OS=Homo sapiens]**	**0**	**2**	**0.901250463**	**2.114036081**	**0.012894685**
P14678	SNRPB	Small nuclear ribonucleoprotein-associated proteins B and B' [OS=Homo sapiens]	0	5	0.888842681	1.905275996	0.008852424
P18124	RPL7	60S ribosomal protein L7 [OS=Homo sapiens]	0	11	3.182145935	4.438277888	1.20009E-09
P19823	ITIH2	Inter-alpha-trypsin inhibitor heavy chain H2 [OS=Homo sapiens]	0	6	11.00433455	6.453134074	2.4869E-14
P20674	COX5A	Cytochrome c oxidase subunit 5A, mitochondrial [OS=Homo sapiens]	0	3	1.117287138	1.717130873	0.029712026
P25787	PSMA2	Proteasome subunit alpha type-2 [OS=Homo sapiens]	0	3	0.752623374	1.647182035	0.04309544
P30049	ATP5F1D	ATP synthase subunit delta, mitochondrial [OS=Homo sapiens]	0	2	0.628506687	0.411795509	0.000216983
P31431	SDC4	Syndecan-4 [OS=Homo sapiens]	0	2	3.073750363	5.388934307	6.16486E-10
P31949	S100A11	Protein S100-A11 [OS=Homo sapiens]	0	5	3.226567037	23.10286713	1E-17
P41567	EIF1	Eukaryotic translation initiation factor 1 [OS=Homo sapiens]	0	2	0.939522749	0.283220971	0.000703541
P42330	AKR1C3	Aldo-keto reductase family 1 member C3 [OS=Homo sapiens]	0	4	1.328685814	1.815038311	0.015645043
P46108	CRK	Adapter molecule crk [OS=Homo sapiens]	0	2	3.555370725	7.464263932	1.25926E-11
P46778	RPL21	60S ribosomal protein L21 [OS=Homo sapiens]	0	3	3.944930818	1.681792831	0.035917534
P47914	RPL29	60S ribosomal protein L29 [OS=Homo sapiens]	0	2	4.890561111	4.34693945	2.10954E-09
P52948	NUP98	Nuclear pore complex protein Nup98-Nup96 [OS=Homo sapiens]	0	3	1.319507911	3.052518418	0.000899288
P55265	ADAR	Double-stranded RNA-specific adenosine deaminase [OS=Homo sapiens]	0	2	0.952637998	2.584705661	0.011158305
P56385	ATP5ME	ATP synthase subunit e, mitochondrial [OS=Homo sapiens]	0	2	0.895025071	1.866065983	0.020020091
P56856	CLDN18	Claudin-18 [OS=Homo sapiens]	0	5	0.784584098	0.366021424	3.06083E-05
P57088	TMEM33	Transmembrane protein 33 [OS=Homo sapiens]	0	5	1.140763716	1.815038311	0.01538457
P61088	UBE2N	Ubiquitin-conjugating enzyme E2 N [OS=Homo sapiens]	0	4	1.443929196	2	0.004854279
P61604	HSPE1	10 kDa heat shock protein, mitochondrial [OS=Homo sapiens]	0	8	0.993092495	0.590496331	0.028429882
P61803	DAD1	Dolichyl-diphosphooligosaccharide--protein glycosyltransferase subunit DAD1 [OS=Homo sapiens]	0	3	0.946057647	0.598739352	0.03152274
P62195	PSMC5	26S proteasome regulatory subunit 8 [OS=Homo sapiens]	0	10	1.064370182	1.670175839	0.038205318
P62266	RPS23	40S ribosomal protein S23 [OS=Homo sapiens]	0	4	1.591072968	2.584705661	0.0001117
P62701	RPS4X	40S ribosomal protein S4, X isoform [OS=Homo sapiens]	0	12	1.790050142	2.751083636	3.68156E-05
P62917	RPL8	60S ribosomal protein L8 [OS=Homo sapiens]	0	10	3.482202253	5.540437872	2.89813E-12
P62942	FKBP1A	Peptidyl-prolyl cis-trans isomerase FKBP1A [OS=Homo sapiens]	0	2	1.613283518	3.655325801	2.15949E-05
P62993	GRB2	Growth factor receptor-bound protein 2 [OS=Homo sapiens]	0	2	0.972654947	0.450625231	0.019539435
P63167	DYNLL1	Dynein light chain 1, cytoplasmic [OS=Homo sapiens]	0	3	0.801069878	1.670175839	0.039716352
P63218	GNG5	Guanine nucleotide-binding protein G(I)/G(S)/G(O) subunit gamma-5 [OS=Homo sapiens]	0	2	1.021012126	1.892115293	0.049207778
P63313	TMSB10	Thymosin beta-10 [OS=Homo sapiens]	0	2	1.021012126	9.063071082	9.4813E-14
P78347	GTF2I	General transcription factor II-I [OS=Homo sapiens]	0	3	1.265756594	0.366021424	0.004436544

Table 14 (cont'd). List of proteins whose quantification changes significantly in the presence of oipA protein in infection compared to control

P99999	**CYCS**	**Cytochrome c [OS=Homo sapiens]**	**0**	**7**	**0.952637998**	**1.681792831**	**0.035554333**
Q06210	GFPT1	Glutamine--fructose-6-phosphate aminotransferase [isomerizing] 1 [OS=Homo sapiens]	0	22	0.986232704	0.607097442	0.036660554
Q07021	C1QBP	Complement component 1 Q subcomponent-binding protein, mitochondrial [OS=Homo sapiens]	0	4	1.197478705	0.50697974	0.004497419
Q12874	SF3A3	Splicing factor 3A subunit 3 [OS=Homo sapiens]	0	2	0.939522749	2.549121255	0.0061062
Q13501	SQSTM1	Sequestosome-1 [OS=Homo sapiens]	0	8	2.0139111	3.20427951	2.2019E-06
Q13867	BLMH	Bleomycin hydrolase [OS=Homo sapiens]	0.001	2	1.414213562	3.249009585	0.002388647
Q14061	COX17	Cytochrome c oxidase copper chaperone [OS=Homo sapiens]	0	2	0.659753955	0.283220971	6.54834E-05
Q15056	EIF4H	Eukaryotic translation initiation factor 4H [OS=Homo sapiens]	0	4	0.742261785	0.348685917	2.78296E-05
Q15185	PTGES3	Prostaglandin E synthase 3 [OS=Homo sapiens]	0	3	0.972654947	1.840375301	0.013442004
Q15363	TMED2	Transmembrane emp24 domain-containing protein 2 [OS=Homo sapiens]	0	4	1.094293701	0.496546248	0.008003692
Q16186	ADRM1	Proteasomal ubiquitin receptor ADRM1 [OS=Homo sapiens]	0	3	0.801069878	0.52850902	0.031579175
Q5R3I4	TTC38	Tetratricopeptide repeat protein 38 [OS=Homo sapiens]	0	3	1.375541818	3.89061979	7.0938E-06
Q5TBC7	BCL2L15	Bcl-2-like protein 15 [OS=Homo sapiens]	0	3	0.659753955	0.441351498	0.001510602
Q5VYY1	ANKRD22	Ankyrin repeat domain-containing protein 22 [OS=Homo sapiens]	0	2	2.234574276	3.810551992	0.000405764
Q6NUK1	SLC25A24	Calcium-binding mitochondrial carrier protein SCaMC-1 [OS=Homo sapiens]	0	13	1.094293701	0.607097442	0.037661932
Q6P1N0	CC2D1A	Coiled-coil and C2 domain-containing protein 1A [OS=Homo sapiens]	0	2	4.531535541	8.397733469	1E-17
Q6UX06	OLFM4	Olfactomedin-4 [OS=Homo sapiens]	0.002	2	1.394743666	0.171942727	2.38513E-06
Q6ZTI6	RFLNA	Refilin-A [OS=Homo sapiens]	0	3	1.132883885	3.095129987	0.000963147
Q8WUH6	TMEM263	Transmembrane protein 263 [OS=Homo sapiens]	0	2	0.888842681	3.138336392	0.000784174
Q99436	PSMB7	Proteasome subunit beta type-7 [OS=Homo sapiens]	0	2	1.064370182	2.234574276	0.00747922
Q99714	HSD17B10	3-hydroxyacyl-CoA dehydrogenase type-2 [OS=Homo sapiens]	0	6	1.172834949	2.848100391	4.82148E-05
Q99961	SH3GL1	Endophilin-A2 [OS=Homo sapiens]	0	3	1.231144413	2.394957409	0.005064399
Q99988	GDF15	Growth/differentiation factor 15 [OS=Homo sapiens]	0	5	2.128740365	3.482202253	1.17078E-05
Q9BPX5	ARPC5L	Actin-related protein 2/3 complex subunit 5-like protein [OS=Homo sapiens]	0	2	0.757858283	0.41754396	0.002318467
Q9BRA2	TXNDC17	Thioredoxin domain-containing protein 17 [OS=Homo sapiens]	0	3	0.986232704	0.517632462	0.006162316
Q9BSH5	HDHD3	Haloacid dehalogenase-like hydrolase domain-containing protein 3 [OS=Homo sapiens]	0	3	1.132883885	2.770218936	0.000688493
Q9BT78	COPS4	COP9 signalosome complex subunit 4 [OS=Homo sapiens]	0	3	1.094293701	2.928171392	0.000563467
Q9BUP3	HTATIP2	Oxidoreductase HTATIP2 [OS=Homo sapiens]	0	3	0.408951029	1.945309895	0.032001302
Q9BXP5	SRRT	Serrate RNA effector molecule homolog [OS=Homo sapiens]	0	10	0.972654947	2.084931522	0.002684686
Q9H0U3	MAGT1	Magnesium transporter protein 1 [OS=Homo sapiens]	0	2	0.920187651	0.463294031	0.00440784
Q9H190	SDCBP2	Syntenin-2 [OS=Homo sapiens]	0	5	0.993092495	1.681792831	0.03501867
Q9NS71	GKN1	Gastrokine-1 [OS=Homo sapiens]	0	4	0.742261785	2.29739671	0.00076345
Q9UDT6	CLIP2	CAP-Gly domain-containing linker protein 2 [OS=Homo sapiens]	0	2	0.895025071	2.462288827	0.004409851

Table 14 (cont'd). List of proteins whose quantification changes significantly in the presence of oipA protein in infection compared to control

Q9UEW8	**STK39**	**STE20/SPS1-related proline-alanine-rich protein kinase [OS=Homo sapiens]**	**0**	**3**	**0.876605721**	**0.339151082**	**0.000529802**
Q9UL25	RAB21	Ras-related protein Rab-21 [OS=Homo sapiens]	0	7	1.086734863	0.607097442	0.046654641
Q9Y295	DRG1	Developmentally-regulated GTP-binding protein 1 [OS=Homo sapiens]	0.001	2	0.858565436	2.584705661	0.001591282
Q9Y2A9	B3GNT3	N-acetyllactosaminide beta-1,3-N-acetylglucosaminyltransferase 3 [OS=Homo sapiens]	0	3	0.895025071	0.524858342	0.033268142

APPENDIX 2

The approval of the ethics committee

9 CURRICULUM VITAE